8-4-2007

Structural, Kinetic and Mutational Analysis of Two Bacterial Carboxylesterases

Ping Liu

STRUCTURAL, KINETIC AND MUTATIONAL ANALYSIS OF TWO BACTERIAL CARBOXYLESTERASES

by

Ping Liu

Under the Direction of Irene T. Weber

ABSTRACT

The crystal structures of two thermostable carboxylesterase Est30 and Est55 from *Geobacillus stearothermophilus* were determined to help understand their functions and applications in industry or medicine. The crystal structure of Est30 was determined at 1.63 Å resolution by the multiple anomalous dispersion method. The two-domain Est30 structure showed a large domain with a modified alpha/beta hydrolase core including a seven, rather than an eight-stranded beta sheet, and a smaller cap domain comprising three alpha helices. A 100 Da tetrahedral ligand, propyl acetate, was observed to be covalently bound to the side chain of Ser94 in the catalytic triad. This ligand complex represents the first tetrahedral intermediate in the reaction mechanism. Therefore, this Est30 crystal structure will help understand the mode of action of all enzymes in the serine hydrolase superfamily.

Est55 is a bacterial homologue of the mammalian carboxylesterases involved in hydrolysis and detoxification of numerous peptides and drugs and in prodrug activation. Est55 crystals were grown at pH 6.2 and pH 6.8 and the structures were determined at resolutions of 2.0 and 1.58 Å, respectively. Est55 folds into three domains, a catalytic

domain, an α/β domain and a regulatory domain. This structure is in an inactive form; the side chain of His409, one of the catalytic triad residues, is pointing away from the active site. Moreover, the adjacent Cys408 is triply oxidized and lies in the oxyanion hole, which would block the entry of substrate to its binding site. This structure suggested a self-inactivation mechanism, however, Cys408 is not essential for enzyme activity. Mutation of Cys408 showed that hydrophobic side chains at this position were favorable, while polar serine was unfavorable for enzyme activity.

Both Est30 and Est55 were shown to hydrolyze the prodrug CPT-11 into the active form SN-38. Therefore, Est30 and Est55 are potential candidates for use with irinotecan in cancer therapy. The catalytic efficiency (k_{cat}/K_m) of Est30 is about 10-fold lower than that of Est55. The effects of the Cys408 substitutions on Est55 activity differed for the two substrates, *p*-NP butyrate and CPT-11. Mutant C408V may provide a more stable form of Est55.

INDEX WORDS: thermostable carboxylesterase, *Geobacillus stearothermophilus*, crystal structure, multiple anomalous dispersion, alpha/beta hydrolase, tetrahedral intermediate, reaction mechanism, prodrug activation, CPT-11, cancer gene therapy

STRUCTURAL, KINETIC AND MUTATIONAL ANALYSIS OF TWO BACTERIAL CARBOXYLESTERASES

by

PING LIU

A Dissertation Submitted in Partial Fulfillment of Requirements for the Degree of

Doctor of Philosophy

In the College of Arts and Sciences

Georgia State University

2006

STRUCTURAL, KINETIC AND MUTATIONAL ANALYSIS OF TWO BACTERIAL CARBOXYLESTERASES

by

PING LIU

Major Professor: Irene T. Weber
Committee: Xiaodong Cheng
Robert W. Harrison
Chung-Dar Lu

Electronic Version Approved:

Office of Graduate Studies
College of Arts and Sciences
Georgia State University
August 2006

ACKNOWLEDGMENTS

I would like to thank my supervisor Dr. Irene Weber who introduced me into the world of protein crystallography where I found how much fun to be a scientist. Over the years, she gave me constant support, encouragement and sound guidance in my research. She always cares about me not only in science but also in my personal life. I really owe her a lot. I would like to acknowledge all of my Committee members: Dr. Robert Harrison, Dr. Xiaodong Cheng and Dr. Chung-Dar Lu. They always gave me constructive advice and brilliant ideas during our committee meetings.

I am also very thankful to my collaborators for their great help, especially Dr. Lu who was always welcoming me when I wanted to use his lab equipments to perform the enzyme kinetics and protein purification experiments. I would also like to thank Dr. Teryl Frey for allowing me to use his lab facilities. Many thanks for his lab members for assisting me during undertaking some of my experiments.

I want to thank all my colleagues: Yuan-Fang Wang, who taught me basic crystallographic principles from data collection to analysis using various software tools; Peter Boross, who helped me in HPLC enzymatic assay; Johnson Agniswamy, Xianfeng Chen, Alexander Chumanevich, Bin Fang, Anna Fominykh, LaQuasha Gaddis, Andrey Kovalevsky, Fengling Liu, Bhuvaneswari Mahalingam, John Petock, Amit Sabnis, Yunfeng Tie, Hao Wang, Patra Volarath, who gave me sincere advice and help for research and presentations. I truly appreciate all the help from Dr. Xiaodong Cheng and

John Horton in Emory University and James Liu in University of Georgia during crystal screening.

I am deeply grateful to my parents, Lijuan Zhang and Minxiu Liu, my brother Feng Liu for their constant support and love. Special thanks go to my husband Hosam Ewis. He was always there for me during my difficult times. He is my partner not only in life but also in science. Without him, I would not go that far. In the end, I would like to thank all the faculty, staff and colleagues in our department.

TABLE OF CONTENTS

LIST OF TABLES

LIST OF FIGURES

LIST OF ABBREVIATIONS

Å	Angstrom
Ab	antibody
ADEPT	antibody-directed enzyme prodrug therapy
ALA	alanine
ASP	aspartic acid
BLAST	basic local alignment search tool
Cα	alpha carbon
cDNA	complementary deoxyribonucleic acid
CE	carboxylesterase
CPT-11	irinotecan
C-terminal	carboxyl terminal
Da	dalton
DDT	dithiothreitol
EDTA	ethylene diamine tetraacetic acid
Glu	glutamic acid
Gln	glutamine
Gly	glycine
4PP	4- piperidino-piperidine
hCE	human carboxylesterase
hiCE	human intestine carboxylesterase

HIS	histidine
γ-IFN	γ-interferon
IL-2	Interleukin 2
ILE	isoleucine
L	liter
LB	Luria-Bertani
Leu	leucine
kDa	kilodaltons
MAD	multiplewavelength anomalous diffraction
MET	methionine
mM	millimolar
MW	molecular weight
NMR	nuclear magnetic resonance
N-terminal	amino terminal
PAGE	polyacrylamide gel electrophoresis
PCR	polymerase chain reaction
PDB	Protein Data Bank
PEG	polyethylene glycol
PHE	phenylalanine
rCE	rabbit carboxylesterase
RMSD	root mean square deviation

SDS	sodium dodecyl sulphate
SeMet-Est30	Est30 with selenomethionine
SER	serine
SN38	7-ethyl-10-hydroxycamptothecin
THR	threonine
TRP	tryptophan
TYR	tyrosine
VAL	valine
VDEPT	viral-directed enzyme prodrug therapy

CHAPTER 1

General Introduction

Carboxylesterases and their classifications

Carboxylesterases (carboxylic ester hydrolase, EC 3.1.1.1) are a group of enzymes that hydrolyze carboxylic ester bonds with relatively broad substrate specificity. They are members of the α/β hydrolase family and can hydrolyze short chain aliphatic and aromatic esters (Krish 1971). Both mammalian carboxylesterases and bacterial carboxylesterases have enormous interest because of their important physiological, industrial and medical roles in the synthesis and hydrolysis of stereospecific compounds including the metabolic processing of drugs, and antimicrobial agents (Krish 1971; Takayama 1998; Bornscheuer 2002).

Several carboxylesterases from bacterial origins have been identified and studied (Morana 2002; Mnisi 2005). Generally, for bacterial carboxylesterases, attention has been focused on their biotechnological potential because of their special characteristics such as high regioselectivity, enantioselectivity and thermostability. Their potential in medicine is rarely explored.

Enzymes can be classified based on either their substrate specificity or their sequence similarity. The substrate specificity of carboxylesterases is very wide (Walker 1983). It has been shown that carboxylesterases have broad and overlapping substrate specificity towards amides and esters and a single esterolytic reaction is mediated by several enzymes. Therefore, it is impossible to classify carboxylesterases based on their

substrate specificity. Arpigny (Arpigny 1999) and Satoh (Satoh 1998) have classified microbial and mammalian carboxylesterases based on sequence similarities.

Microbial lipolytic enzymes including carboxylesterases and true lipases are classified into eight families. Members of Family I are true lipases. The enzymes in Family II (GDSL family) have a Gly-Asp-Ser-(Leu) (GDSL) motif instead of the conventional pentapeptide Gly-Xaa-Ser-Xaa-Gly. Few enzymes have been identified in Family III and the majority of them are lipases. Their structures display a canonical fold. Family IV is called the hormone sensitive lipase (HSL) family because enzymes in this family have a striking amino acid sequence similarity to the mammalian HSL. Enzymes grouped in Family IV originate from mesophilic bacteria (*Pseudomonas oleovorans*, *Haemophilus influenzae*, *Acetobactr pasteurianus*) as well as from cold-adapted (*Moraxella sp*) or thermostable (*Sulfolobus acidocaldarius*) organisms. The unique feature of enzymes in Family VI is their low molecular weight (23-26 KDa). They are the smallest esterases known. Esterases from Family VII are rather large (~55 KDa) and share significant homology to eukaryotic acetylcholine esterases and intestine or liver carboxylesterases. A *p-nitrobenzyl* esterase from *Bacillus subtilis* and an esterase from *Arthrobacter oxydams* belong to this group (Pohlenz 1992; Moore 1996; Arpigny 1999). Interestingly, Family VIII enzymes show a significant similarity to several class C β-lactamases. A region of 150 residues (from position 50 to 200) is 45% similar to an *Enterobacter cloacae ampC* gene product (Arpigny 1999).

Mammalian carboxylesterases (EC 3.1.1.1) are from multiple gene families. The gene products are located in the endoplasmic reticulum of many tissues (Hosokawa 1987;

Hosokawa 1990; Yamada 1994; Hosokawa 1995; Satoh 1998; Mori 1999; Hosokawa 2001). Satoh and Hosokawa proposed a novel classification and nomenclature of carboxylesterase isozymes (Satoh 1998). Based on the sequence identity and the enzyme characteristics, they proposed that carboxylesterase isozymes be classified into four families, CES1, CES2, CES3, and CES4. According to the classification, human liver carboxylesterase and rabbit liver carboxylesterase (rCE) belong to the CES1 family.

Carboxylesterase reaction mechanism

Carboxylesterase can perform ester hydrolysis and substrate transesterfication reactions. The cleavage of the esters by carboxylesterases is base-mediated and requires water as co-reactant. The reaction is achieved by the catalytic triad of Ser, Glu and His. Site-directed mutagenesis of the catalytic Ser, His and Glu to Ala significantly reduced the carboxylesterase activity, thus confirming the role of Glu and His in forming a putative charge relay system with Ser (Taylor 1994). Frey (Frey 1994) demonstrated the importance of low-barrier hydrogen bonds in the serine esterase reacion. The low-barrier hydrogen bonds formed between His and Glu facilitate the action of nucleophilic attack by the β-OH group of Ser on the acyl carbonyl group of chymotrypsin (Frey 1994). The charged glutamic acid facilitates removal of a proton from histidine, resulting in the transfer of proton from the adjacent serine to the opposing nitrogen of histidine. The generated oxygen nucleophile subsequently attacks the carbonyl group of substrate. The transition state is stabilized by low-barrier hydrogen bonds, which include the hydrogen bond between His and Glu and the hydrogen bond between the tetrahedral oxyanion and

the amides of two Gly. Then, the acyl-enzyme complex forms after removing a proton from His and the alcohol is released. The deacylation reaction is the reverse of the acylation step, which starts from a nucleophilic attack by a water molecule in identical fashion to form the second tetrahedral intermediate, leading to the release of the carboxylic acid and return of the enzyme in the original state (Satoh 1998).

Carboxylesterase structures

Although several carboxylesterase families have been identified, the molecular structures are known for only a few carboxylesterases. Crystal structures are available for two members of the hormone-sensitive lipase (HSL) family (Family IV), (De Simone 2000; De Simone 2001), one carboxylesterase from the Family VI (Kim 1997) and pNB esterase from Family VII (Figure 1.1). These structures have a typical α/β hydrolase fold (Ollis 1992; Heikinheimo 1999; Nardini 1999), with a central eight-stranded β sheet, flanked by helices and connecting loops (Figure 1.2). The catalytic center contains a triad of amino acid residues (Ser-His-Asp/Glu), responsible for the nucleophilic attack on the carbonyl carbon atom of the ester bond. The nucleophile is located at the apex of a sharp turn between a β strand and an α helix that is known as the nucleophile elbow.

Only two mammalian carboxylesterase structures have been determined (Figure 1.3). The first crystal structure of a mammalian carboxylesterase was that of rCE (Bencharit 2002). rCE has the serine hydrolase fold observed in other esterases. Human carboxylesterase 1 (hCE1) and rCE share 81% sequence identity and have a 0.68 Å root

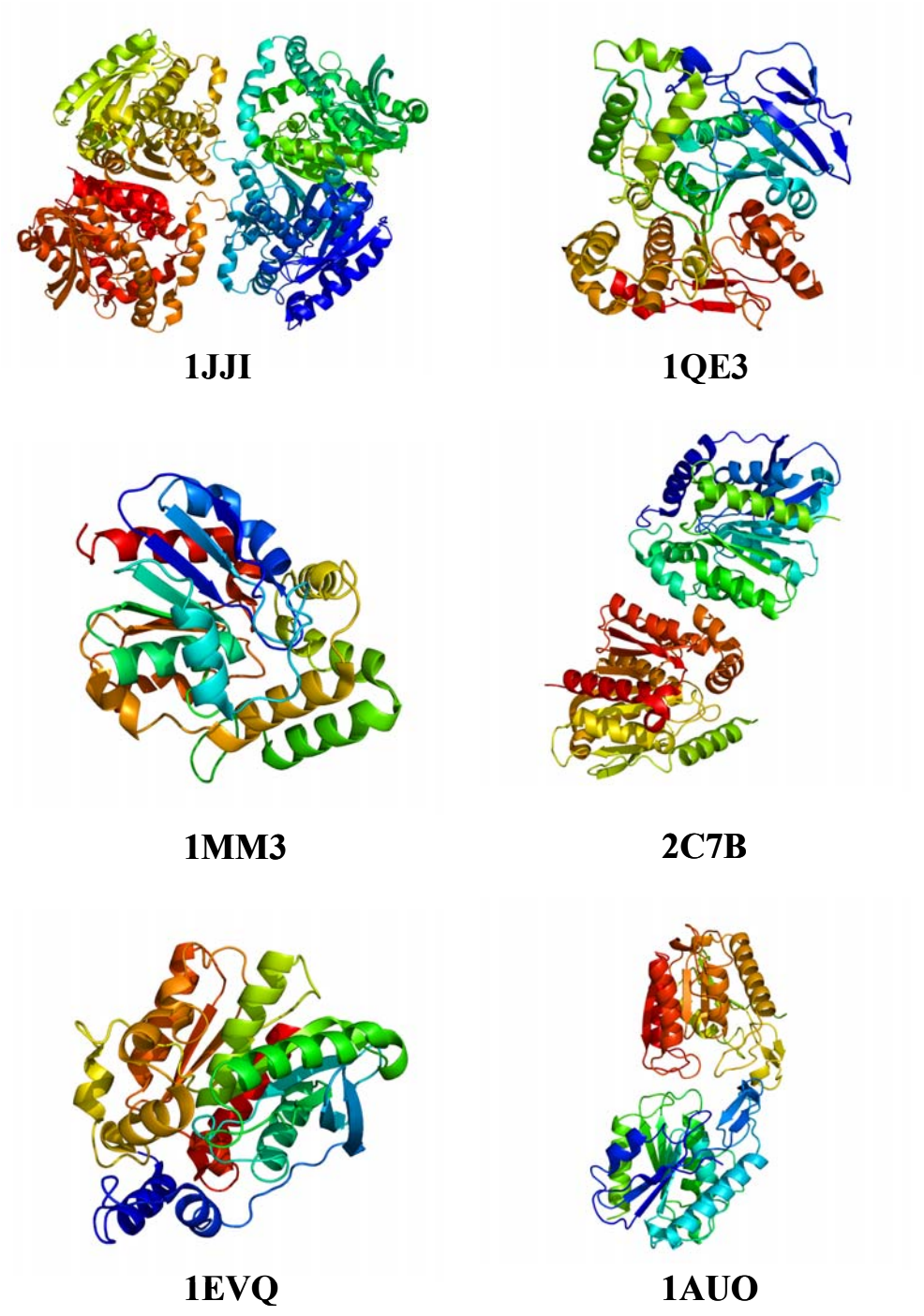

Figure 1.1 Bacterial carboxylesterase structures. The four-letter code under each structure is its code in the protein data bank.

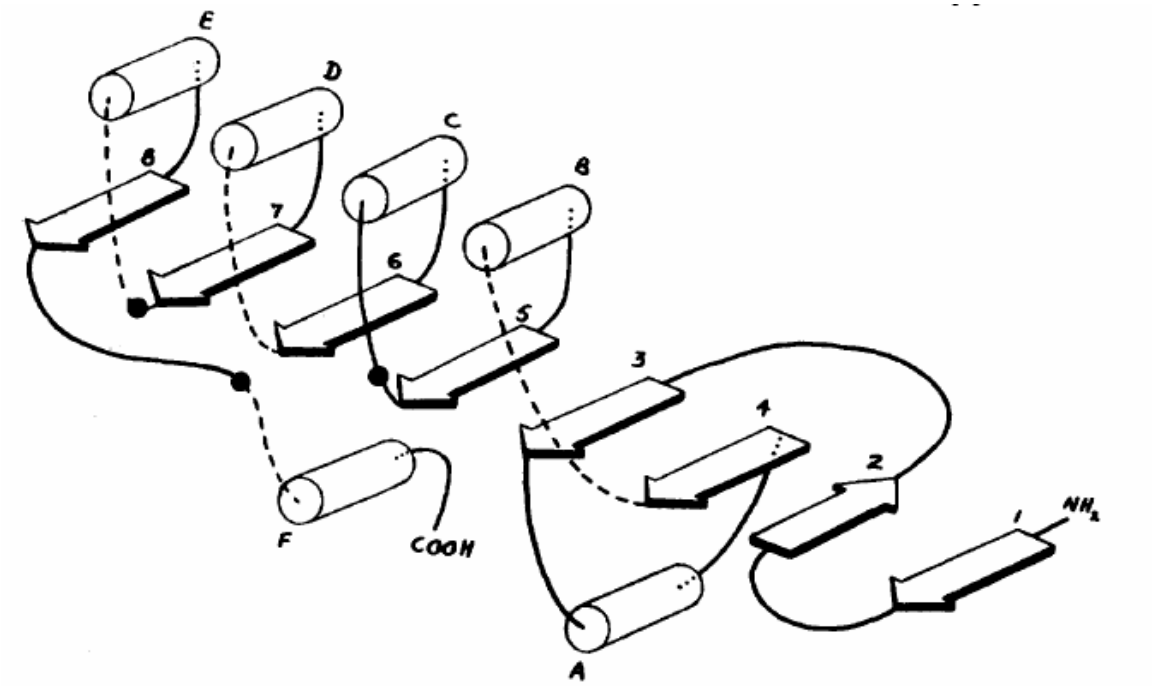

Figure 1.2 A schematic diagram of the α/β hydrolase fold (Ollis 1992). The secondary structure is indicated by arrows for beta strands and cylinders for alpha helices.

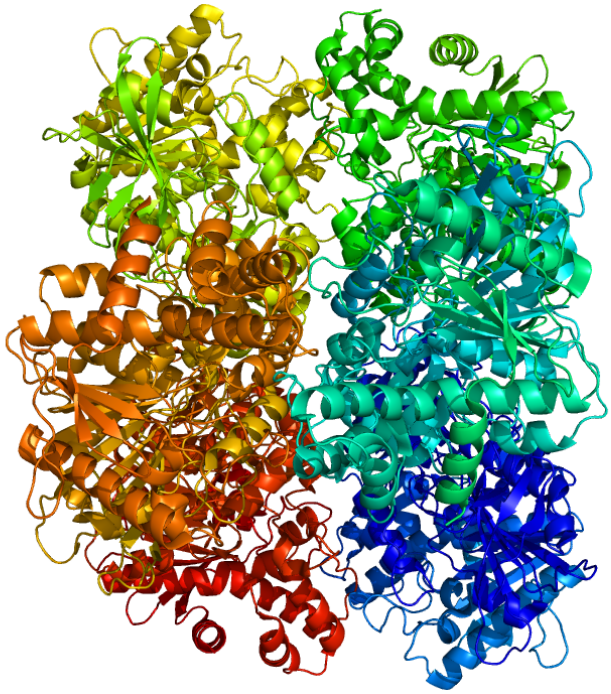

1MX1

1K4Y

Figure 1.3 Mammalian carboxylesterase structures. The four-letter code under each structure is its code in the protein data bank.

mean square deviation (RMSD) over Cα carbons (Bencharit 2003; Bencharit 2003). Both enzymes form trimers and the serine hydrolase fold exhibited by their structures includes a central 15-stranded β sheet surrounded by several α helices and β strands.

Biological roles of carboxylesterases

The specific biological functions have not been defined for many carboxylesterases due to their wide substrate specificity. Carboxylesterases have been found to play a role in processing endobiotic compounds, for example, in cholesterol homeostasis (Becker 1994). Although cholesterol is essential in the structural integrity of plasma membranes, it is toxic if present in excess. Thus, systemic trafficking of cholesterol is crucial to the delivery and clearance of this compound. Fatty acids are added to the 3-position of cholesterol by carboxylesterase to create cholesteryl esters, which are packaged with high-, intermediate- and low density lipoproteins for systemic delivery and clearance (Redinbo 2005).

Carboxylesterases are involved in drug metabolism. Many clinically useful drugs containing ester groups are subject to catalysis by carboxylesterases (Tang 1995). Carboxylesterases are essential in the hydrolysis of cocaine (Brzezinski 1994; Dean 1995), heroin (Brzezinski 1997), aspirin, procalin (Joly 1986), dipivefrin hydrochloride (Nakamura 1992), carbonates (McCracken 1993), salicylates (White 1994), capsaicin (Park 1994), palmitoyl-coenzyme A (Hosokawa 1987; Hosokawa 1990), haloperidol (Nambu 1987), imidapril (Yamada 1992), pyrrolizidine alkaloids (Dueker 1992; Dueker 1992; Dueker 1995) and steroid (Lund-Pero 1994). Therefore, strategies to modulate the

levels of the drugs such as cocaine and heroin in patients who have overdosed on these substances are proposed (Kamendulis 1996; Pindel 1997). For example, human carboxylesterase 1 can convert cocaine into benzoylecgonine, a non-toxic derivative. This approach is especially useful for those cases where drug levels are extremely high and would result in significant clinical problems that cannot be resolved by standard emergency hospital care (Redinbo 2005).

The applications of carboxylesterases

Carboxylesterases are important enzymes in the hydrolysis and detoxification of numerous peptides and drugs. Carboxylesterase-mediated hydrolysis of esters has been used to design several ester-containing drugs including development of the chemotherapeutic agent CPT-11 (Senter 1996; Kojima 1998) 10-hydroxycampothecin fatty acid esters (Takayama 1998), and the drug lovastatin for the activation of the blood cholesterol (Tang 1995).

The main application of microbial carboxylesterases is in biocatalysis, especially in organic compound synthesis. The best studied enzyme is the carboxylesterase NP (NP from naproxen, a non-sterodial anti-inflammatory drug) from *Bacillus subtilis* (Quax 1994). NP esterase is used in resolution of (*R*, *S*)-naproxen methylester and (*R*, *S*)-ibuprofen methylester. Another enzyme used in organic synthesis is an esterase from *A. globiformis*, which is used in the synthesis of (+)-*trans*-(1*R*, 3*R*)- chrysanthemic acid, an important precursor of pyrethrin insecticides (Nishizawa 1995). Carboxylesterases can also be used in the chemo- or regioselectivity reaction such as the release of ferulic acid

from plant cell wall polysaccharides such as pectin or xylan (Falconnier 1994; Lesage-Meessen 1996; Gasson 1998). Microbial carboxylesterases are involved in the catabolism of aryl esters, as shown by the example of an enzyme from *Acinetobacter sp*. that releases an acid from benzyl esters (Jones 1999). *p*-nitro-benzyl benzyl esterase from *Bacillus subtilis* is used to remove protecting groups in the synthesis of the antibiotic Loracarbef (Zock 1994).

Carboxylesterases play important roles in prodrug activation. In the majority of esterase-mediated reactions, the drug compounds are inactivated by esterases. While, in the reaction of hydrolysis of prodrugs CPT-11 and capecitabine, the ester groups are removed to improve their water solubility, resulting in elevated antitumor activity (Kunimoto 1987; Bajetta 1996; Danks 1998; Matsuzaki 1998; Potter 1998). Therefore, these carboxylesterases have a potential role in cancer gene therapy.

Cancer gene therapy

Several strategies have been used in cancer gene therapy. One major strategy is correction of the genetic defect in tumor cells and another is killing the tumor cells. Corrective gene therapy may not be a practical approach because most tumor cells contain multiple genetic mutants. Gene replacement for cancer would require correcting multiple oncogenes in every tumor cell since any nontransduced cells would continue rapid replication. Therefore, cancer gene therapy has expanded the range of transgenes to include those with ability to confer selective cytotoxicity to transduced tumor cells. The purpose of most cancer gene therapy strategies is to kill tumor cells instead of restore

their normal phenotype (Aghi 2000). Therapeutic transgenes that have been utilized include those that (1) correct the primary genetic defect in many cancer cells. An example is the restoration of wild type of tumor suppressor gene p53 expression using a retroviral vector (Roth 1999); (2) enhance the immune response by transferring genes that encode cytokines IL-2 and γ-IFN (Foa 1992; Watanabe 1992); (3) transfer of genes conferring chemotherapy resistance into bone marrow or peripheral blood stem cells in order to allow high dose of chemotherapy to be given, e. g. transfer of multidrug resistance gene that encodes P-glycoprotein (DelaFlor-Weiss 1992); (4) transfer of genes encoding enzymes or active enzymes directly to tumor sites to activate prodrugs (Habib 2001).

The role of carboxylesterases in CPT-11 gene therapy

Carboxylesterases have been evaluated for activation of prodrug CPT-11 (Irinotecan) in cancer gene therapy (Tsuji 1991; Satoh 1994; Senter 1996). CPT-11 is a prodrug that can be activated by a carboxylesterase to generate SN-38 (7-ethyl-10-hydroxycamptothecin), a topoisomerase I poison (Figure 1.4). Irinotecan is a water-soluble derivative of camptothecin, an alkaloid originally extracted from the Chinese tree *Camptotheca acuminata*. CPT-11 has shown significant anti-tumor activity in human tumor xenograft models. So far, irinotecan has been used in the treatment of different types of cancers such as colorectal cancer (Rothenberg 2003), gastric cancer (Comella 2002), lung cancer (Ichiki 2003), cervical cancer (Chitapanarux 2003), ovarian cancer

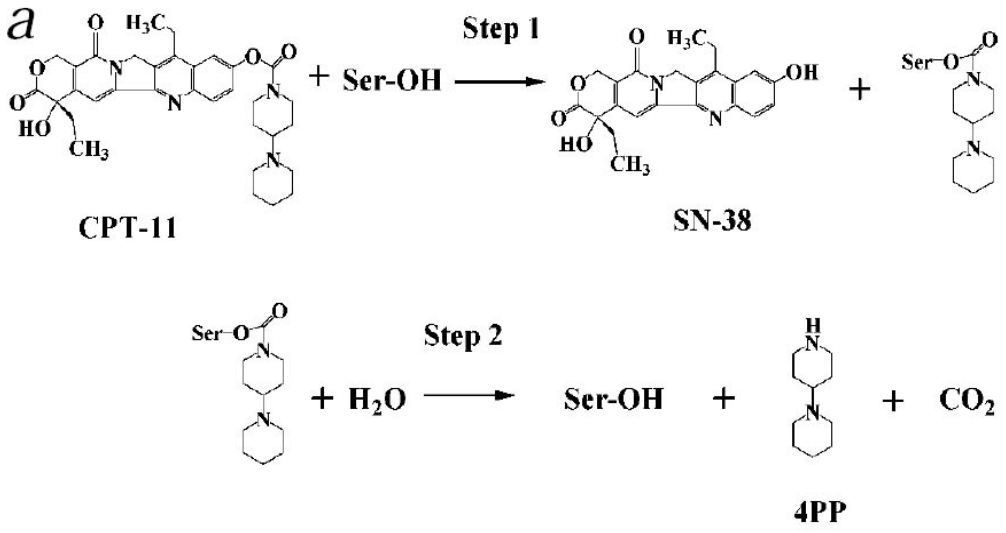

Figure 1.4 Two steps of activation of prodrug CPT-11 to topoisomerase poison SN-38 and 4- piperidino-piperidine (4PP) by carboxylesterase (Bencharit 2002).

(Bodurka 2003), breast cancer (Agelaki 2003), head and neck cancer and brain tumors (Koukourakis 1999; Friedman 2003).

CPT-11 is poorly activated in humans, thus this suggests the potential for the development of an enzyme prodrug therapy (Danks 2004). Such a strategy allows the enzyme to selectively activate inactive prodrugs to produce specific toxicity in desired cell types. For CPT-11 activation, rabbit carboxylesterase (rCE) is considered the most efficient enzyme and is ~5 fold and ~1000 fold more efficient than human intestine carboxylesterase (hiCE) and human carboxylesterase (hCE), respectively (Potter 1998; Danks 1999; Danks 2004). Two different approaches can be applied in this Carboxylesterase/CPT-11 therapy (Figure 1.5).

Viral-directed enzyme prodrug therapy (VDEPT) is a technique that involves physical delivery of a gene encoding a foreign enzyme to tumor cells where prodrugs can be activated after expression of that enzyme (Xu 2001). Transfer of genes is generally facilitated by a vector, which is either viral or non-viral. The ideal vector for gene transfer would be safe and easy to prepare in large quantities. It would be efficient to deliver genetic material and specific for its target, and not recognized by host immune system (Habib 2001). Several viruses have been used for VDEPT, including retroviruses, adenoviruses, herpes simplex virus (HSV), adeno-associated virus, lentivirus, and Epstein-Barr virus (EBV). Retroviruses are used widely and have been utilized in 80 % of gene therapy protocols. They can be integrated into genome and can give rise to stable expression (Habib 2001). The main disadvantage associated with a retrovirus vector is that the retrovirus can only target dividing cells, whereas most tumor cells are slowly

dividing, so this results in a low transduction rate (2-10%) (Hamstra 1999). Vector targeting is usually affected by direct injection into tumor tissues, but the efficiency is very low. In order to increase the efficiency, the bystander effect has been utilized in VEDPT. The Bystander effect is that activated drug can act not only on transduced cells but also on nontransduced cells. This bystander effect requires cell–to- cell contact or facilitation by drug diffusion or extracellular activation to target neighboring tumor cells. Designing a secreted form of genes whose products can be secreted outside of cells is one of the strategies that has been utilized in VEDPT (Howard B 1994). Several viral vectors have been applied to achieve delivery of the cDNA encoding the carboxylesterases to tumor cells (Kojima 1998; Kojima 1998; Wierdl 2002; Oosterhoff 2003; Oosterhoff 2005). A replication-deficient adenoviral vector Ad.C28-sCE2 containing a fusion gene encoding a secreted form of human liver CE2 has been designed to target to the surface antigen epithelial cell adhesion molecule (EpCAM) that is highly expressed on most colon carcinoma cells (Oosterhoff 2005). They demonstrated that active carboxylesterases were expressed and secreted in Ad.C28-sCE2-transduced colon carcinoma cells and bound specifically to EpCAM-expressing cells. The secreted carboxylesterases allow the activated drugs to act not only on transduced cells but also on nontransduced cells. Therefore, Ad.C28-sCE2 provides a promising approach for the treatment of colon carcinoma. Wierdl *et al* developed an adenoviral vector expressing intracellular rabbit carboxylesterase. After transduction, the virus produces very high levels of CE activity in a panel of human tumor cell lines and results in marked sensitization to CPT-11 for all of the transduced cells (Wierdl 2002).

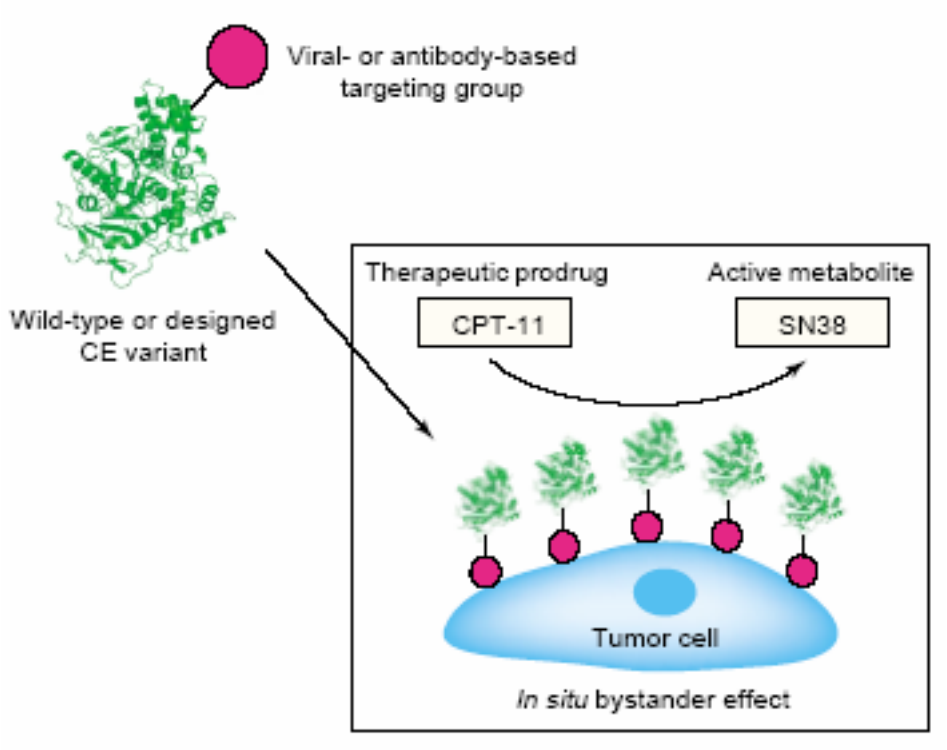

Figure 1.5 Two different approaches, Viral-directed enzyme prodrug therapy (VDEPT) and Antibody-directed enzyme prodrug therapy (ADEPT), could be utilized in carboxylesterase activating prodrug CPT-11 (Redinbo 2005).

An alternative approach is antibody-directed enzyme prodrug therapy (ADEPT). In ADEPT, selectivity for a target is achieved by an antibody (Ab) in an Ab-enzyme conjugate that binds to an antigen that is only expressed on the surface of tumor cells. In the first step, antibody-enzyme conjugates are administrated and accumulate at the tumor site. Enough time is allowed for clearance of the conjugate from blood and normal tissues. In the second step, a nontoxic prodrug is administrated, which can be activated on the surface of tumor cells and diffuse inside tumor cells. The advantage of this approach is that not all tumor cells would be required to bind the antibody because drugs released by the enzyme could diffuse to neighboring cells that are not expressing the antigen. Also, in ADEPT, a single molecule has the potential to cleave many prodrug molecules. The main drawback of ADEPT is that the Ab-enzyme conjugates can elicit the immune response, which can prevent the administration of repeated doses of the conjugate. This method has been applied in the activation of CPT-11 using hiCE and rCE against a melanoma tumor model (Senter 2001). However, little success was achieved by this method. This could be due to several factors including the loss of the enzyme activity after coupling to the antibody, the low affinity of antibody to antigen, or relatively inefficient activation of the drug. Increasing enzyme specificity or activity will help improve this approach for cancer therapy (Redinbo 2005).

Protein Crystallography

Several mammalian and bacterial carboxylesterase structures have been determined as described earlier (Figure 1.1& 1.3). Knowing their structures can help

better understand their functions and explore their potential applications. For example, knowledge of the structure of the starting protein is central to a rational way to redesign the protein function. X-ray crystallographic determination has been the most extensively used approach to obtain three-dimensional structures of various enzymes. Under certain conditions, protein molecules form crystals. The crystal is an orderly three dimensional array of molecules, held together by various noncovalent interactions including hydrogen bonds, salt bridges, and hydrophobic interactions. Figure 1.6 depicts an example of lysozyme crystals. X-ray scattering from a single molecule will be very weak and will not be detected above the noise level, which includes scattering from the air and water. A crystal has a huge number of molecules arranged in the same or a related orientation, so that the scattering waves from all the molecules can add up together to reach a measurable level. Thus, a crystal can act as an amplifier.

A crystal consists of an array of unit cells. Each unit cell is designated by six parameters: the length of three unique edges (a, b and c) and three unique angles (α, β, and γ). The unit cell is the smallest unit, which can build up the whole crystal by a symmetric relationship. Determining crystal symmetry is usually the first step in data collection and analysis (Rhodes 2000).

There are a number of potential bottlenecks in determining a crystal structure such as growing diffraction quality crystals, finding a cryoprotectant and phase determination, but growing a useful crystal can be the most serious one. There is no general protocol for crystallizing proteins. The crystallization conditions vary from one protein to the other. Even a single mutation and the addition of a small ligand can result

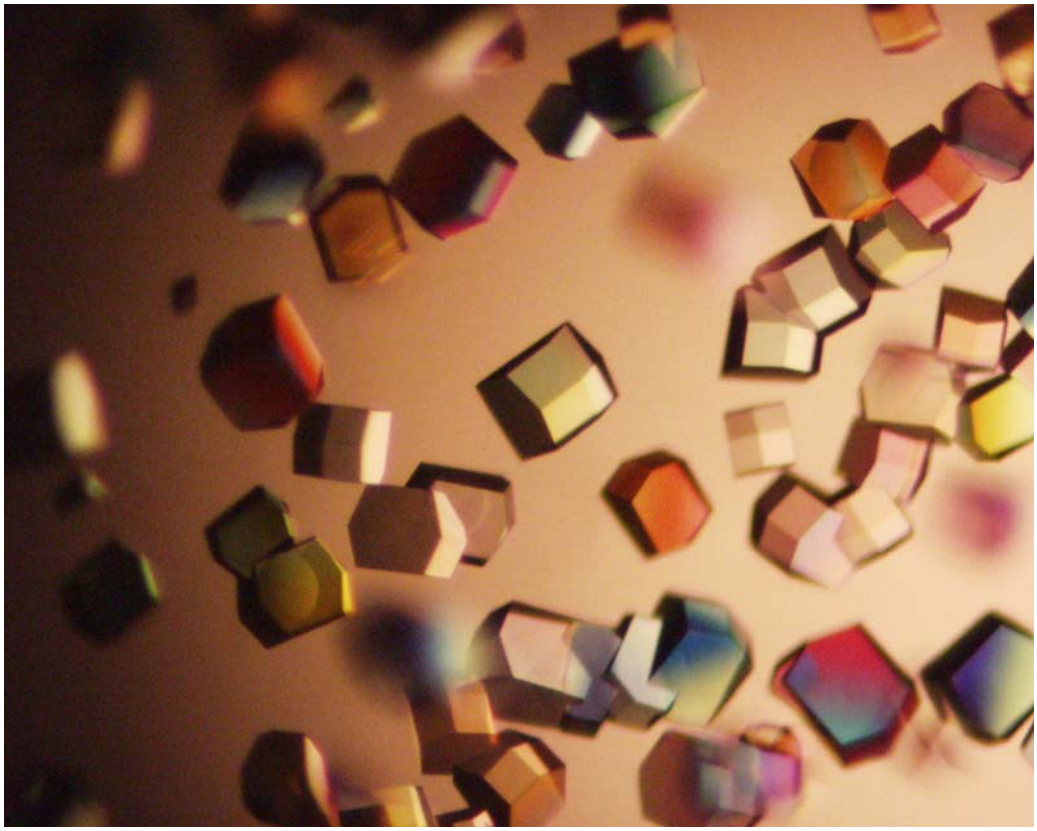

Figure 1.6 Lysozyme crystals (Grown by Sonia Iyer in Dr. Weber's lab)

in a dramatic change of crystallization condition. Crystallization could be affected by various factors such as protein concentration, temperature, pH, buffer, and salt. Finding the exact conditions to produce good crystals of one specific protein often requires many trials. Sometimes crystallization can be achieved by efforts of many years. By far the most popular technique for crystallization is vapor diffusion. Hanging drop method under the category of vapor diffusion is frequently used (Figure 1.7). In this method, a droplet containing purified protein, buffer and precipitate is allowed to equilibrate with a reservoir containing the precipitate in higher concentrations. Usually a few microliter of purified protein is mixed with an equal amount of the reservoir solution. This solution is suspended as a droplet underneath a cover glass, which is sealed on the top of the reservoir. Because the precipitate concentration in the drop is about 50 % of that in the reservoir, water vaporizes from the drop and transfers to the reservoir. When the system comes to equilibrium, the net transfer of water ceases. If the precipitant concentration in the drop increases to the level optimal for crystallization, protein molecules will be crystallized (Rhodes 2000).

After obtaining a reliable source of suitable crystals, data collection can begin. First, crystals must be positioned between an X-ray source and an X-ray detector. The classical method of mounting crystals is to transfer them to a fine glass capillary along with the mother liquor. In recent years, crystallographers have been able to take advantage of collecting X-ray data of crystals at very low temperature, for example liquid nitrogen (boiling point -196 ℃). Theoretically, lowering the temperature should increase molecular order in the crystals and improve diffraction data quality. However, practically,

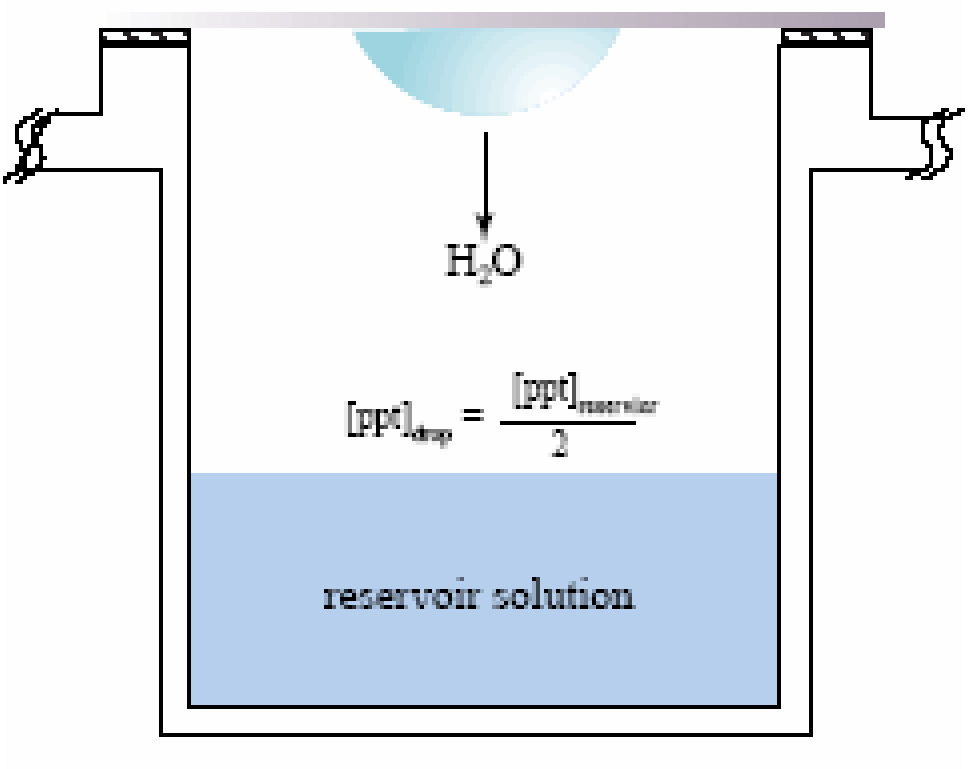

Figure 1.7 Hanging drop method is a common used approach in crystallization.

freezing crystals directly will result in damage due to formation of ice crystals. Crystallographers have developed a technique for flash freezing crystals in the presence of chemical agents called cryoprotectants, such as glycerol, small molecular weight polyethylene glycol, sugar, oil. However, searching for a suitable cryoprotectant can be another bottle-neck in the way of solving crystal structures due to the fragile nature of protein crystals and the lack of a general protocol for this procedure (Rhodes 2000).

The crystal diffracts the source of X-ray beam into discrete directions, shown as distinct spots (reflections) on the detector. Generally, the goal of data collection is to maximize the data resolution and completeness with the shortest time. Usually the data collection strategy is guided by the information of crystal symmetry, the unit cell parameters, the crystal orientation and the resolution limit obtained from a few crystal diffraction images in the initial trials.

The determination of protein structure by X-ray crystallography requires not only crystallizing the proteins and experimental collection of diffraction data as intensities of diffracted X-rays scattered from a protein crystal but also the phase angle. The intensity and phase data can be transformed using the Fourier Transform equation to produce a three-dimensional visualization of the scattering matter, which is called the electron density map. But what we measure in the experiment is the number of X-ray photons in each reflection. There is no practical way of measuring the relative phase angles of different diffracted spots experimentally. The number of photons gives the intensity, which is proportional to the square of the amplitude of the diffracted wave. But the phase has been lost.

The Phase problem is one of the most difficult problems in crystallography. There are three commonly used strategies for determining accurate phases, namely, multiple isomorphous replacement, multiple wavelength anomalous dispersion and molecular replacement. The isomorphous replacement is achieved by comparison of the diffraction data from two crystals, which differ because one or more strong scattering centers exist in one crystal and are absent in the other. Usually a heavy metal ion or a heavy metal compound, which can bind tightly to one or more sites of the protein molecule, was directly added into crystallization solution or "soaked" into crystals. In most cases, a protein is first crystallized in the absence of heavy atoms. The crystals without the heavy atoms may be referred to as the parent or native form, and a crystal including the heavy atom may be called the derivative. The word isomorphous means that the parent and derivative crystals have the same unit cell dimensions and symmetry. The binding of heavy atom ions or compounds usually disturbs the structure including distorting the surrounding protein structure and probably forcing some solvent out of the crystal, so isomorphism is never perfect. The isomorphous replacement method is based on the theory that the scattering by a derivative crystal, containing heavy atoms is the sum of the scattering by the parent crystal and the scattering by the added heavy atoms. It usually requires at least two derivatives to determine the phase angles (Blow 2002).

The multiple anomalous dispersion method, which was developed later, is now frequently used in phase determination. It provides extra phase information through the violation of Friedel's law. The integers h, k, and l are used to identify each of the diffracted waves forming the diffraction pattern. In the normal diffraction, a pair of

reflections *h*, *k*, *l* and –*h*, -*k*, -*l* have the same structure amplitude and the phases have the opposite sign. This is known as Friedel's law. But at a wavelength close to the absorption edge of an atom, the scattering violates the Friedel's law. The heavy atom structure factors F_H (*h*,*k*,*l*) and F_H (-*h*,-*k*,-*l*) have the same magnitudes, but they do not have the opposite phases. The anomalous scattering method is based on the idea that the total scattering by the structure is the sum of the normal scattering and the anomalous scattering. But the anomalous scattering has the opposite effects on Friedel-related reflections. Phase information can be obtained from measurement of the total scattering for each member of the Friedel pair (Blow 2002). Anomalous scattering effects are smaller than those obtained by isomorphous replacement, but the measurement is more accurate because the diffraction data was collected on the same crystal. Useful anomalous scatters can be far lighter than the heavy atoms used for macromolecular isomorphous replacement. From iron (Z = 26) to palladium (Z = 46) the *K* absorption edges are at convenient wavelengths. The K absorption of selenium (Z = 34) at 0.98 Å is easily accessible in synchrotron radiation. Selenomethionine has similar chemical properties to methionine and similar shape and volume. Cohen and Cowie first discovered that the *E.coli* strain, which is auxotrophic for methionine, can grow in the medium containing selenomethionine (Cowie 1957). Later, Hendrickson and co-workers found that selenium is a very useful anomalous scatterer and they solved the structures of selenobiotyl streptavidin (Hendrickson 1989) and of selenomethionyl proteins (Yang 1990).

The Molecular replacement method determines the orientation and position of a molecule in the unit cell using an existing solved structure as a search model. The search

and the target molecule must have reasonable sequence identities (>>25%) for this to succeed. Generally there are two steps in this method known as rotation and translation function (Blow 2002).

Model building is the next step where the electron density map is interpreted in terms of a set of atomic coordinates. It is very straightforward in the case of molecular replacement because many atoms have been positioned. However, in the case of the multiple isomorphous replacement and multiple wavelength dispersion methods, we simply have the electron density map. Normally, a protein backbone will be fit into the density first and then the side chains of protein will be inserted based on the protein sequence. The amount of the detail depends on the resolution and the quality of the phases. Often the regions of high flexibility are not visible at all due to disorder. Automated procedures using software such as ArpWarp (Lamzin 1993) to fit maps are successful for data at higher resolutions (usually < 2 Å).

After we obtain a model from an electron density map and have interpreted it, the next task of improving the interpretation is structural refinement, in which the atomic model is adjusted to improve the agreement with the measured diffraction data. In structural refinement, the measurement of discrepancy between the X-ray structure factors calculated for the model structure $|F_{cal}|$ and the observed intensities $|F_{obs}|$ is defined as an R factor:

$$R = \frac{\sum_h \left\| F_{obs} \right| - \left| F_{cal} \right\|}{\sum_h \left| F_{obs} \right|} \qquad (1)$$

The purpose of structure refinement is to get the lowest R factor consistent with correct geometry and interpretation of the electron density maps.

Structure-based protein engineering

Many proteins, especially enzymes, become therapeutic and commercial targets. Most of the time, enzymes isolated from organisms do not fulfill the specific demands of their therapeutic uses and industrial applications. To improve the properties of proteins or enzymes for different purposes, protein engineering concepts have been developed. Two main approaches, directed evolution and rational design, are utilized in protein engineering (Svendsen 2004; Zhao 2004).

Directed evolution has emerged as a powerful approach for improving enzyme properties and has been widely used in engineering many enzymes (Farinas 2001; Altamirano 2002). Proteins in nature have evolved to perform specific biological tasks through selective pressures. They are generally not optimized for nonnatural applications. For instance, as potential chemical catalysts, they often are not stable, have low specificity or low catalytic efficiency. Similarly, as potential therapeutic agents, natural proteins often have low efficiency and low stability. As a result, naturally occurring proteins have to be tailored in the laboratory to increase specificity and stability. Structure-based rational design does not always result in success due to our limited knowledge of protein folding, structure, function and dynamics. In comparison, directed evolution does not always require any structural information and can often solve a protein design problem in a short time. Sometimes, directed evolution can provide unexpected

solutions for protein design problems. Random mutation and gene recombination are two natural evolutionary processes that have been mimicked by directed evolution (Zhao 2004). Random mutations can be classified into four types: substitution, deletion, insertion, and inversion. Gene recombination is a reassortment of a series of nucleotides along a nucleic acid molecule, usually double-stranded DNA. The main differences between random mutagenesis and gene recombination are elucidated as follows: Random mutation starts from a single gene and creates a library of variants containing point mutations or insertion/deletions. Whereas gene recombination usually starts from a pool of variants from a single gene or a pool of closed related parent genes of different origins and creates an exchange of sequence information among parent genes (Zhao 2004). Random mutagenesis by point mutation is the simplest way to create mutations. Effective methods to introduce point mutations include chemical mutagens (Myers 1985), UV radiation (Botstein 1985), mutator strains (Greener 1997), or error prone PCR (Leung 1989; Rice 1992). Among these methods, error prone PCR, introducing point mutations based on inaccurate copying by DNA polymerase, is the most widely used method. Random mutagenesis by insertion/deletion is another effective method to introduce molecular diversity. Unlike point mutation, random mutagenesis by insertion or deletion will alter the full length of the target gene. In contrast to random mutagenesis, gene recombination is a "sexual" evolutionary process. Several approaches, both *in vitro* and *in vivo*, have been developed to mimic nature's recombination strategy. Usually *in vitro* recombination offers higher recombination efficiency than *in vivo* approaches. DNA shuffling starts from a pool of parent genes, which are first fragmented and then

reassembled into full-length products by repeated cycles of overlap extension reaction. Recombination occurs when fragments derived from parent genes prime each another (Zhao 2004). Several other *in vitro* recombination approaches such as the staggered extension process (StEP) method (Zhao 1998), random chimeragenesis on transient template (RACHITT) (Coco 2001), family shuffling (Crameri 1998), degenerate oligonucleotide gene shuffling (DOGS) (Gibbs 2001), sequence homologous-independent protein recombination (SHIPREC) (Sieber 2001), and exon shuffling (Kolkman 2001) are widely used (Svendsen 2004).

The alternative approach for protein engineering is structure-based rational design. With the advent of structural genomics and the concomitant growth of PDB (Protein Data Bank) (Berman 2000), it has become more likely that a protein engineer will know the structure of their target protein or its homologs. The basic idea of rational design is as follows: although there are many interactions that control the folding of a protein or catalysis of a chemical reaction, a 3-D structure alone or in combination with additional information, such as the biochemical and biophysical properties of a protein or the structure of a homologous protein, together with understanding how the enzymes work, will give ideas on how to improve selected protein properties (Lehmann 2004). Many catalytic properties of an enzyme including pH activity profile, the specific activity, the substrate specificity or enantioselectivity have been engineered to meet the specific needs. To improve any of those properties by rational design, a high resolution protein structure in complex with an inhibitor, a substrate or a product of the enzyme reaction is generally required. If the protein-ligand complex structure is not available,

computer modeling is an alternative way to model a substrate or a product into the active site and provides ideas about which amino acids are important for substrate binding, stabilizing the transition state of the reaction and for catalysis of the reaction (Svendsen 2004).

Est30 and Est55

Est30 and Est55 are two carboxylesterases isolated from *Geobacillus stearothermophilus* (Ewis 2004). Est30 is a thermostable enzyme with optimal activity for short chain acyl derivatives of length C4-C8 at a temperature of 70°C. Est30 showed low sequence identity with the closest members in the eight previously classified families of microbial carboxylesterases (Arpigny 1999). Therefore, Est30 represents a new carboxylesterase family that includes enzymes from several pathogenic Gram-positive bacteria. Est55 belongs to the microbial carboxylesterase Family VII. Sequence alignment by BLAST (Basic Local Alignment Search Tool) (Altschul 1997) shows that Est55 shares 32% identity and 48% similarity with rabbit carboxylesterase, which is considered most efficient enzyme so far for activating prodrug CPT-11 (Danks 1999). Est55 also showed higher enzymatic activity than rCE towards the same *p*-nitrophenyl esters, which have a similar molecular diameter as CPT-11.

In this work, we describe studies of the structure, reaction mechanism, and medical application of Est30 and Est55. The first chapter describes the structure determination of carboxylesterase Est30 at 1.63 Å resolution using multiple anomalous dispersion data. Est30 represents a new microbial carboxylesterase family. A 100 Da

tetrahedral ligand was observed to be covalently bound to the side chain of catalytic residue Ser94. This tetrahedral ligand was deduced to be propyl acetate, and represents the first tetrahedral intermediate in the reaction mechanism. Therefore, this Est30 crystal structure will help understand the mode of action of all enzymes in the serine hydrolase superfamily. In the second chapter, the main focus is on the structure and reaction mechanism study of carboxylesterase Est55. The Est55 structure was determined by the molecular replacement method at 1.58 Å. An oxidized Cys408 was observed in one of loops located in the active site of Est55 structure. This loop can mimic an "inhibitor" to block the active site of Est55. Mutational analysis was used to explore the role of Cys408 in the Est55 enzymatic activity toward *p*-nitrophenyl substrates. The third chapter describes the potential applications of Est30 and Est55 in cancer therapy.

CHAPTER 2

Crystal Structure and Reaction Mechanism of A Thermostable Carboxylesterase Est30 from *Geobacillus stearothermophilus*

CONTENTS

I. INTRODUCTION

Carboxylesterases are ubiquitous enzymes with important physiological, industrial and medical roles in the synthesis and hydrolysis of stereospecific compounds, including the metabolic processing of drugs, and antimicrobial agents (Krish 1971; Takayama 1998; Bornscheuer 2002). Carboxylesterases (carboxylic ester hydrolase, EC 3.1.1.1) are members of the α/β hydrolase family. They hydrolyze short chain aliphatic and aromatic esters and are inhibited by low concentrations of organophosphorus compounds (Krish 1971). The biochemical properties and industrial applications of microbial carboxylesterases have been reviewed recently by Bornscheuer (Bornscheuer 2002). Carboxylesterases exhibit high regio- and stereospecificity, require no cofactor in the reaction, and are stable and active in organic solvents (Moher 1989; Bornemann 1992; Margolin 1993). The hydrolysis reaction is believed to proceed through several steps including formation and dissociation of two tetrahedral intermediates (Satoh 1998).

Microbial carboxylesterases have been classified into eight families based on their sequences (Arpigny 1999). However, the molecular structures are known for only a few bacterial carboxylesterases. Crystal structures are available for two members of the hormone-sensitive lipase (HSL) family (Family IV), (De Simone 2000; De Simone 2001) and one carboxylesterase from the Family VI (Kim 1997). These structures have a typical α/β hydrolase fold (Ollis 1992; Heikinheimo 1999; Nardini 1999) with a central parallel-stranded β sheet surrounded by α helices on both sides. The enzymes contain the same catalytic triad (Ser-Asp-His), with the serine located in a sharp turn between a β strand

and α helix that is known as the nucleophile elbow. The major structural differences are in the conformation of the substrate binding pockets.

The esterase gene *est30* was recently isolated from the genomic library of the Gram-positive bacterium *Geobacillus stearothermophilus* and cloned and expressed in *E. coli* (Ewis 2004). The *est30* gene encodes 247 amino acids with a calculated molecular mass of 28257 Da. Est30 was shown to be active as a dimer with optimal activity for short chain acyl derivatives of length C4-C8 at a temperature of 70°C. Est30 showed no more than 21% sequence identity with the closest members in the eight previously classified families of microbial carboxylesterases (Arpigny 1999). Therefore, Est30 represents a new carboxylesterase family that includes enzymes from several pathogenic Gram-positive bacteria. This chapter describes the crystallization and preliminary diffraction data for Est30 (Liu 2003) and the crystal structure of Est30 with a covalent ligand that represents a trapped reaction intermediate (Liu 2004). This structure will help to understand the reaction mechanism for this widespread class of enzymes.

II. MATERIALS AND METHODS

Expression and purification of recombinant Est30

The coding sequence of *est*30 amplified by PCR was cloned into the pBAD-HisA vector (Invitrogen) and the resulting recombinant plasmid was designated pHE30. *Escherichia coli* Top10 (Invitrogen) harboring pHE30 was induced for 4 h by 1 m*M* arabinose in 1 liter culture and then harvested at 5000 *g* for 15 min at 277 K. The cell pellet was suspended in 40 ml of hypertonic solution consisting of 20 m*M* Tris-HCl pH 7.5, 2.5 m*M* EDTA and 20% sucrose. The suspension was incubated on ice for 30 min and vortexed every 10 min. Cells were removed by centrifugation at 13 000 *g* for 20 min at 277 K and the cell pellet was resuspended in 60 ml of 20 *mM* Tris-HCl pH 7.5, 2.5 m*M* EDTA (hypotonic solution) and further incubated on ice for 30 min with intermittent vortexing every 10 min. Cells were removed by high-speed centrifugation at 22 000 *g* for 20 min at 277 K and the supernatant applied to a Pharmacia Q-Sepharose Hiload 26/10 HP that was equilibrated with 50 m*M* Tris-HCl pH 8.0. The column was washed with 150 ml of the equilibration buffer to remove unbound proteins, followed by a linear gradient to 50 m*M* Tris-HCl pH 8.0 and 1 *M* KCl. The esterase peak eluted at 0.65 *M* KCl. Fractions containing esterase activity were pooled (32 ml), concentrated to 5 ml by ultrafiltration and applied to a Sephacryl S 200 HR column (Pharmacia, 26/60). The enzyme was eluted using 50 m*M* potassium phosphate pH 7.0 and 0.15 *M* NaCl.

The selenomethionine Est30 derivative (SeMet-Est30) was prepared following the same protocol with some modifications. *E. coli* top 10 cells carrying the recombinant

clone pHE30 were grown in M9 medium with 19 amino acids (40 µg/ml final concentration) and selenomethionine (60 µg/ml final concentration) using glycerol as a carbon source. SeMet-Est30 was purified under reduced conditions in order to avoid oxidation of the selenium by adding 10-20 mM DTT to the purification buffers and storing the protein under vacuum in each purification step.

Mass spectrometry

An electrospray-quadrupole/time-of-flight spectrometer (Waters Micromass Q-TOF^{TM} micro, Waters Corporation, Milford, Massachustts, USA) was used to carry out the mass spectrometric experiments in a positive mode. Nitrogen supplied by a nitrogen generator (Model 75-72, Parker Balston, Haverhill, MA, USA) was used as the cone gas at 50 L/hr, and as the drying gas heated to 150°C at a flow-rate of 450 L/min to evaporate solvents in the spray chamber. Argon was used as the collision gas. The voltage settings for the API electrospray interface were capillary, 2700 V; sample cone, 35 V; Extraction Cone, 0.5V. The source temperature was at 80 ^{o}C and the desolvation temperature was at 150 ^{o}C. The sample at 2.5 mg/ml was diluted 10 times with 50 % MeOH containing 0.1 % formic acid. All solutions were continuously infused by means of a syringe pump at a typical flow-rate of 5 µl min^{-1} into the electrospray probe. MassLynx (version 4.0) software was used for instrument control, data acquisition and processing.

Crystallization

Purified native and SeMet-Est30 were dialyzed into Tris buffer at pH 8.0 and were concentrated to 4.6 mg/ml and 2.5 mg/ml, respectively. Est30 was crystallized at

room temperature by hanging drop vapor diffusion at 24 ^{o}C using 1 μl of protein and 1 μl of mother liquor. Crystals were initially grown with 45-50 % ammonium sulfate pH 8.0, Tris pH 7.5-8.1 or HEPES pH 7.5, MPD 8-12 %, and 0.1 % sodium azide as described previously (Figure 2.1) (Liu 2003). During freezing it was found that the crystals dissolved in all tested cryoprotectants except for high concentration of lithium sulfate. These crystals showed disorder in the diffraction pattern; the spots were smeared and the mosaicity was very high (more than 0.6). Therefore, different growth conditions were tried. Finally, single native Est30 and SeMet-Est30 crystals were grown using lithium sulfate as the precipitant. The optimum conditions were 70 % lithium sulfate, 5 % PEG400, 5 % Dioxane, and 100 mM HEPES pH 7.5.

X-ray data collection

Crystals were mounted on a nylon loop and frozen directly in liquid nitrogen. X-ray diffraction data were collected on a MAR CCD 165 detector for SeMet-Est30 crystals and a MAR CCD 225 detector for native crystals at the SER-CAT beam line of the national synchrotron light source at the Advanced Photon Source. Selenium X-ray multiplewavelength anomalous diffraction (MAD) data with crystal to detector distance of 130 mm and oscillation angle of 0.5° were collected at four wavelengths: 0.9792 Å, (peak), 0.97933 Å (inflection point), and 0.971602 Å (high energy remote) and 0.987072 Å (low energy remote) (Table 1). Two 180° datasets of high and low resolution were collected from a native crystal.

Structure determination

The X-ray data were integrated using the HKL2000 program (Otwinowski 1997). The space group was orthorhombic $C222_1$ with cell dimensions of a = 55.476 Å, b = 58.474 Å and c = 179.163 Å, and contained one molecule per asymmetric unit. Phasing and automatic structure tracing were tried using the SOLVE/RESOLVE package (Terwilliger 1997; Terwilliger 2001) with scaled but unmerged data. Eight of the ten expected selenium sites were identified in residues 34, 74, 115, 119, 127, 153, 161, and 195 (except for the N-terminal residues 1 and 2) using the program SOLVE (Terwilliger 1997). RESOLVE was run to perform density modification and automated model building (Terwilliger 2001). The partial model from RESOLVE containing 7 α helices and 5 β strands was used as a starting point for automated model building and side chain docking by ARP/WARP (Lamzin 1993). 90% of the structure was automatically traced by ARP/WARP (Lamzin 1993). The subsequent manual building of one missing loop on the surface of structure was performed using the graphics program O (Jones 1991).

Model refinement

Crystallographic refinement was initially carried out using the CNS package. (Brunger 1998)Manual adjustments and rebuilding were performed using O and σA-weighted electron density maps. After simulated annealing and B-group refinement, the missing loop was built. Individual B factor refinement resulted in a model with R_{factor} = 24.0 % and R_{free} =26.5 %.

The crystal structure of the Se-Met Est30 was used to solve the native Est30 crystal structure by molecular replacement using AMoRe (Navaza 1994) The native crystal structure was refined in space group $C222_1$ with one molecule per asymmetric unit. SHELX 97 (Sheldrick 1997) was used to refine the structure with solvent and anisotropic temperature factors. During refinement, the F_o-F_c difference Fourier map showed positive electron density connecting with the catalytic residue Ser94, suggesting a covalent bond modification of the Ser94. Therefore, the density was modeled with a tetrahedral intermediate in the active site. The size of the intermediate was determined by mass spectrometry. The structure was analyzed with PROCHECK (Laskowski 1993)

Sequence analysis

Sequence similarity searches were performed using BLAST at (http://www.ncbi.nlm.nih.gov/BLAST) (Altschul 1997). Multiple sequence alignments used the CLUSTALX and GENEDOC programs (Nicholas 1997; Thompson 1997)

Structural analysis

The native and SeMet-Est30 crystal structures were superimposed on all Cα atoms using an implementation of the algorithm described in [Ferro & Hermans, (1977)] (Ferro 1977). The structures of Est30 and the carboxylesterase from *Pseudomonas fluorescens* were superimposed on all Cα atoms using the program ALIGN (Cohen 1997). Figures were generated with MolScript (Kraulis 1991) BobScript (Esnouf 1999) and Raster3D (Merritt 1997).

Protein Data Bank accession numbers

The coordinates have been deposited in the Protein Data Bank with accession code 1TQH.

III. RESULTS and Discussion

Crystallization

The recombinant Est30 from *G. stearothermophilus* was expressed and purified for crystallographic analysis. The total yield of pure esterase was 6 mg per liter of culture. The purified Est30 was judged to be in excess of 95% homogeneous. Crystals were grown by hanging-drop vapor diffusion using ammonium sulfate as precipitant. Under the optimal crystallization conditions, Est30 crystals appeared after 2 or 3 d and reached maximum dimensions of 0.6 × 0.15 × 0.05 mm after one week. An example is shown in Figure 2.1. The crystallographic statistics are summarized in Table 2.1. The crystals diffracted to better than 2.0 A resolution. X-ray diffraction data were reduced in space group $C222_1$, with unit-cell parameters a = 55.83, b = 58.15, c = 179.65 A. R_{merge} was 0.038 for 17,449 independent reflections with a completeness of 85.1%. V_M was calculated to be 2.43 A^3 Da^{-1} (Matthews 1968) and the solvent content was 0.49, which suggested that there was one molecule of Est30 in the asymmetric unit. However, crystallographic diffraction of crystals grown from this crystallization condition showed high mosaicity (Figure 2.2A), which is not suitable for phase determination using either isomorphous replacement or multiple anomalous dispersion method. Different crystallization conditions were tried and finally high quality diffraction data were obtained from both native and SeMet-Est30 crystals grown from lithium sulfate (Figure 2.2B).

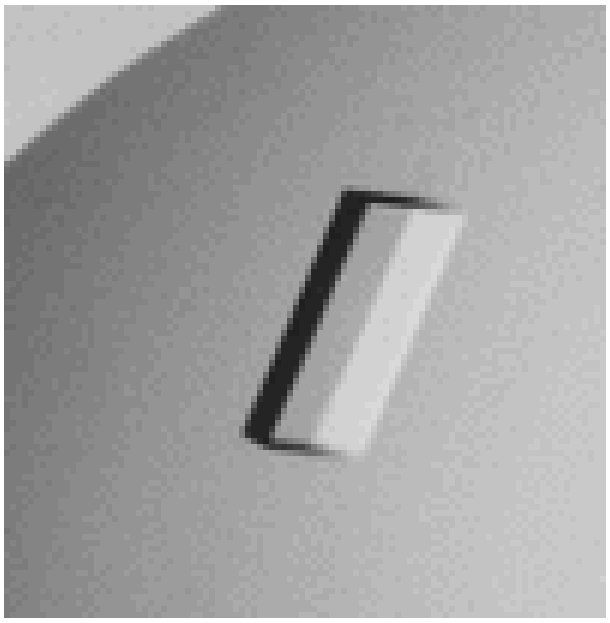

Figure 2.1 Crystal of Est30 grown in 50% ammonium sulfate, 10% MPD, 0.1% sodium azide, 100 m*M* HEPES pH 7.5 at room temperature. The size of this crystal is approximately 0.3 × 0.17 × 0.05 mm.

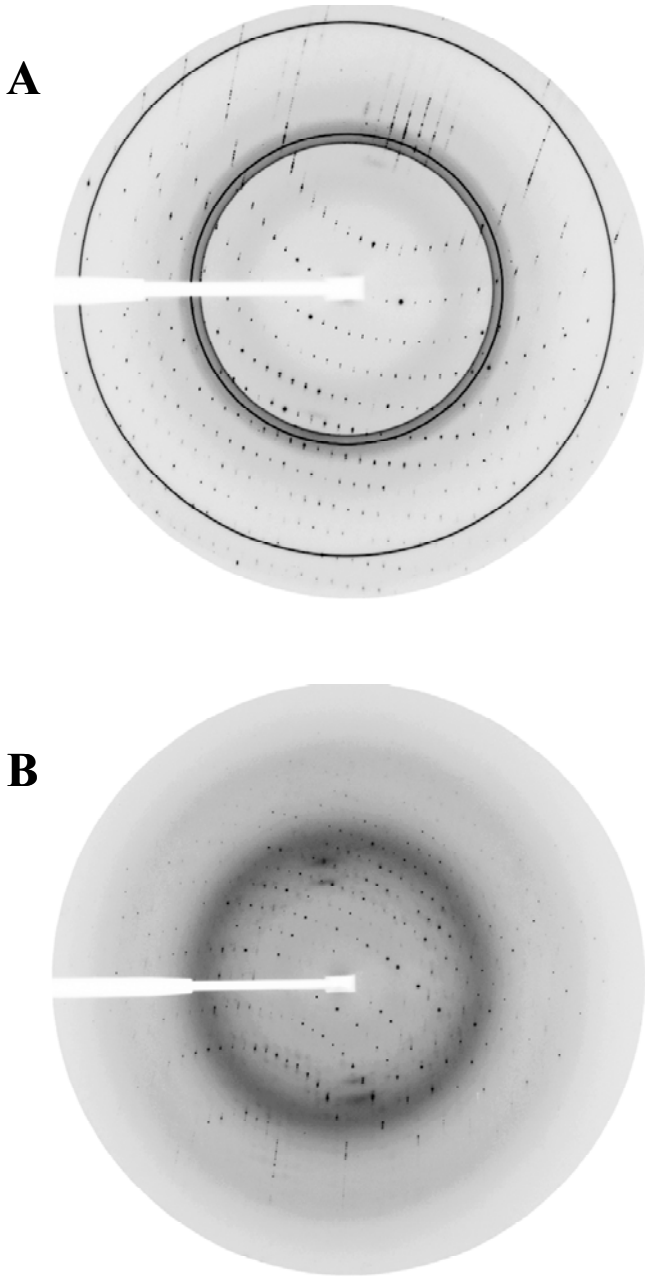

Figure 2.2 Diffraction pattern of Est30 crystals. Crystallographic diffraction of crystals grown from ammonium sulfate as precipitate (A) and lithium sulfate as precipitate (B).

Table 2.1 Data collection statistics of crystals grown from ammonium sulfate as precipitant

Space group	$C222_1$
Resolution Å	1.99 (2.07-1.99)
Unit-cell parameters Å	a = 55.83, b = 58.15, c = 179.65
No. reflections with $I > 3\ \sigma(I)$	16997 (1182)
$\langle I/\sigma(I) \rangle$	19.4 (7.6)
Independent reflections	17449 (1388)
R_{merge} [#]	0.038 (0.112)
Completeness %	85.1 (69.4)
Redundancy	4.8 (2.2)

[#] $R_{merge} = \sum |I - \langle I \rangle| / \sum I$.

Overall structure

The Est30 structure could not be solved by molecular replacement owing to the lack of an available structure with homologous protein sequence. Multiple isomorphous data or anomalous dispersion data were needed to obtain phase information. Halide soaks were not successful. However, Est30 has two cysteine and ten methionine residues. Therefore, SeMet-enriched protein was prepared for phase determination using the multiple wavelength anomalous diffraction (MAD) method. The native Est30 crystal structure was solved in space group $C222_1$ using multiple anomalous dispersion (MAD) phasing and automated tracing, and refined to an R-factor of 17.1% at 1.63 Å resolution. The crystallographic statistics for data collection and refinement are shown in Tables 2.2 and 2.3. No density was visible for the N-terminal five residues. The Est30 structure includes residues 6-247 with a covalent ligand on Ser94, as described later. The side chains of residues Leu35, The114, Met127, Lys165, Met195, Glu207 and Glu220 were modeled with alternate conformations. The solvent density was fit with two sulfate ions and 153 water molecules (including full and half occupancy sites).

Est30 folds into two domains with the catalytic triad and substrate-binding site located at the interface between the domains (Figure 2.3). The smaller domain consists of three α helices B_1', D_1' and D_2' that form a cap over the active site. The larger domain resembles the classical α/β hydrolase fold.(Ollis 1992) It contains a central seven-stranded β-sheet surrounded by six α-helices, αA (Ala30-Ser41), αB (Pro66-Asn82), αC (Leu95-Gly104), αD (Leu164-Leu180), αE (Ser200-Glu207) and αF (Lys231-Ser244).

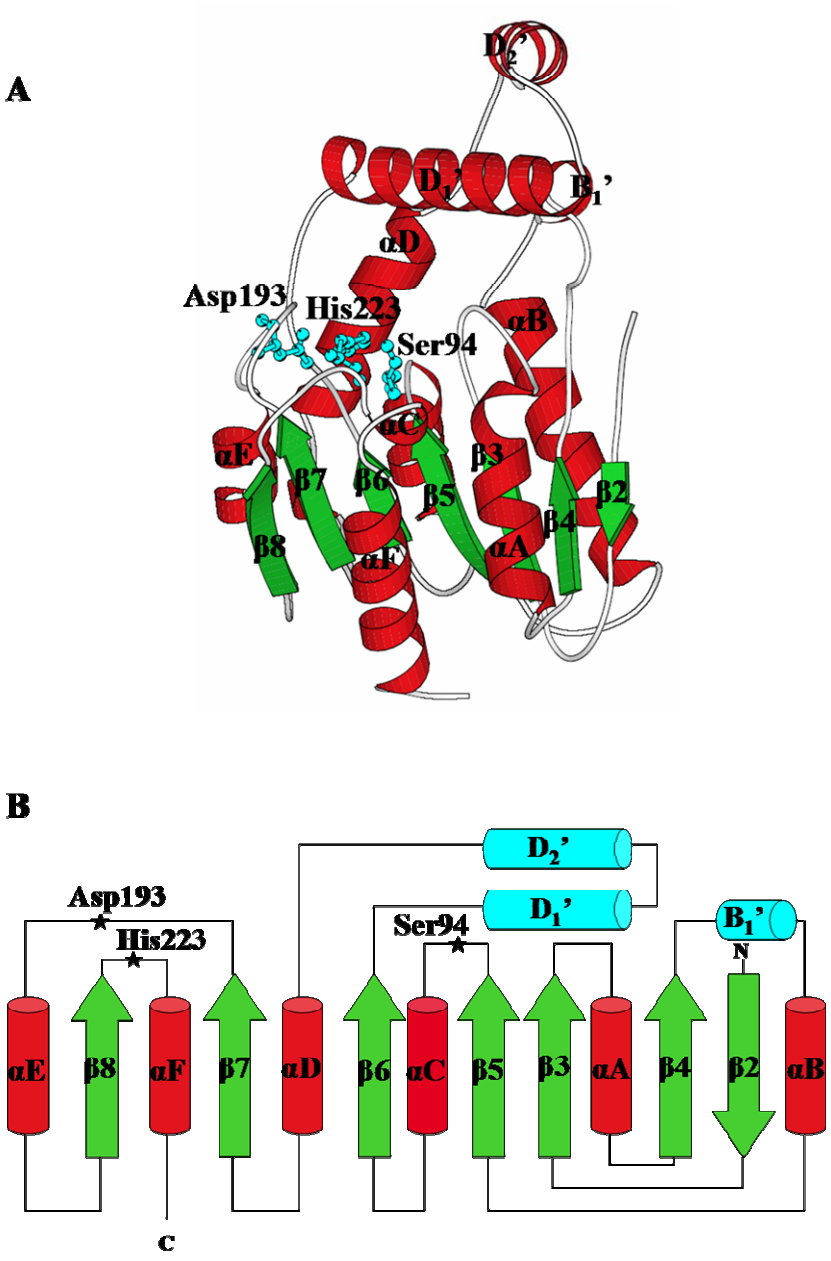

Figure 2.3. (a) Overall structure of carboxylesterase Est30. Six α-helices A–F (red), and seven β-strands 2–8 (green) are labeled using the nomenclature for the classical α/β hydrolase fold(Ollis 1992), and the three cap helices are labeled B′$_1$, D′$_1$ and D′$_2$. The catalytic residues Ser94, Asp193, and His223 (cyan) are shown in ball and stick representation. **(b) Topology diagram of Est30**. The secondary structure is indicated as in (a); β-strands are shown as arrows, α-helices are presented as cylinders. The cap (cyan) is composed of three helices unlike the typical α/β hydrolases. The catalytic triad residues Ser94, Asp193, and His223 are indicated by black stars.

Table 2.2 Data collection statistics of crystals grown from lithium sulfate as precipitant

	MAD Data				Native
	Peak	Inflection point	High energy remote	Low energy remote	
Wavelength Å	0.97920	0.97933	0.971602	0.987072	0.9997
Resolution (last shell) Å	50-2.0 (2.3-2.0)	50-2.05 (2.09-2.05)	50-2.0 (2.03-2.0)	50-2.4 (2.49-2.4)	50-1.63 (1.69-1.63)
R_{merge} (last shell)	0.09 (0.37)	0.09 (0.39))	0.07 (0.36)	0.06 (0.29)	0.16 (0.18)
Unique Reflections	20147	18778	20175	11571	35555
Redundancy	7.0	6.8	6.8	4.4	6.2
Completeness (last shell) %	100 (100)	99.9 (100)	99.8 (99.6)	96.0 (83.4)	97.5 (90.5)
$\langle I/\sigma \rangle$	12.1	12.9	14.6	13.3	14.3

Table 2.3 Crystallographic Refinement Statistics

Resolution range (Å) (last shell)	10-1.63 (1.70-1.63)
R_{factor} /R_{free}	17.14 / 22.79
No. residues	242
No. water molecules	153
No. sulfates	2
rms deviation from ideality	
Bond length (Å)	0.008
Bond angles (deg.)	0.024
Ramachandran plot	
Most favored regions (%)	92.4
Additional allowed regions (%)	7.6
Averaged B-values (Å^2)	
Main chain atoms	23.4
Side chain atoms	28.1
Covalent ligand atoms	31.7
Solvent atoms	35.1
All atoms	26.5

The β-sheet of the typical α/β hydrolase fold consists of eight strands with the second β strand antiparallel to the others. However, the first β strand of the typical α/β hydrolase fold is missing from the Est30 structure. Therefore, the β-sheet of Est30 only has seven strands (β2 - β8) with the N-terminal β2 strand antiparallel to the others.

The Est30 structure also differs from the classical α/β hydrolases in the presence of the smaller cap domain comprising three helices. The existence of the cap has been reported in the structures of carboxylesterases from the thermophile *Alicyclobacillus acidocaldarius* and from archaeon *Archaeoglobus fulgidus* (De Simone 2000; De Simone 2001). However, the cap in Est30 lies mainly near the N-terminal end of the central β sheet instead of near the C-terminal end of the β sheet as is observed in the other two carboxylesterases. Also, the cap in the archaeon carboxylesterase is composed of 5 α helices (De Simone 2001) instead of the three helices in Est30. Therefore, the cap structure of Est30 is different from those of the other known bacterial carboxylesterase structures.

Catalytic triad

The three dimensional structure of Est30 shows that the catalytic triad consists of Ser94, Asp193, and His223 (Figure 2.4). Ser94 is in the conserved sequence Gly-X-Ser-X-Gly.(Brenner 1988) All three catalytic residues are located on the top of the C-terminal β sheet. Ser94 is positioned at a sharp turn between β5 and helix αC that is called the nucleophile elbow. The main chain φ and ψ angles of Ser94 are outside the favored regions of Ramachandran plot (φ =57.7, ψ = -120.9), which is common for the

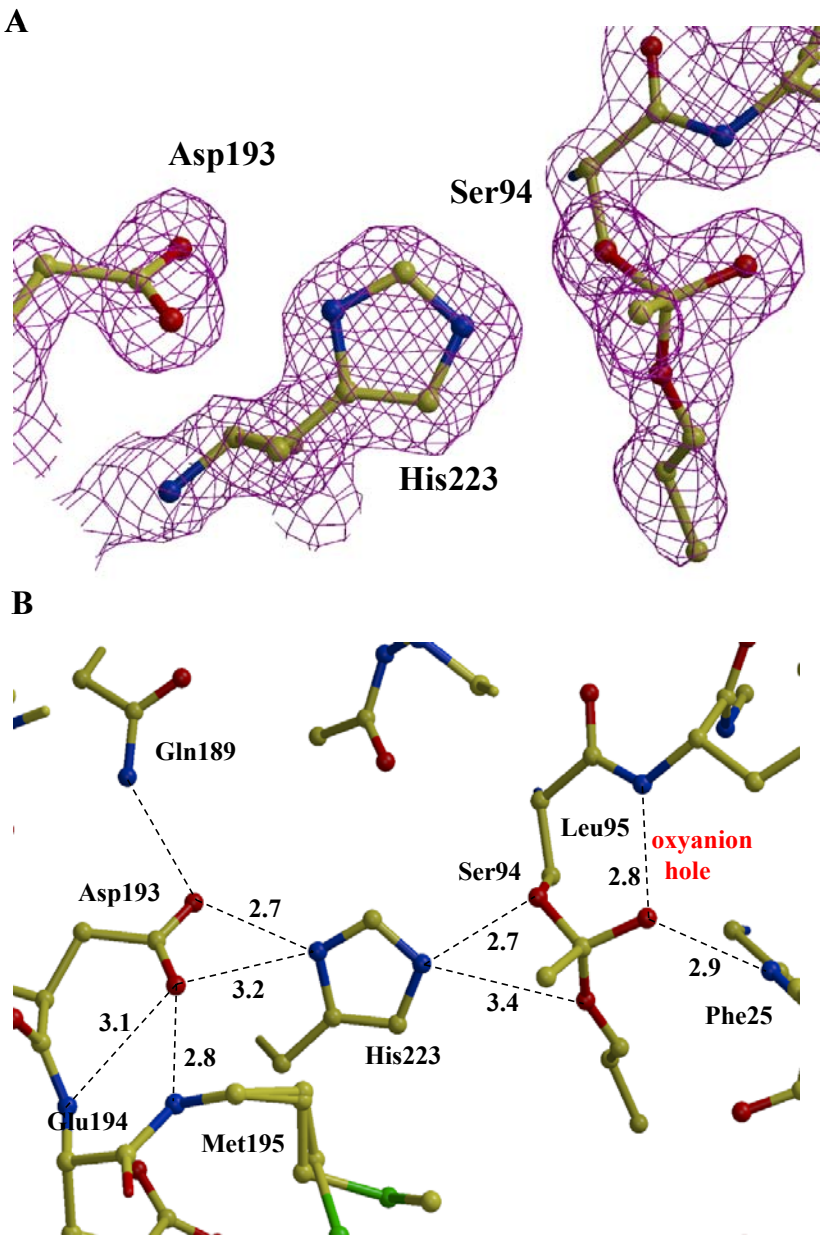

Figure 2.4 The active site region of Est30. (a) $2F_o-F_c$ electron density map contoured at 1.6σ. (b) Interacting residues. Interatomic interactions are shown in broken lines with distances in Å. The negative charge of the oxygen atom of the tetrahedral intermediate and the NH groups of Leu95 and Phe25 form an oxyanion hole (labeled in red).

nucleophile in α/β hydrolases (Nardini 1999). The conformation of Ser94 is stabilized by hydrogen bond interaction of the hydroxyl group with the side chain of His223. Asp193 and His223 are positioned at loops between β7 and αE and β8 and αF, respectively. A network of hydrogen bonds stabilizes the side chains of Asp193 and His223 (Figure 2.4B). The OD1 atom of Asp193 has hydrogen bond interactions with ND1 in His223 and the NE2 atom in Gln189. The OD2 atom in Asp193 has hydrogen bond interactions with ND1 of the His223 side chain, and the amides of Glu194, Met195 and Ile196. Similar hydrogen bond networks are observed in the catalytic triad structures of other carboxylesterases (Kim 1997).

Est30 Contains a Tetrahedral Reaction Intermediate

Unexpectedly, extra density was observed near the side chain of Ser94 (Figure 2.5). This density indicated that a tetrahedral ligand was covalently bound to the side chain of Ser94. The existence of a covalent ligand was confirmed by mass spectrometry. The Est30 sample was 28356 Da, or 99 Da more than the calculated protein mass. Two tetrahedral intermediates are formed during the esterase reaction. The reaction mechanism is considered to proceed through several steps as shown in Figure 2.6 (Bornemann 1992; Hakulinen 2000). Initially, the hydroxyl of the active Ser94 binds to the substrate forming the first tetrahedral intermediate. The negative charge of the oxygen atom of the intermediate is stabilized by hydrogen bond interactions in the oxyanion hole. Then, the alcohol product is released and the acyl-enzyme complex is formed. His223 stabilizes the nucleophile oxygen of water, which attacks the carbonyl carbon of the

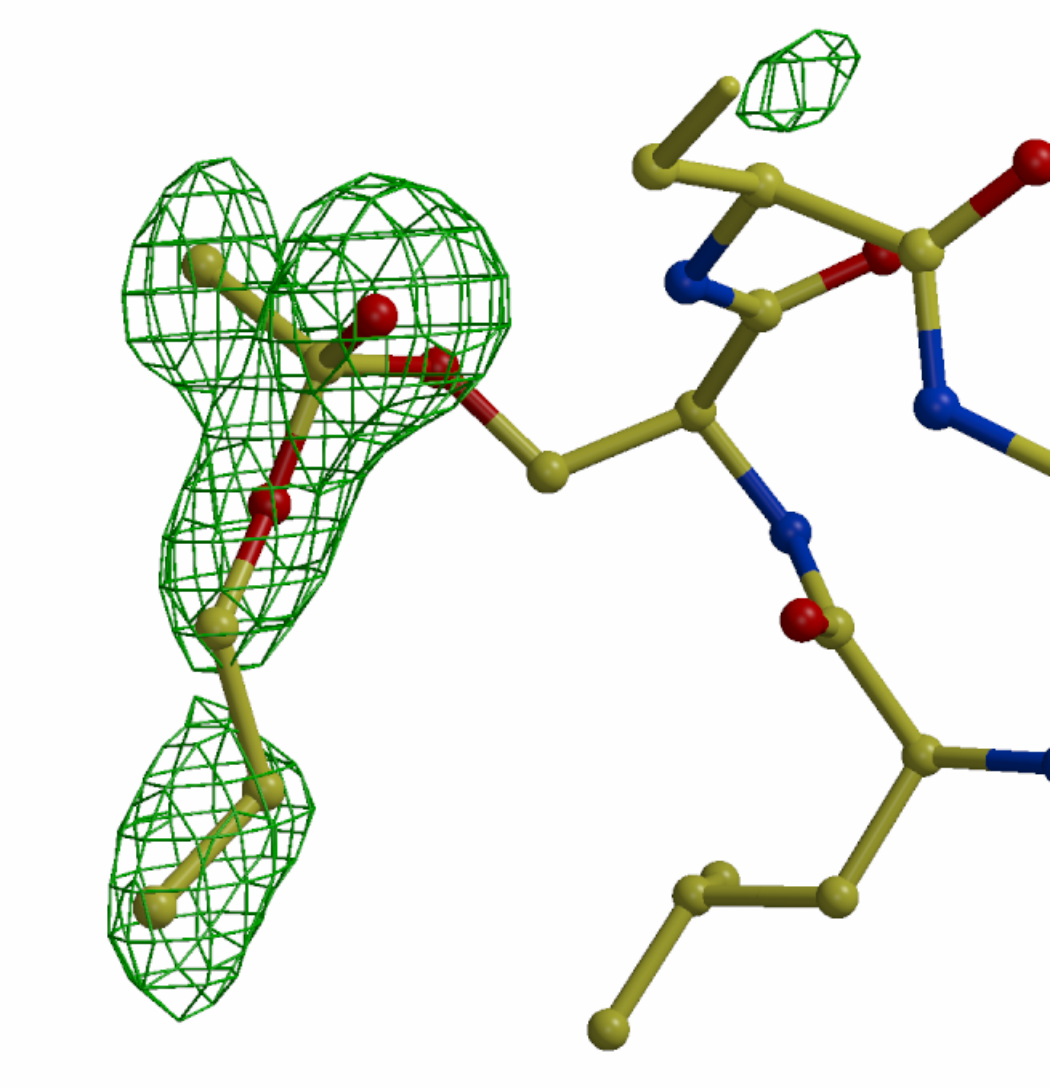

Figure 2.5 Covalent ligand. Omit F_o-F_c electron density map contoured at 2.5σ.

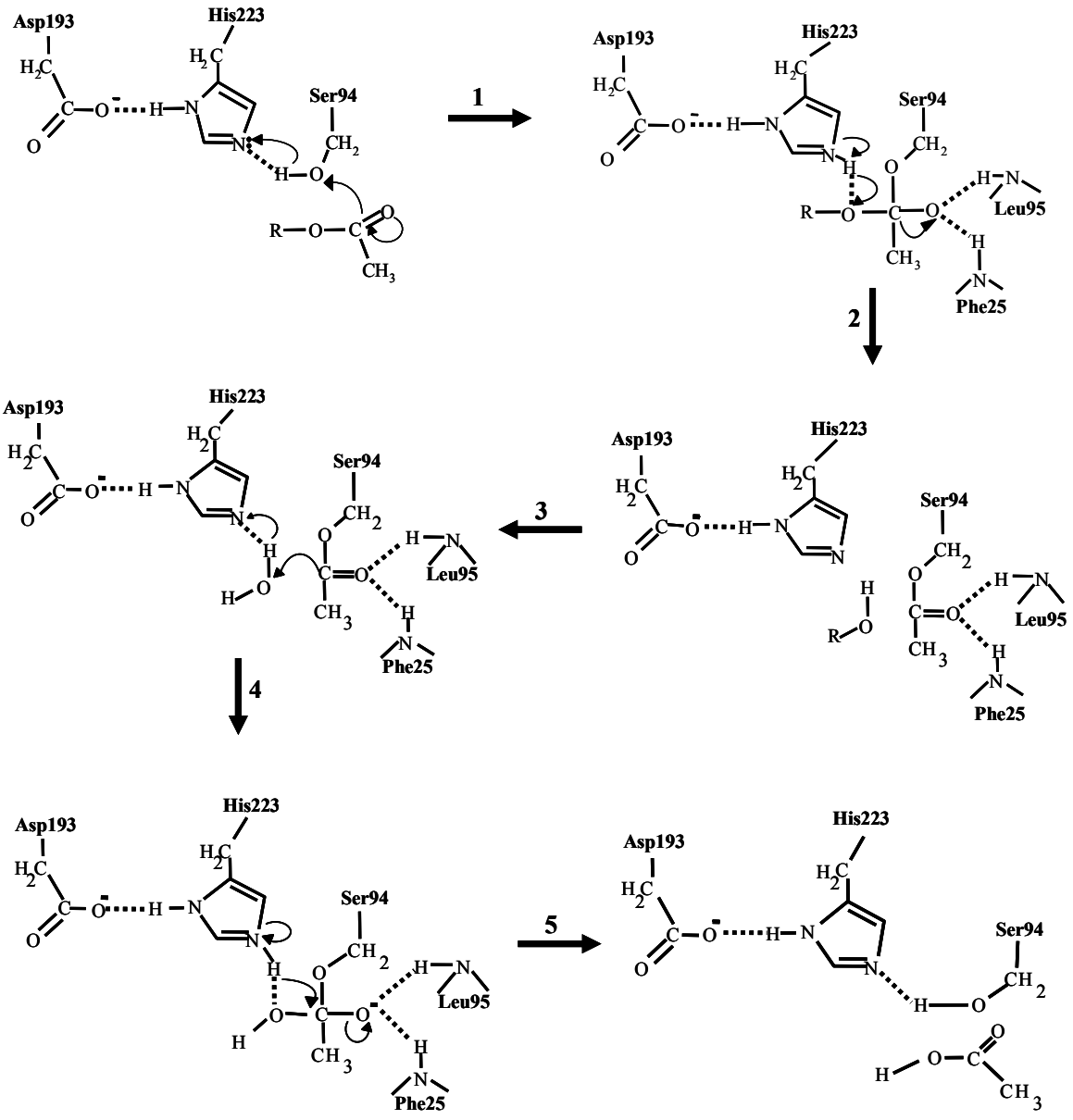

Figure 2.6 Possible reaction mechanism (Satoh 1998). Six intermediates in the Est30 reaction are shown. The reaction proceeds through the following steps. (1) Nucleophilic attack to form the first tetrahedral intermediate. (2) Formation of the acyl–enzyme complex. (3) Release of the alcohol product. (4) Nucleophilic attack forming the second tetrahedral intermediate. (5) Release of carboxylate product.

acetyl group of the substrate to form a second tetrahedral intermediate. Finally, the carboxylate product is released from Ser94.

The two possible tetrahedral intermediates (Figure 2.6) of about 100 Da were evaluated. Geometrical constraints and the X-ray data were consistent with the presence of propyl acetate (101 Da) as the first tetrahedral reaction intermediate with the R group of CH2-CH2-CH3. The omit map for the tetrahedral intermediate is shown in Figure 2.5. The tetrahedral carbon, the three oxygens and the methyl carbon atoms were well defined with atomic B factors similar to those of the protein atoms. Switching the positions of the oxygen and methyl group resulted in difference density at the atoms, which confirmed the geometry. The B factors increased along the flexible propyl group to give an average for the ligand atoms of 31.7 $Å^2$. The intermediate is stabilized by hydrogen bond interactions with the amides of Phe25 and Leu95 in the oxyanion hole and with a water molecule, as shown in Figure 2.4. The stable existence of the trapped tetrahedral intermediate suggests that its dissociation is the rate limiting step for Est30. Consequently, the Est30 complex provides important geometrical details for the reaction mechanism.

Est30 showed hydrolysis activity in the temperature range of 40-70 °C (Ewis 2004). Therefore, the reaction intermediate appears to have been trapped when the temperature was reduced during the Est30 reaction at a higher temperature. No acyl esters were added during protein expression, purification or crystallization. Hence, the substrate is presumed to have bound during the expression in *E. coli*. At the 37 °C used for bacterial growth the Est30 activity is 34 % of its maximum at 70 °C (Ewis 2004). Therefore, it is possible that the reaction commenced during bacterial expression and the

tetrahedral intermediate was trapped when the cells were harvested at 4 °C. Subsequent purification and crystallization of Est30 occurred at room temperature, where the enzyme activity is only 7 % of the maximum activity.

Substrate binding pocket

The putative substrate-binding cavity extends on both sides of Ser94 in a cleft between the cap and the larger hydrolase domain. The propyl alcohol side of the substrate lies within a larger, more exposed groove between the cap and the larger domain. The groove extends to approximately 10-14 Å from Ser94 and could fit a longer, more polar ligand. The groove is formed by hydrophobic side chains of Leu93, Val224 and Leu227 on one side, Gly24, Gly27 and the side chain of Asp31 at the base, and by the polar side chains of Glu133, Tyr134, Glu137 and Arg141 from the cap on the other side. The ligand atoms have van der Waals contacts with Gly24, Gly27, and Val224.

The acetate product would fit in a less exposed hydrophobic pocket of approximately 8 Å wide and 8-10 Å long, consistent with the observed activity on acyl chain derivatives of length C2-C12 (Ewis 2004). This pocket is formed by the loops of residues 23-29, 191-199, 219-224, and helices αD and D_2'. The hydrophobic side chains comprising this pocket are Phe25, Thr26, Trp69, Leu95, Val98, Phe99, Pro118, Ile121, Met127, Val131, Leu167, Leu170, Ile171, Met195, and Ile196. The side chains of Met127 and Met195 showed two alternative conformations. Because Met195 is located about 3.8 Å from the side chain of His223 (Figure 2.4) these two conformations might have a role in substrate binding.

Subunit interactions in the dimer

Est30 is catalytically active as a dimer in solution (Ewis 2004) The Est30 homodimer can be constructed from the 2-fold crystallographic symmetry. The residues 211 to 219 of the two C-terminal β8 strands lie antiparallel at the interface between two subunits. Residues Asn202, Tyr205, Asn206 located on helix αE and Arg191 on strand β7 also contribute to stabilizing the intermolecular packing. The side chains of several residues are involved in intersubunit hydrogen bond interactions. There are intersubunit hydrogen bonds of the side chains of Tyr205 with Asn202 and Trp217, the side chain of Gln214 with the side chain of Glu219 and with the carbonyl oxygen and amide of Trp217, the side chain of Arg191 with the carbonyl oxygen of Lys213. The dimeric arrangement is similar to that of the carboxylesterase from the achaeon *Archaeoglobus fulgidus* (De Simone 2001).

Comparison with Est30-HEPES Complex

Subsequent to solution of this Est30 structure the crystal structure of an inhibited form of the Est30 dimer was deposited in the protein databank (PDB entry 1R1D) (Cuff). This structure shows seleno-methionine-Est30 with 4-(2-hydroxyethyl)-1-piperazine ethane sulfonic acid (HEPES) bound in the active site. The Est30-HEPES structure was compared to the Est30-reaction intermediate structure. The two structures superimposed with a root mean square difference of 0.33 Å on Cα atoms. Most of the residues forming the substrate-binding site are in nearly identical positions in both structures, except for the side chains of Leu95 and Lys122. The side chain of Lys122 has moved to interact

with the carbonyl oxygen of SeMet195, and the Leu95 side chain has moved away to allow a water molecule to interact with the HEPES sulfate. Both the HEPES and the tetrahedral intermediate interact with His223 (Figure 2.7). However, there was a small change in position of the catalytic His223 (0.5 Å for Cα atom). The hydrogen bond interaction between the side chains of His223 and Ser94 is 3.1 Å in the Est30-HEPES structure and 2.7 Å in the Est30-tetrahedral intermediate complex, concurrent with the small change in position of His223. The HEPES formed a hydrogen bond interaction with Ser94 rather than the covalent linkage of the tetrahedral intermediate. This comparison suggests that the HEPES is bound approximately in the position of the released alcohol product.

Comparison of Est30 with other microbial carboxylesterases

The most interesting structural difference between the Est30 and the typical α/β hydrolases is the presence of three helices forming a second small domain on the top of the larger domain. This smaller domain forms a cap over the active site. The presence of the cap has been reported in the structures of carboxylesterases from the thermophile *Alicyclobacillus acidocaldarius* and from archaeon *Archaeoglobus fulgidus* (De Simone 2000; De Simone 2001) However, the cap in Est30 covers mainly the N-terminal end of the central β sheet instead of the C-terminal end of the β sheet as observed in the other two carboxylesterases. Another difference is that the cap in the carboxylesterase from achaeon *Archaeoglobus fulgidus* is composed of 5 α helices (De Simone 2001) instead of three in Est30. Therefore, the Est30 cap structure differs from those of the other known.

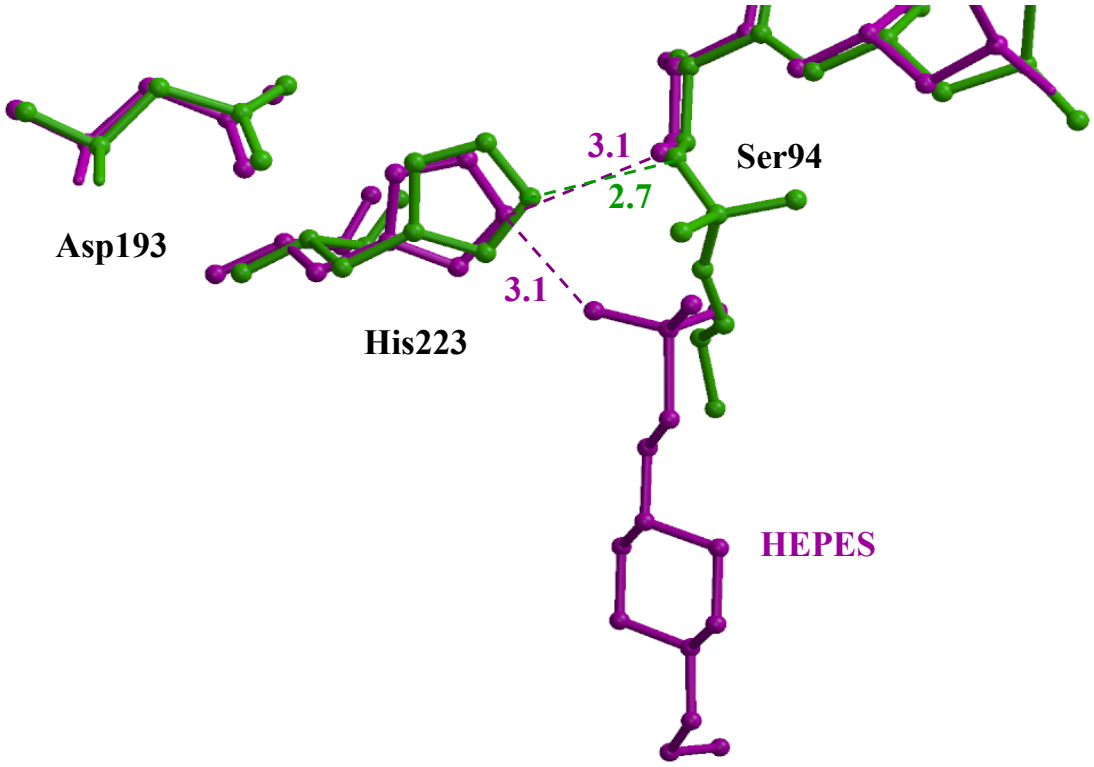

Figure 2.7 Comparison of Est30 complex with covalent ligand (green) and Est30-HEPES complex (1R1D) (red). Hydrogen bond interactions with His223 are shown in dashed lines.

bacterial carboxylesterase structures. The cap is adjacent to the active site of the enzyme and forms part of the substrate binding pocket. Therefore, the different cap structures might contribute to the different substrate specificities.

The carboxylesterase from *Pseudomonas fluorescens* is the most similar structurally to Est30 (Figure 2.8), although the two proteins share very low sequence identity (18.3%) (Kim 1997). Both proteins have seven β strands surrounded by six α helices in the larger domain. Est30 has a relatively large cap, consisting of the small B_1' helix and the two large helices D_1' and D_2', that lies over the N-terminal strands of the central β sheet. However, the carboxylesterase from *P. fluorescens* forms a smaller cap consisting of a winding loop and two β strands after β4 that covers the C-terminal strands of the β sheet. Superimposing these two structures after removing the cap gave a RMSD value of 1.75 Å, which indicates that the typical α/β hydrolase fold is conserved among bacterial species. Both enzymes share a similar active-site cleft formed by six loops at the C-terminal ends of the parallel β strands. The *P. fluorescens* carboxylesterase is active on acyl chains from C2 to C10 in length, compared to C2 to C12 for Est30. These differences in substrate specificity are consistent with the presence of a more open substrate-binding site in Est30, as well as differences in the cap structures.

The catalytic triad displays virtually indistinguishable geometry in both enzymes. The RMSD values for the residues of the catalytic triad (Ser94/Asp193/His223 in Est30 and Ser114/Asp168/His199 in *P. fluorescens*) are 0.88 Å, 0.94 Å and 1.32 Å, respectively. Also, *P. fluorescens* has similar interactions between catalytic triad residues to those in Est30. The OD1 and OD2 atoms in Asp168 have hydrogen bond interactions

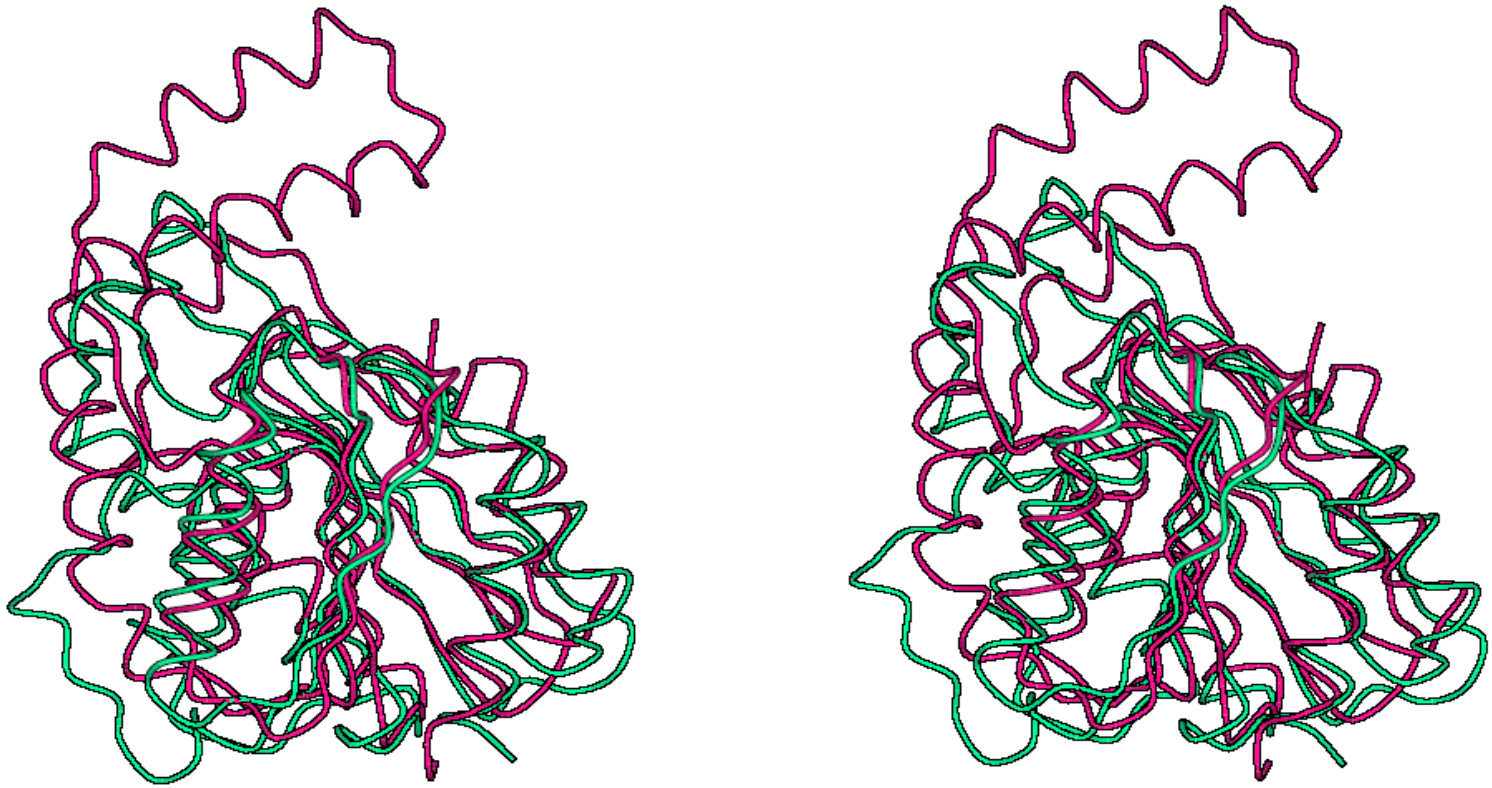

Figure 2.8 Superposition of Est30 and closest other esterase structure from *P. fluorescens* (1AUO) in a stereoview. Est30 is colored in red and 1AUO is colored in green.

with ND1 atom in His199. The distance between the Ser114 OG atom and the NE atom of His199 (2.76 Å) of *P. fluorescens* is similar to that between the corresponding residues in Est30 (2.72 Å), which suggests that the interactions among the catalytic triplet residues are highly conserved among the carboxylesterases.

The Est30 sequence was compared to the sequences of members of the related enzyme families. Microbial lipases and carboxylesterases have been classified into eight families based on their sequences (Arpigny 1999). The differences between the carboxylesterases and lipases lie mainly in their substrate specificity. Carboxylesterases hydrolyze at least partly soluble small ester-containing molecules, while true lipases work on water-insoluble long chain fatty acids. Est30 was identified as a carboxylesterase because it has maximal activity towards short chain acyl derivatives of length C6, decreased activity towards the longer C8 to C12 derivatives, and undetectable activity towards C14 and C18 chains (Ewis 2004). Est30 is closest to family VI enzymes in the classification of Arpigny (Arpigny 1999). This family of enzymes has molecular weight in the range 23-26 kDa and the active form is a dimer. Est30 is also active as a dimer with the higher molecular weight of 30 kDa for a monomer. The family VI enzymes, like Est30, have no activity towards long-chain triglycerides. The family VI enzymes show a classical α/β hydrolase fold unlike the modified fold with a seven-stranded β sheet observed for Est30. Moreover, Est30 showed only 10-21% sequence identity with family VI members. Most significantly, Est30 has none of the conserved sequence motifs observed for this family (Arpigny 1999). Instead, Est30 has high sequence identity (76-97%) with carboxylesterases in other Gram-positive strains, such as *Bacillus subtilis*,

Bacillus cereus, and *Bacillus anthracis* (Figure 2.9) (Kunst 1997; Read 2002; Ivanova 2003). This analysis suggests that Est30 is a member of a new enzyme family. The sequence similarities suggest that all members of this family have a similar tertiary structure, including the 3-helix cap of Est30. The hydrophobic specificity pocket for substrate consists of mostly identical residues in the family members, except for two residues indicated on helix D_1' and one on αD (Figure 2.9). The residues in D_1' are Met127 and Val131 in Est30, but the equivalent positions have Val or Leu, and Ile or Phe, respectively, in the other enzymes. Leu167 of Est30 is substituted by Val in the esterase from *O. iheyensis*. These differences in the hydrophobic side chains may alter the substrate specificity.

The crystal structure of Est30 provides fundamental insights into the reaction mechanism and substrate specificity of this new family of carboxylesterases. Moreover, the detailed geometry of the tetrahedral intermediate will help understand the mode of action of the broad category of physiologically important enzymes in the serine hydrolase superfamily. The Est30 structural data will be valuable for design of new transition-state analog inhibitors for a wide variety of processes catalyzed by these enzymes.

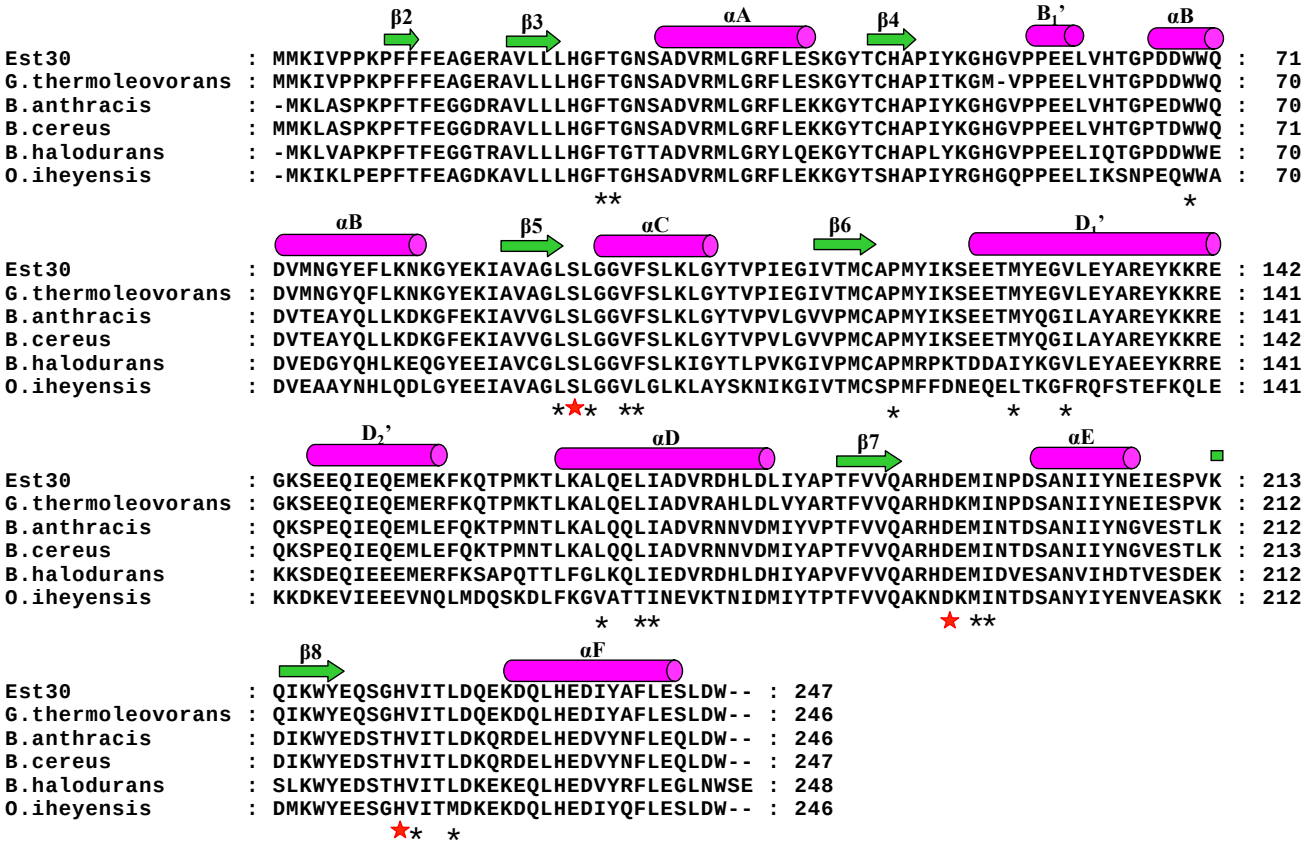

Figure 2.9 Sequence alignment of Est30 and related proteins. Est30 showed 76-97% sequence identity with carboxylesterases from *Geobacillus thermoleovorans, Bacillus anthracis, Bacillus cereus*, *Bacillus halodurans*, and *Oceanbacillus iheyensis*. The secondary structure of Est30 is indicated by green arrows for beta strands, and red cylinders for alpha helices. The catalytic triad residues (Ser94, Asp193, and His223 in Est30) are indicated by large red asterisks. The residues forming the hydrophobic specificity pocket are indicated by small black asterisks. These residues are Phe25, Thr26, Trp69, Leu93, Leu95, Val98, Phe99, Pro118, Met127, V131, Leu167, Leu170, Ile171, Met195, Ile196, Val224 and Leul227 in Est30.

CHAPTER 3

Crystal Structure and Reaction Mechanism of A thermostable Carboxylesterase Est55 from *Geobaccilus stearothermophilus*

CONTENTS

I. INTRODUCTION

Carboxylesterases are important enzymes in the hydrolysis and detoxification of numerous peptides and drugs. Carboxylesterase-mediated hydrolysis of esters has been used to design several ester-containing drugs including the development of chemotherapeutic agents CPT-11 (Senter 1996; Kojima 1998), and 10-hydroxycampothecin fatty acid esters (Takayama 1998) and the drug lovastatin for the activation of the blood cholesterol (Tang 1995). Carboxylesterases are also essential in the hydrolysis of cocaine, heroin, aspirin, procaline and meperidine (Lotti 1983; Joly 1986; Brzezinski 1997; Pindel 1997). It is therefore important to study the catalytic mechanism responsible for carboxylesterase induced hydrolysis.

Bacterial lipolytic enzymes have been classified into eight families based on their sequence identities and enzyme properties (Arpigny 1999). Family VII consists of rather large number of bacterial esterases with a molecular weight of 55 kDa that share about 30-40% sequence identity. This group of enzymes is widely utilized in several industrial applications. For example, *B. subtilis* carboxylesterase was found to efficiently hydrolyze *p*-nitrobenzyl esters, which makes it valuable in the final removal of the *p*-nitrobenzyl group used as a protecting group in synthesis of the *β*-lactam antibiotic. Interestingly, this group of enzymes is also homologous to mammalian carboxylesterases that are involved in hydrolysis and detoxification of numerous peptides and drugs and in prodrug activation. Therefore, enzymes in this family can be used as models to study the reaction mechanism of the related mammalian carboxylesterases.

The esterase gene *est55* was recently isolated from the genomic library of the Gram-positive bacterium *Geobacillus stearothermophilus* and cloned and expressed in *E. coli* (Ewis 2004). The *est55* gene encodes 498 amino acids with a calculated molecular mass of 54867 Da. Est55 is active as a monomer with optimal activity for short chain acyl derivatives of length C4-C6 at a temperature of 60 °C. Est55 belongs to microbial family VII and shares homology with mammalian carboxylesterases. Est55 shares 32 % sequence identity with human liver carboxylesterase 1 (hCE1) and 31 % rabbit liver carboxylesterase (rCE). We hypothesized that Est55 could be used as a model system to study the catalytic mechanism responsible for mammalian carboxylesterase induced hydrolysis. In this chapter, the crystal structure of Est55 was determined and mutational analysis was used to explore the role of C408 in the Est55 enzymatic activity toward *p*-nitrophenyl substrates. This work will help to design a new generation of prodrugs and pharmaceuticals or to select a new carboxylesterase for prodrug activation or detoxification of compounds.

II. MATERIALS and METHODS

Site-directed mutagenesis

Random mutations of C408 were generated by the Quick-Change mutagenesis kit (Stratagene) using the following degenerate primers: CYS408_f (5'-GCTGAAAGCANNNCACGCGCTCGAGCTGCCGTTTGTG-3') and CYS408_r (5'-CGAGCGCGTGNNNTGCTTTCAGCTGGCCGCCGAACAC-3'). 20 ng of plasmid encoding the *est55* gene were mixed with two degenerate primers and 2.5U of *pfu*Turbo DNA polymerase, followed by 20 cycles of denaturing, annealing and extension using a thermal cycler. The reaction mixture was digested by 10 U of *Dpn* I enzyme at 37 °C for 1h and then transformed into the expression host *E. coli* Top 10 cells. The mutations were confirmed by DNA sequencing.

Expression and purification of recombinant Est55

Est55 and the Cys408 mutants were expressed and purified to homogeneity as described previously (Ewis 2004). Briefly, the enzyme was expressed using *E. coli* Top 10 cells carrying the recombinant clone pHE55. The wild type Est55 and the mutants were purified in two steps, ionic exchange using high-load Q-Sepharose HR 26/10 (Pharmacia) and gel filtration using Sephacryl S200 (HR26/60).

Carboxylesterase assay

The esterase activity of the wild type and the mutant enzymes was measured as described with modification (Ewis 2004). *p*-nitrophenyl butyrate was used as the substrate. The reaction mixture (2 ml) contained 10 mM Tris HCl (pH 8.5) and 0.5 mM substrate. The amount of *p*-nitrophenol liberated during the reaction was monitored continuously at 405 nm in a Carey 3E spectrophotometer (Varian) with a temperature control module. One unit of activity was defined as the amount of enzyme that releases 1 μmol of *p*-nitrophenol/min at 37 °C. The molar extinction coefficient of *p*-nitrophenol is 18,380 M^{-1} cm^{-1} at 405 nm. The protein concentration was measured by the Bradford method (Bradford 1976) with bovine serum albumin as the standard.

Crystallization

Purified Est55 was dialyzed into Tris-HCl buffer at pH 8.0 and concentrated to 7-10 mg/ml. Est55 was crystallized by hanging drop vapor diffusion at 24 °C using 1 μl of protein and 1 μl of mother liquor**.** Crystallization trials used the Hampton PEG/ION screen. Crystals grew after 7-15 days with 20 % w/v Polyethylene Glycol 3350, 0.2 M Ammonium Iodide pH 6.2, or 0.2 M Potassium Iodide pH 6.8.

X-ray data collection

Crystals were mounted on a nylon loop and cryo-protected in 20 % (v/v) PEG400 before flash cooling in liquid nitrogen. X-ray diffraction data were collected on a MAR CCD 225 detector at the SER-CAT beamline of the Advanced Photon Source (APS) at

the Argonne National Laboratory. The crystal-to-detector distance was 142 mm. The oscillation angle was 0.25° and the rotation range was 180° for the complete dataset. X-ray diffraction data for the crystals grown at pH 6.8 and pH 6.2 were measured to 1.58 Å and 2.02 Å resolution, respectively.

Structure determination

The X-ray data were integrated using the HKL2000 program (Otwinowski 1997). The structure of Est55 at pH 6.8 (Est-pH6.8) was determined by molecular replacement with the CNS package (Brunger 1998). The structure of Pnb esterase (1QE3) from *Bacillus subtilis* was used as a search model (40 % sequence identity) (Spiller 1999). Data between 15 and 4 Å were used in the rotation research, resulting in one peak. The rotation solution was then applied in a translation search, yielding a distinct solution with a correction coefficient of 0.20. After rigid body refinement (CNS) and density modification using the phase probability distribution calculated from the model and the experimental amplitudes and solvent flipping, the figures-of-merit improved to 0.82. The Est55-pH6.2 structure was determined by molecular replacement with the Est55-pH6.8 structure using the program MolRep (Vagin 1997) in CCP4i (Potterton 2003).

Model refinement

Crystallographic refinement of the Est55-pH6.8 structure was initially carried out using the CNS package (Brunger 1998). The manual building of missing residues of structure was performed using the graphics program O (Jones 1991). After iteratively

subjecting the model to several rounds of stimulated annealing and B-group refinement with CNS and manual rebuilding, the R_{factor} and R_{free} dropped to 26.4 % and 28.5 %, respectively. After manual building of the missing residues, SHELX 97 (Sheldrick 1997) was used to refine the Est55-pH6.8 structure with solvent and isotropic temperature factors. Crystallographic refinement of the Est55-pH6.2 structure was carried out using CNS. The final R_{factor} and R_{free} were 20.0 % and 23.0 %, respectively.

Structural analysis

The Est55 crystal structures at different pHs were superimposed on all Cα atoms using an implementation of the algorithm described in [Ferro & Hermans, (1977)] (Ferro 1977). The structures of Est55 and the rabbit carboxylesterase were superimposed on all Cα atoms using the program ALIGN (Cohen 1997). Figures were generated with MolScript (Kraulis 1991), BobScript (Esnouf 1999) and Raster3D (Merritt 1997).

III. RESULTS AND DISCUSSION

Crystal structures of Est55

Est55 was crystallized under two different conditions in the presence of the iodine ion. An example is shown in Figure 3.1. Crystals with similar morphology were obtained from conditions with different pHs. Est55 was crystallized in 20% PEG3350, 0.2 M Ammonium Iodine (pH 6.2), or 20% PEG3350, 0.2 M Potassium Iodine (pH 6.8). The higher the pH, the longer the crystals took to grow. The crystallographic statistics for data collection and refinement are shown in Table 3.1. Both of the Est55 crystal structures were observed in the space group $P2_12_12_1$ with one molecule per asymmetric unit. The structures were solved by molecular replacement using Pnb esterase (1QE3) as a search model(Spiller 1999). The pH 6.2 structure (Est55-pH6.2) was refined to an R-factor of 20.0 % at 2.02 Å resolution. The pH 6.8 structure (Est55-pH6.8) was refined to R-factor of 17.2 % at 1.58 Å resolution. The higher resolution structure of Est55-pH6.8 had more disorder than the lower resolution structure of Est55-pH6.2. 479 and 463 residues of 498 amino acids of the Est55 structure were positioned in the pH 6.2 and pH 6.8 structures, respectively. Two residues at both termini were not visible in the electron density maps. Residues were not visible in one or two surface loops and before His409 of the catalytic triad. Residues 66-76 in a surface loop and 401-404 near the catalytic His were not visible in Est55-pH6.2. In Est55-pH6.8 the disordered residues were located in the two surface loops of residue 66-79, 349-358 and 401-407. Cys408 is oxidized with three oxygen atoms in Est55-pH6.2 (The detail will be described later).

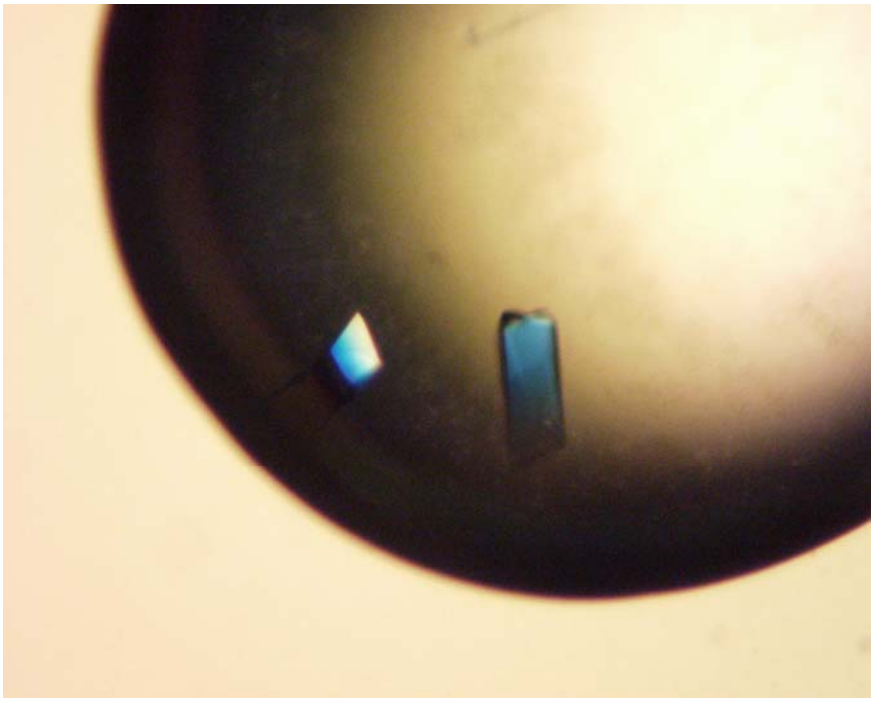

Figure 3.1 Crystals of Est55 grown after a few days using hanging drop vapor diffusion method.

.

Table 3.1 Crystallographic data collection and refinement statistics for the Est55 crystal structures.

	Est55-pH6.2	Est55-pH6.8
Data collection		
Space group	$P2_12_12_1$	$P2_12_12_1$
Unit cell Å	a=69.529, b=73.485, c=99.034	a = 69.361 Å, b = 74.430 Å, c = 98.606 Å
Unique reflections	67530	71770
R_{merge} (last shell)	0.07 (0.5)	0.08 (0.4)
Redundancy	5.3	5.1
Completeness (last shell) %	99.1 (95.6)	97.8 (91.5)
$\langle I/\sigma \rangle$	17.6	17.5
Refinement		
Resolution Å	10-2.02	10-1.58
R_{factor} /R_{free} %	20.0/23.0	17.2/23.7
No. residues	479	463
No. water molecules	151	159
No. Iodine atoms	3	1
rms deviation from ideality		
Bond length (Å)	0.006	0.018
Bond angles	1.3[a]	0.028[b]
Ramachandran plot		
Most favored regions (%)	89.3	89.4
Additional allowed	10.2	10.1
Averaged B-values (Å^2)		
Main chain atoms	35.4	27.9
Side chain atoms	39.4	33.5
Solvent atoms	36.1	39.4

[a] degree [b] angle distances

Est55 is folded into three domains, a catalytic domain, an α/β domain and a regulatory domain (Figure 3.2). The catalytic domain shows the typical α/β hydrolase fold, with a central antiparallel β sheet surrounded by α helices. The two structures of Est55-pH6.2 and Est55-pH6.8 superimposed with a RMSD value of 0.2 Å for Cα atoms, which indicated that there were no significant conformation changes in the overall structure. The Est55 structure was similar to that of rabbit carboxylesterase (rCE) (Bencharit 2003) (PDB entry 1K4Y) with an RMSD of 1.32 Å over 379 Cα atoms, although the regulatory domains showed significant differences (Figure 3.3).

Iodine in the Est55 structure

Iodine was present during crystallization. Three iodine atoms were identified in the Est55-pH6.2 structure, and one iodine in the Est55-pH6.8 structure (Figure 3.4). One iodine binding site was conserved in both structures with 0.65 occupancy in the Est55-pH6.2 structure and 0.34 occupancy in the Est55-pH6.8 structure, respectively. The iodine atom was identified by the very high level of electron density, even in the 2Fo-Fc map contoured at 10σ level, as shown in Fig 4a. The iodine had a potential hydrogen bond interaction with the amide of Asp309 and van der Waals interactions with the hydrophobic side chains of Phe488, Val372, and Thr367 and Arg393. Two other iodines were observed in the Est55-pH6.2 structure. One iodine atom with 0.65 occupancy was located near the active site and had hydrogen bond interactions with amides of Ala407 and Cys408, the carbonyl oxygen of Cys408 and two water molecules. It formed van der Waals interactions with the side chains of Phe112, Lys406, Cys408 and the main chain of

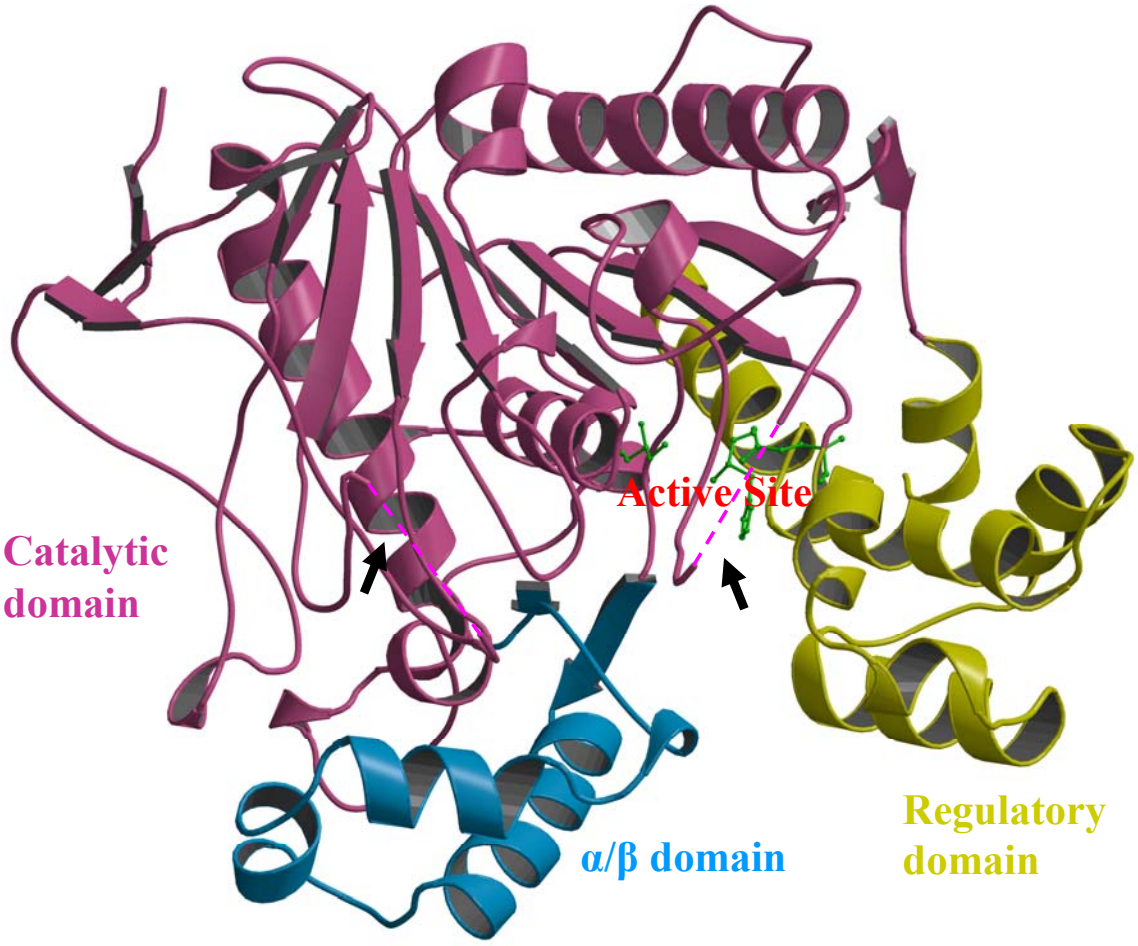

Figure 3.2 Overall structure of carboxylesterase Est55 comprising three domains. The catalytic domain is in magenta, the α/β domain is in blue and the regulatory domain is in yellow. The catalytic residues Ser194, Glu310, and His409 are shown in green ball and stick representation. Black arrows point to two missing loops in the Est55-pH6.2 structure, which are indicated by the dashed lines.

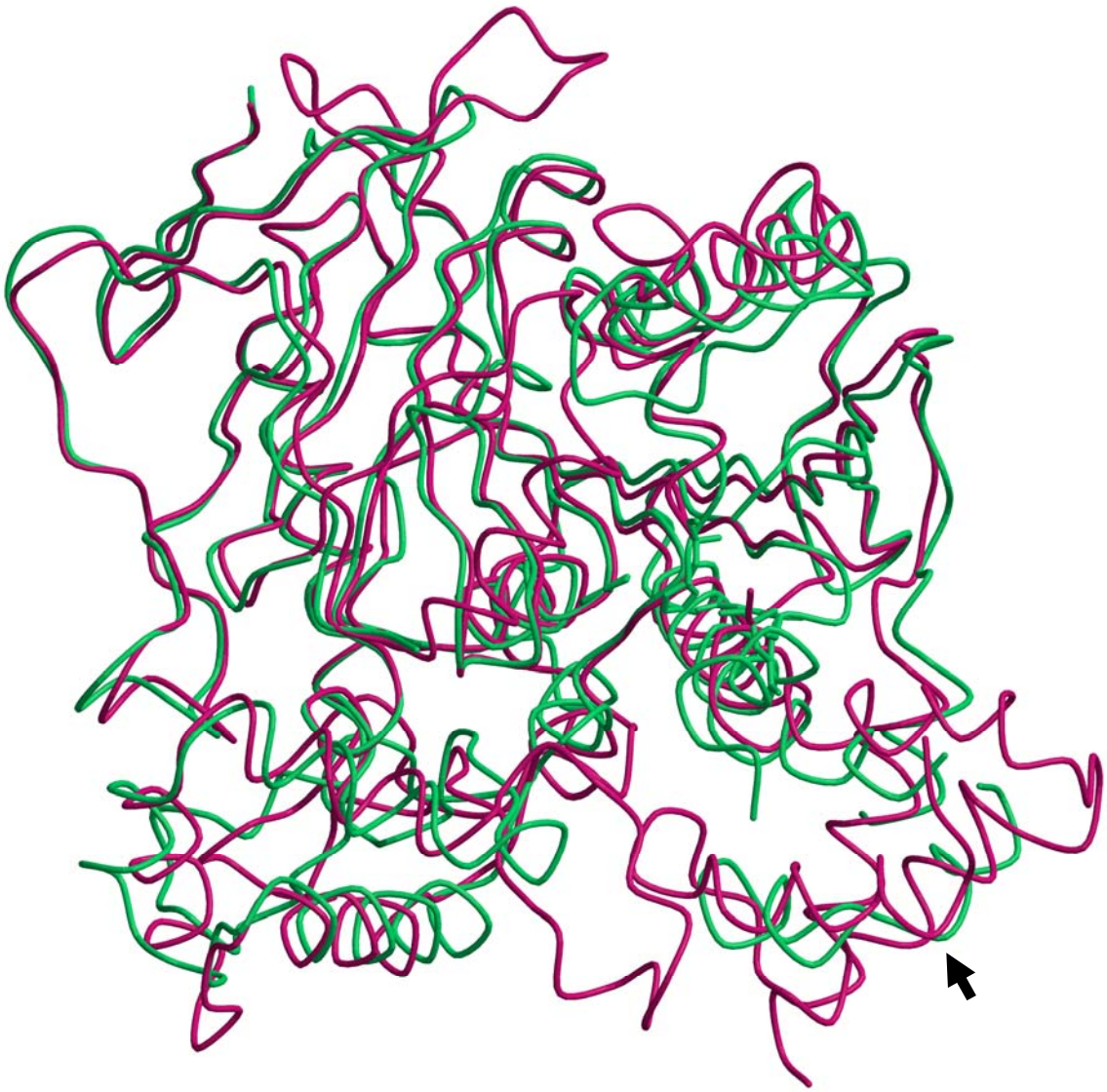

Figure 3.3 Superposition of Est55 and rabbit carboxylesterase (1K4Y) structures. Est55 is colored green and 1K4Y is colored red. The black arrow indicates the regulatory domain, which shows significant difference in the two structures.

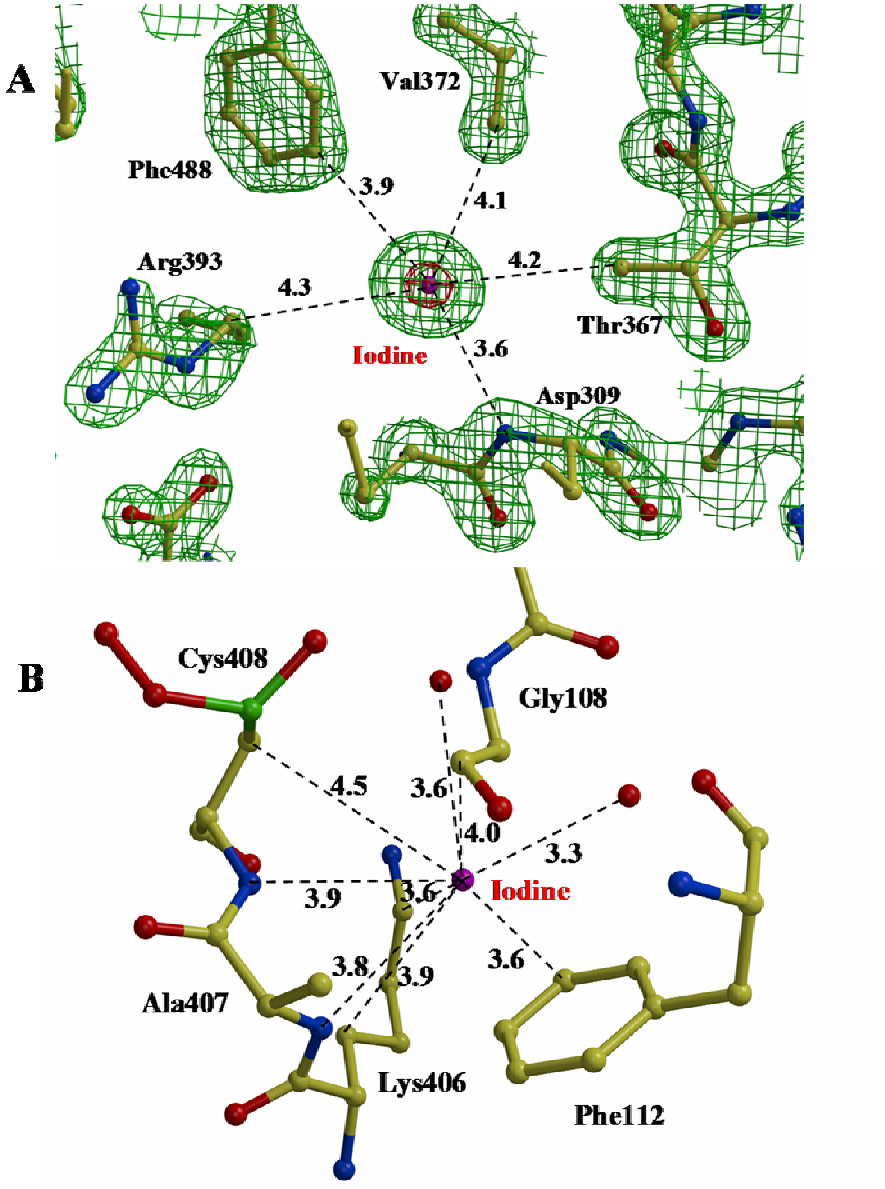

Figure 3.4 Iodine in the crystal structure. $2F_o$-F_c electron density map contoured at 2.0σ. Interatomic interactions are shown as dashed lines with distances in Å. A) conserved iodine site and B) second site in Est55-pH6.2. Cys408 is oxidized with three oxygen atoms.

Gly108 (Fig 3.4b). The third iodine was refined with partial occupancy and was located on the surface of the protein with an ionic interaction with the side chain of Arg377, a hydrogen bond interaction with amide of Ala400, and van der Waals interactions with main chain atoms of Pro399 and side chain of Glu290. This iodine was located right next to the disordered loop 401-404 in the active site. It was positioned partly in the density for one alternate conformation of the side chain of Arg293, indicating that the Arg293 side chain is in the other conformation in the presence of iodine ion. The hydrogen bond interactions observed between three iodine atoms and the amides of the protein are N-H….I interactions, with N….I distances in the range of 3.3-3.9 Å. Similar hydrogen bond distances were observed in the small molecule crystal structures (Sheldrick 1970; Dale 2005).

Flexibility of the active site

The electron density in the active site region showed partial disorder in Est55-pH6.8, while the residues were clearly visible in Est55-pH6.2. In the Est55-pH6.8 structure, the loop containing the catalytic His409 was partially disordered and residues 401-407 were not visible. Only one water molecule was visible and it formed hydrogen bond interactions with the side chains of Ser220 and two of catalytic triad residues Ser194 and Glu310. However, the structure of Est55-pH6.2 showed more ordered density near the active site. The loop around His409 showed clear electron density and residues 405-409 were fit into the electron density unambiguously. The conformation of this loop

was stabilized by several hydrogen bond and van der Waals interactions with the surrounding residues in the active site (Figure 3.5).

The catalytic triad of Est55 consists of Ser194, Glu310, and His409. The catalytic Ser194 was located at the bottom of a deep active site cleft and formed water-mediated hydrogen bond interactions with the carboxylate side chain of Glu310 (Fig 3.5). Although, the side chain of His409 was positioned unambiguously in Est55-pH6.2 and Est55-pH6.8 structure, it was directed away from the other members of the catalytic triad, Ser194 and Glu310, and did not show the hydrogen bond interactions with their side chains that are expected for the catalytic triad. Moreover, His409 was located near a disordered loop in both Est55 structures. These observations suggested that the flexibility of the loop where His409 is located plays an important role in substrate binding and catalysis. It is likely that the active site is not formed until the substrate is bound within the catalytic gorge. The rCE structure also showed flexibility near the catalytic site. Disorder was observed for two loops in the rCE structure adjacent to the catalytic triad residues Glu353 and His467. Also, the catalytic Glu353 was rotated away from the active site relative to the conserved orientations observed in other esterases. Therefore, the existence of disordered active sites suggests that Est55 and rCE enzymes will bind substrate by an induced fit mechanism.

Est55 contains an oxidized cysteine in the active site.

Extra electron density was observed near the side chain of Cys408 in Est55-6.2 structure (Figure 3.6a). This density indicated the presence of three oxygen atoms within

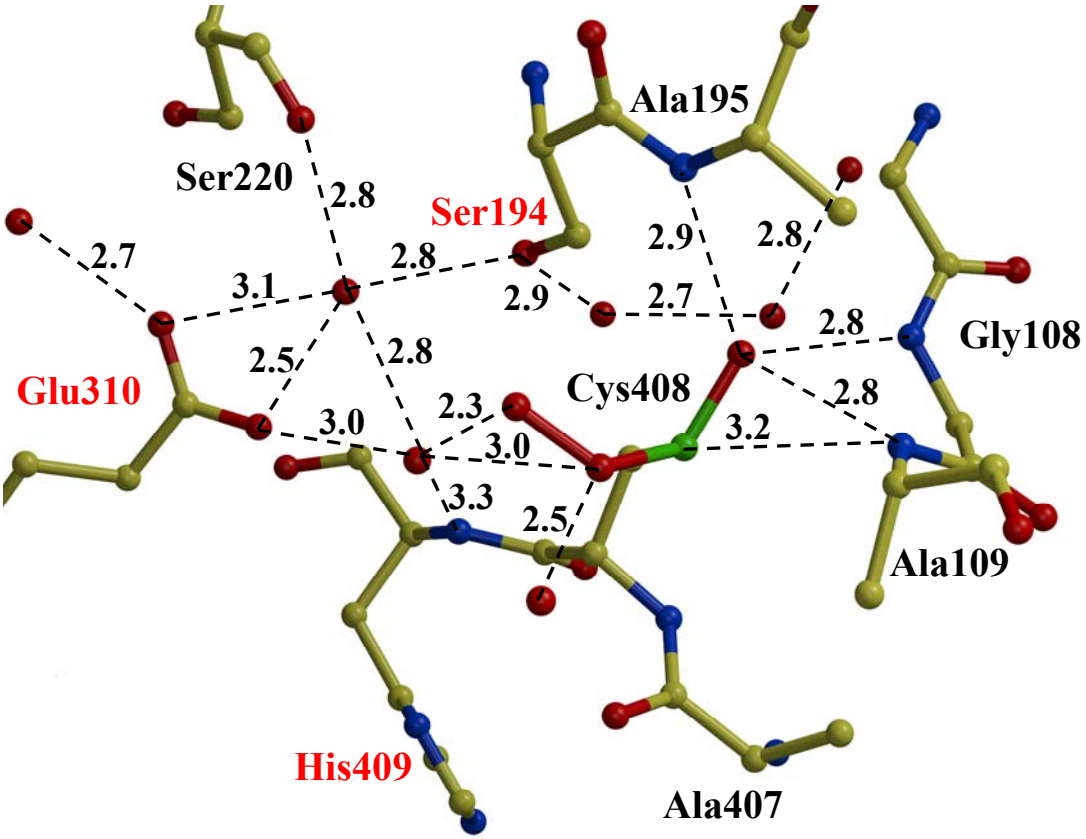

Figure 3.5 The active site region of Est55. Interatomic interactions are shown in dashed lines with distances in Å. The catalytic residues Ser194, Glu310 and His409 are labeled in red.

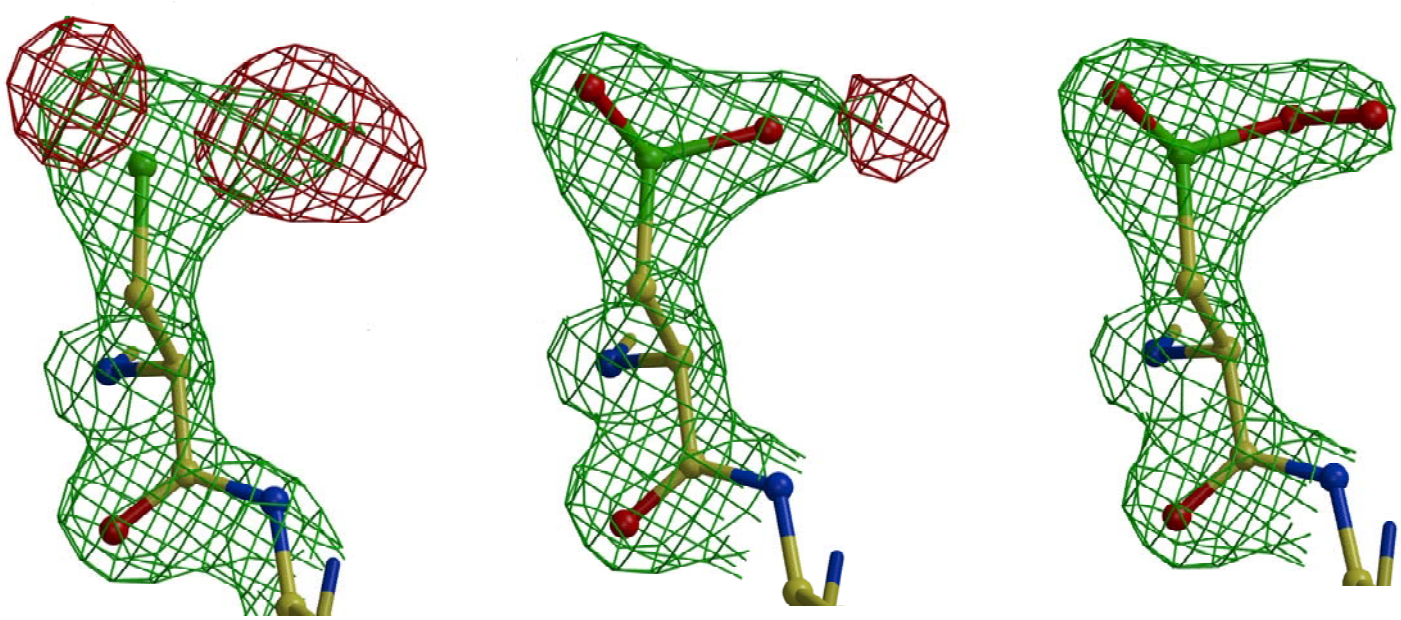

Figure 3.6 Oxidized cysteine. A) $2F_o$-F_c electron density map contoured at 1.6 σ and F_o-F_c electron density map contoured at 3.5 σ before three oxygen atoms were positioned. B) $2F_o$-F_c electron density map contoured at 1.6 σ after addition and refinement of two oxygen atoms and C) three oxygen atoms.

bonded distance of the cysteine sulfur. Refinement confirmed that the cysteine was oxidized to the sulfinylperoxy form of SO_2O^- (Figure 3.6c). This oxidation state is unusual, however, similar forms have been observed in oxidized small molecules at low temperatures. The small molecule sulfinylperoxy intermediate ($-SO_2O^-$) and cysteine sulfonyl peroxyl radicals ($-SO_2^-$ and SO_2OO^-) have been reported (Kim 1988; Sevilla 1990). In Est55 the oxidized cysteine was stabilized by hydrogen bond interactions with amides of Gly108, Ala109 and Ala195 and two water molecules in the oxyanion hole, as shown in Figure 3.5. Unexpectedly, Cys408 occupied the oxyanion hole of the active site and blocked the entrance of the active site cavity, and appeared to mimic an inhibitor. Five water molecules occupied the active site and made hydrogen bond interactions with the side chains of Ser194, Ser220, Glu310, Cys408 and the amide of His409.

The presence of oxidized cysteine has been described in several protein structures, mainly in the form of cysteine sulfenic acids (Cys-SOHs), sulfinic acids (Cys-SO_2 H) and sulfonic acids (Cys-SO_3H). Some of these oxidized cysteines have been reported to play roles in enzyme catalysis (Stehle 1993; Mande 1995; Mizohata 2005). In NADH peroxidase, a conserved cysteine functions as a redox center that cycles between sulfhydryl (Cys-SH) and sulfenic acid (Cys-SOH) states (Stehle 1993; Mande 1995). In peroxiredoxins, a conserved redox-active cysteine is oxidized to a cysteine sulfenic acid after attacking the peroxide substrate (Mizohata 2005). Oxidized cysteines with no apparent roles in catalysis have also been reported in some enzymes. Cysteine sulfinic acid has been described in the crystal structure of α-glucosidase AglA with a possible

role in enzyme inactivation. The oxidized cysteine prevents the catalytic histidine from interacting with an Mn^{2+} ion and the potential nucleophile Asp (Lodge 2003).

Several studies have indicated a correlation between the cysteine oxidation and the oxidative stress response (Canet-Aviles 2004). Cysteine-sulfinic acid resulting from cysteine oxidation of human Parkinson's disease protein DJ-1 can signal mitochondrial relocalization and protect against cell death in response to the oxidative stress (Canet-Aviles 2004; Kim 2005; Moore 2005). The cysteine oxidization was also observed in a prokaryotic homologue of DJ-1, the YajL protein from *Eschericha coli* (Wilson 2005). Furthermore, the NADH peroxidase and peroxiredoxin, which contain oxidized cysteines, are involved in the defense mechanism against oxidative stress. Interestingly, it has been observed that Est55 is secreted during the stationary phase (unpublished observation). During this stage of cell growth, bacteria are exposed to several environmental stresses, one of which is oxidative stress. Based on the crystal structure of Est55-pH 6.2, it is tempting to suggest that cysteine oxidation of Est55 may provide a possible cellular mechanism in response to oxidative stress during the stationary phase. The activity of Est55 would be inhibited by the oxidization of Cys408.

Role of Cys408 in the enzymatic activity of Est55

In order to investigate the role of C408 in the reaction mechanism of Est55, a random mutant library of C408 was constructed using the Quick-change site-directed mutagenesis kit with degenerate primers. Mutations to the hydrophobic amino acids C408A, C408P, C408V, the polar amino acid C408S, and the flexible amino acid C408G

were selected to test the enzymatic roles of cysteine. The different mutants were identified by DNA sequencing. All mutants were purified to homogeneity and their enzymatic activities were compared with that of the wild type enzyme. The enzymatic activity for *p*-nitrophenyl substrate (*p*-nitrophenyl butyrate, *p*-NP butyrate) was measured for both the wild type and the mutants to evaluate the effect of the mutants on catalysis. The kinetic parameters are shown in Table 3.2. Little variation was observed in the K_m for the wild type Est55 and the mutants, except for C408S. Mutations to hydrophobic amino acids, C408A, C408P, and C408V, showed similar K_m values as the wild type. However, mutation to polar serine in C408S resulted in 4-fold increased K_m value, suggesting that a polar environment is less favorable for substrate binding. Substitutions of Cys408 showed conserved or improved k_{cat} value, except for C408G that showed a 4 fold decrease in k_{cat} relative to wild type Est55. Overall, the C408S and C408G mutants demonstrated decreased catalytic efficiency for *p*-NP butyrate hydrolysis. The lower activity of the serine mutant is consistent with the hydrophobic nature of the Est55 substrate binding pocket. This pocket is formed by the hydrophobic side chains of Phe112, Trp119, Leu225, Leu226, Met274, Leu313, Phe314, Leu316, Val370, Phe371, and Leu411. Moreover, the lower activity of C408G suggested that the very flexible amino acid glycine was unfavorable at this position. Overall, the analysis of these mutations suggested that cysteine408 is not essential for activity, and the substitution of hydrophobic side chains of alanine or valine in fact produces higher enzyme activity. However, these results do not rule out a possible role of C408 in the regulation of Est55 activity *in vivo*.

Table 3.2 Effects of mutation at Cys408 on the hydrolysis of *p*-NP butyrate.

	K_m (μM)	k_{cat} (s^{-1})	k_{cat}/K_m (s^{-1} μM^{-1})
WT	24.2 ± 2.5	(7.9 ± 0.3) x 10^5	(3.3 ± 0.4) x 10^4
C408A	32.8 ± 2.9	(13.7 ± 0.4) x10^5	(4.2 ± 0.4) x 10^4
C408G	23.1 ± 2.7	(2.2 ± 0.09) x 10^5	(0.95 ± 0.17) x10^4
C408P	26.0 ± 3.2	(6.5 ± 0.3) x 10^5	(2.5 ± 0.3) x10^4
C408S	97.5 ± 4.3	(12.7 ± 0.6) x 10^5	(1.1 ± 0.05) x 10^4
C408V	28.3 ± 3.8	(10.7 ± 0.3) x 10^5	(4.5 ± 0.6) x10^4

CHAPTER 4

The Potential for Use of Bacterial Carboxylesterase Est30 and Est55 in Cancer Gene Therapy

CONTENTS

I. INTRODUCTION

Carboxylesterases were introduced in cancer therapy for activating the prodrug irinotecan (7-ethyl-10-[4-(1-piperidino)-1-piperidino] carbonyloxycamptothecin; CPT-11) in 1998 (Kojima 1998). CPT-11 is a prodrug that can be activated by a carboxylesterase to generate SN-38 (7-ethyl-10-hydroxycamptothecin), a topoisomerase I poison. CPT-11 is a water-soluble derivative of camptothecin, an alkaloid originally extracted from the Chinese tree *Camptotheca acuminata*. CPT-11 has shown significant anti-tumor activity in human tumor xenograft models, especially for colon cancer (Taguchi 1990). Although SN-38 can be detected in the plasma of patients within minutes after administration of CPT-11 (Gupta 1997), only a small percentage of CPT-11 was converted into SN-38 (Rivory 1997). Therefore, several cDNAs encoding different carboxylesterases, including rabbit liver carboxylesterase (rCE), human small intestine (hiCE) and human liver carboxylesterase 2 (hCE2) have been isolated and their enzymatic roles for CPT-11 activation were explored (Potter 1998; Humerickhouse 2000; Khanna 2000). To date, rabbit carboxylesterase (rCE) is considered the most efficient enzyme, which activates CPT-11 within 22 hours under the conditions of applying 2000 units of the enzyme (Danks 1999).

The application of mammalian enzymes has the advantage of lower immunogenicity, which supports longer periods of prodrug activation (Aghi 2000). However, they lack the advantage of the large therapeutic index and high thermostability that can be achieved with enzymes from thermostable bacterial origins. The esterase genes *est55* and *est30* were recently isolated from the genomic library of the Gram-

positive bacterium *Geobacillus stearothermophilus* and cloned and expressed in *E. coli* (Ewis 2004). They showed high thermostability and remained active at mesophilic temperature. Est55 shares 32 % sequence identity with human liver carboxylesterase 1 (hCE1) and 31 % rabbit liver carboxylesterase (rCE). It also showed higher enzymatic activity than rCE towards the same *p*-nitrophenyl esters (Ewis 2004), which have a similar molecular diameter to CPT-11. Therefore, we hypothesized that Est55 can activate CPT-11. Although there is no sequence homology between Est30 and Est55, they share similar substrate specificity (Ewis 2004), which suggests the possibility that Est30 also may activate CPT-11. In this chapter, we measured the ability of these two enzymes to activate CPT-11 and compared their catalytic efficiency. We also analyzed the role of Cys408 in the Est55 enzymatic activity towards CPT-11. Finally the effects of Cys408 mutants were compared for hydrolysis of *p*-NP butyrate and CPT-11.

II. MATERIALS and METHODS

Site-directed mutagenesis of Est55

Random mutations of C408 were generated by the Quick-Change mutagenesis kit (Stratagene) using the following degenerate primers: CYS408_f (5'-GCTGAAAGCANNNCACGCGCTCGAGCTGCCGTTTGTG-3') and CYS408_r (5'-CGAGCGCGTGNNNTGCTTTCAGCTGGCCGCCGAACAC-3'). 20 ng of plasmid encoding the *est55* gene were mixed with two degenerate primers and 2.5 U of *pfuTurbo* DNA polymerase, followed by 20 cycles of denaturing, annealing and extension in a thermal cycler. The reaction mixture was digested by 10 U of *Dpn* I enzyme at 37 °C for 1h and then transformed into the expression host *E. coli* Top 10 cells. The mutation sites were confirmed by DNA sequencing.

Expression and Purification of Recombinant Est55

Est55 and Cys408 mutants were expressed and purified to homogeneity as described previously (Ewis 2004). Briefly, the enzyme was expressed using *E. coli* Top 10 cells carrying the recombinant clone pHE55. The wild type Est55 and the mutants were purified in two steps, ionic exchange using high-load Q-Sepharose HR 26/10 (Pharmacia) and gel filtration using Sephacryl S200 (HR26/60).

Expression and Purification of Recombinant Est30

The coding sequence of *est*30 amplified by PCR was cloned into the pBAD-HisA vector (Invitrogen) and the resulting recombinant plasmid was designated pHE30. *Escherichia coli* Top10 (Invitrogen) harboring pHE30 was induced for 4 h by 1 mM arabinose in 1 liter culture and then harvested at 5000 *g* for 15 min at 277 K. The cell pellet was suspended in 40 ml of hypertonic solution consisting of 20 mM Tris-HCl pH 7.5, 2.5 mM EDTA and 20% sucrose. The suspension was incubated on ice for 30 min and vortexed every 10 min. Cells were removed by centrifugation at 13 000g for 20 min at 277 K and the cell pellet was resuspended in 60 ml of 20 mM Tris-HCl pH 7.5, 2.5 mM EDTA (hypotonic solution) and further incubated on ice for 30 min with intermittent vortexing every 10 min. Cells were removed by high-speed centrifugation at 22 000g for 20 min at 277 K and the supernatant applied to a Pharmacia Q-Sepharose Hiload 26/10 HP that was equilibrated with 50 mM Tris-HCl pH 8.0. The column was washed with 150 ml of the equilibration buffer to remove unbound proteins, followed by a linear gradient to 50 mM Tris-HCl pH 8.0 and 1 M KCl. The esterase peak eluted at 0.65 M KCl. Fractions containing esterase activity were pooled (32 ml), concentrated to 5 ml by ultrafiltration and applied to a Sephacryl S 200 HR column (Pharmacia, 26/60). The enzyme was eluted using 50 mM potassium phosphate pH 7.0 and 0.15 M NaCl.

HPLC Assay for Enzymatic Conversion of CPT-11 to SN-38

The enzymatic reaction was carried out as described before with minor modifications (Guichard 1998). In brief, freshly purified Est55 and Est30 were incubated

with different concentrations of CPT-11 from 1.67 μM to 100 μM in a final volume of 300 μl of 50 mM HEPES (pH 7.4) at 37 °C for 8hrs. The reaction was terminated with the addition of one volume of 75mM Ammonium acetate (pH 4.0), vortexed, and centrifuged at 14,000 g for 2 min. The kinetic parameters for conversion of CPT-11 were obtained from HPLC separation of substrate and product.

HPLC analysis for CPT-11 and SN-38 was performed as described (Danks 1999). An aliquot of the reaction was injected onto an Anlantis^{TM} dC $_{18}$ chromatography column (4.6 x 50 mm) using an automatic injector (Amersham A-900) and was run by HPLC on an AKTA Purifier. A linear gradient was run with 75mM ammonium acetate (pH 4.0), and 0 to 25% acetonitrile to separate the substrate and product. The reaction mixture was eluted at 1ml/min. Under these conditions, the CPT-11 and SN-38 were eluted at 3.8 ml and 5.1 ml, respectively. The two compounds were detected by UV absorbance at wavelengths of 266 nm and 375 nm, respectively. The absorbance was converted to SN-38 concentration via the standard calibration curve of UV peak area generated by known concentrations of SN-38. Kinetic parameters were determined by fitting the data obtained at less than 20 % substrate hydrolysis for the Michaelis-Menton equation using the SigmaPlot 8.0.2 program (SPSS, Inc.).

RESULTS AND DISCUSSION

Both Est30 and Est55 can convert CPT-11 to SN-38

Freshly purified Est30 and Est55 were used to measure their ability to convert CPT-11 to SN-38. The enzymatic conversion of CPT-11 to SN-38 was quantitated by HPLC separation of the substrate and product. The peak positions for CPT-11 and SN-38 were confirmed by using the pure compounds. Also, the presence of SN-38 was confirmed by mass spectrometry of the isolated fraction giving the molecular mass of 393.1. Est55 activated CPT-11 with a k_{cat}/K_m value of 0.84 ± 0.08 min^{-1} mM^{-1} (Table 1). Est30 activated CPT-11 with a k_{cat}/K_m value of 0.09 ± 0.01 min^{-1} mM^{-1}. In comparison with the published kinetic data for other carboxylesterases, these two enzymes showed lower catalytic efficiency than rabbit carboxylesterase (180 min^{-1} mM^{-1}) (Wierdl 2004). However, Est55 and Est30 have the advantages of high thermostability and catalytic efficiency at mesophilic temperature. Proteins of bacterial origin are relatively easy to overexpress, purify and engineer, which is an advantage for the long term goal of selecting efficient stable enzymes for CPT-11 activation. Therefore, Est55 and Est30 can provide enzymes with high stability for efficient cancer therapy with CPT-11.

The kinetic constants were used to compare the differences between Est55 and Est30 in catalytic efficiency towards CPT-11 (Table 4.1). A Lineweaver–Burk plot showed a linear response over the tested concentration range. The K_m and k_{cat} values of Est55 were estimated to be 18.6 ± 1.8 μM and (15.6 ± 0.5) $\times 10^{-3}$ min^{-1}, while those of Est30 were 202 ± 20 μM and (17.2 ± 1.2)$\times 10^{-3}$ min^{-1}. These results indicate that Est30

Table 4.1 Kinetic parameters for Est55 and Est30 with CPT-11.

	K_m (μM)	k_{cat} (min^{-1})	k_{cat}/K_m (min^{-1} mM^{-1})
Est55	18.6 ± 1.8	(15.6 ± 0.5) × 10^{-3}	0.8 ± 0.08
Est30	202 ± 20	(17.2 ± 1.2) × 10^{-3}	0.09 ± 0.01

has much lower substrate binding affinity than Est55, and consequently the catalytic efficiency (k_{cat}/K_m) of Est30 (0.09 ± 0.01 min^{-1} mM^{-1}) is about 10-fold lower than that of Est55 (0.8 ±0.08 min^{-1} mM^{-1}).

Effects of mutation of Est55 at Cys408 on the hydrolysis of CPT-11

The Cys408 mutants of Est55 were evaluated for hydrolysis of CPT-11 to SN-38 (Table 4.2). Various effects on prodrug activation were observed for the different substitutions of Cys408. The most dramatic effect was observed for the C408S mutant, where no product peak for SN-38 was detected even after doubling the incubation time. Therefore, mutation to the polar serine has eliminated the ability to hydrolyze CPT-11. Mutation to glycine resulted in ~four-fold decrease in k_{cat}/K_m. Substitution of hydrophobic amino acids had variable effects on kinetic parameters. The C408A mutant showed more than 2-fold increase in K_m, while C408P and C408V had ~3- to 5-fold decreased k_{cat} relative to wild type Est55. The two mutants C408A and C408P had decreased catalytic efficiency of 40 and 17 % of wild type $k_{cat}/K_{m,}$, respectively. The C408V mutant showed the highest catalytic efficiency of 70 % relative to the wild type Est55.

Table 4.2 Effects of mutation at Cys408 on the hydrolysis of CPT-11.

	K_m (μM)	k_{cat} (min^{-1})	k_{cat}/K_m (min^{-1} mM^{-1})
WT	18.6 ± 1.8	(15.6 ± 0.5) $\times 10^{-3}$	0.8 ± 0.08
C408A	45.3 ± 6.9	(15.5 ± 0.35) $\times 10^{-3}$	0.34 ± 0.05
C408G	22.4 ± 1.4	(5.0 ± 0.12) $\times 10^{-3}$	0.23 ± 0.02
C408P	20.6 ± 2.1	(2.9 ± 0.1) $\times 10^{-3}$	0.14 ± 0.01
C408S	N. D.*	N. D.*	N. D.*
C408V	22.3 ± 2.5	(13.5 ± 0.6) $\times 10^{-3}$	0.6 ± 0.07

* Not detectable

The effects of the Cys408 substitutions on Est55 activity differed for the two tested substrates, *p*-NP butyrate and CPT-11, as shown in Figure 4.1. Hydrolysis of *p*-NP butyrate showed relatively little change (76-140% of wild type Est55) for the mutations to hydrophobic amino acids, alanine, valine and proline, whereas, substitution of glycine or serine was unfavorable and resulted in only about 30% of wild type catalytic efficiency. In contrast, hydrolysis of CPT-11 was substantially reduced for all the tested mutants of Cys408, except C408V. In fact, the serine mutant had no detectable activity. These results suggested that the hydrophobicity of the binding site was more critical for binding and hydrolysis of CPT-11 compared with *p*-NP butyrate. Mutant C408V may provide a more stable construct by removing the only cysteine residue, which can oxidize as shown in the crystal structure and potentially inhibit Est55 activity.

Attempts to obtain structures of Est55 with substrates, products and inhibitors

Although Est55 and Est30 did not show higher catalytic efficiency than that of rCE, their high thermostability and bacterial origins make them promising candidates for activating CPT-11. However, protein engineering has to be pursued. Directed evolution is a very common approach for improving enzyme activity even after the three dimensional structure of enzyme has been determined because the rational design based on the structure usually focuses on the enzyme active site only, while sometimes a mutation far from the active site may have dramatic effects on enzyme activity. Directed evolution has been successfully used to improve the stability and activity of a carboxylesterase from *Bacillus subtilis*, which can selectively cleave the *p*-nitrobenzyl ester of Loracarbef, a

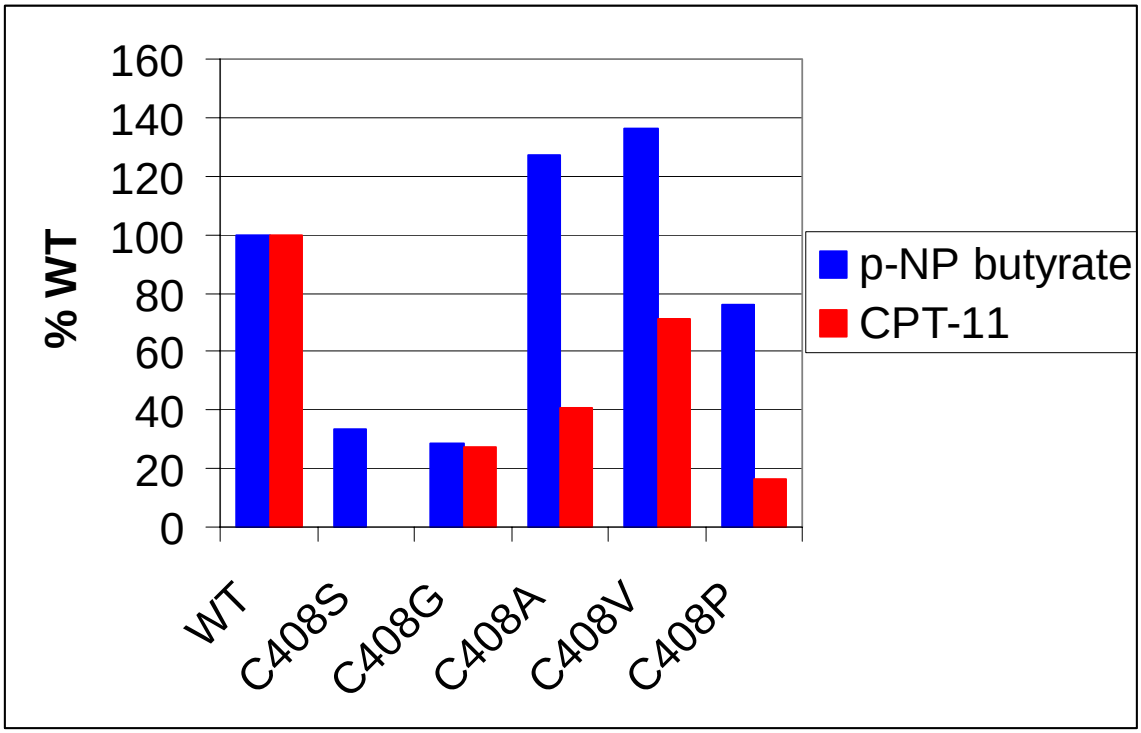

Figure 4.1 Relative activity of Est55 Mutants on *p*-NP butyrate and CPT-11

cephalosporin. The wild type enzyme has very weak activity in the presence of dimethylformamide (DMF), which is used for dissolving the substrate. The combination of DNA shuffling and error-prone PCR generated a mutant with 150 times higher activity compared to the wild type enzyme. Error-prone PCR by the addition of manganese chloride was performed on *est55* gene. A high throughout screening method using a substrate mimicking the size of CPT-11 is under development. Those variants with higher enzymatic activity towards that substrate will be further tested for the activation of CPT-11 by the HPLC assay.

In addition to creating genetic diversity from a pool of variants from a single gene, a recent approach called family shuffling allows two or more naturally occurring homologous genes to be used as the starting genetic material. In family shuffling, the homologous genes are mixed, randomly fragmented and recombined under the conditions that permit annealing and extension of nonidentical complementary strands. Such related genes, which have been selected from nature to be functional and useful, provide functional diversity as opposed to simply random mutants (Svendsen 2004). The power of this method has been demonstrated in the directed evolution of thymidine kinase for AZT phosphorylation using DNA family shuffling (Christians 1999). Since several carboxylesterases have shown the ability to activate CPT-11, family shuffling of this pools of genes is another possible approach to select a more active mutant (Potter 1998; Danks 1999; Danks 2004).

Rational design based on the crystal structure of Est55 to improve its enzymatic activity can be also attempted. Unfortunately, the Est55 structure is in an inactive form,

with the catalytic His409 rotated away from the other two members of the catalytic triad, Ser194 and Glu310. The presence of the inactive form maybe due to the pH of crystallization conditions in the range of pH 6 to pH 7. At these pH conditions, the enzyme maintains only slight activity (Ewis 2004). In order to get a structure in an active form, crystallization at the basic pH in which this protein is more active was tested, however crystals were either in the needle shape or too small and no useful data have been obtained. As a structure of an enzyme in complex with either a substrate or a product may provide more detailed information about the enzyme reaction mechanism, which is critical for designing a mutant with higher enzymatic activity, several experiments have been performed to achieve this goal (Table 4.3). In order to obtain an enzyme-substrate complex structure, the catalytic triad Ser194, Glu310, and His409 were mutated to Alanine individually to eliminate the enzyme activity. All these mutant enzymes were expressed, purified, and cocrystallized with the substrate CPT-11. Glu310Ala-CPT11 crystals appeared after a few days, however, the crystals were not big enough to diffract. Also, co-crystallization of the wild type protein or soaking wild type Est55 crystals with the two products SN-38 and 4PP was tried. No electron density was observed for the products in all the data sets collected, even though the products and the enzyme are in high molar ratio, for example the molar ratio of Est55 and 4PP is 1:1000. Since there was no success in obtaining the enzyme-substrate or enzyme-product complex by either co-crystallization or soaking, and the inactive form of the enzyme structure makes it difficult to model the ligands into the active site, an alternative approach has to be tried. Crystallization of Est55 with inhibitors was attempted.

Table 3 Crystallization trials of Est55 wild type and mutants with different ligands.

	Ligand	Results
Est55	CPT-11	Crystals diffract, No density for substrate
Est55	SN-38	Crystals diffract, No density for product
Est55	4PP	Crystals diffract, No density for product
Ser194Ala	CPT-11	No crystals
Glu310Ala	CPT-11	Crystals are too small
His409Ala	CPT-11	No crystals
Est55	Phenylmethylsulphonylfluoride (PMSF)	No crystals
Est55	N-*p*-Tosyl-L-phenylalanine chloromethyl ketone (TPCK)	No crystals

Unfortunately, Est55 could not be fully inhibited by all known commercial serine protease and carboxylesterase inhibitors. We accidentally found that Est55 can be inhibited by a protease inhibitor cocktail tablet. Although the specific inhibitors have not been identified, crystallization of Est55 with the cocktail will be attempted.

Once a structure is available for Est55 in complex with substrate, a product or an inhibitor, we can elucidate the detailed information of the key residues involved in substrate binding and product release. Site-directed random mutagenesis of those residues in the active site can be performed in the next step. Those improved clones from either directed evolution or rational design will be combined, re-mutated, and screened for higher catalytic efficiency.

LITERATURE CITED

Agelaki, S., Karyda, E, Kouroussis, C.h., Ardavanis, A., Kalbakis, K., Malas, K., Malamos, N., Alexopoulos, A., Tselepatiotis, E., Georgoulias, V. (2003). "Gemcitabine plus irinotecan in breast cancer patients pretreated with taxanes and anthracyclines: a multicenter phase II studyW." Oncology **64**: 477-478.

Aghi, M., Hochberg, F., Breakefield, X.O. (2000). "Prodrug activation enzymes in cancer gene therapy." J Gene Med. **2**: 148-164.

Altamirano, M. M., Blackburn, J.M., Aguayo, C., Fersht, A.R. (2002). "Retraction. Directed evolution of new catalytic activity using the alpha/beta-barrel scaffold." Nature. **417**: 468.

Altschul, S. F., Madden, T. L., Schäffer, A. A., Zhang, J., Zhang, Z., Miller, W. Lipman, D. J. (1997). "Gapped BLAST and PSI-BLAST: a new generation of protein database search programs." Nucleic. Acids. Res. **25**: 3389-3402.

Arpigny, J. L., Jaeger, K. E (1999). "Bacterial lipolytic enzymes: classification and properties." Biochem. J. **343**: 177-183.

Bajetta, E., Carnaghi, C., Somma, L., Stampino, C.G. (1996). "A pilot safety study of capecitabine, a new oral fluoropyrimidine, in patients with advanced neoplastic disease." Tumori **82**: 450-452.

Becker, A., Bottcher, A., Lackner, K.J., Fehringer, P., Notka, F., Aslanidis, C., Schmitz, G. (1994). "Purification, cloning, and expression of a human enzyme with acyl coenzyme A: cholesterol acyltransferase activity, which is identical to liver carboxylesterase." Arterioscler Thromb.. **8**: 1346-1355.

Bencharit, S., Morton, C.L., Howard-Williams, E.L., Danks, M.K., Potter, P.M., Redinbo, M.R. (2002). "Structural insights into CPT-11 activation by mammalian carboxylesterases." Nat Struct Biol. **9**(5): 337-342.

Bencharit, S., Morton, C.L., Hyatt, J.L., Kuhn, P., Danks, M.K., Potter, P.M., Redinbo, M.R. (2003). "Crystal structure of human carboxylesterase 1 complexed with the Alzheimer's drug tacrine: from binding promiscuity to selective inhibition." Chem Biol. **10**: 341-349.

Bencharit, S., Morton, C.L., Xue, Y., Potter, P.M., Redinbo, M.R. (2003). "Structural basis of heroin and cocaine metabolism by a promiscuous human drug-processing enzyme." Nat Struct Biol. **10**(5): 345-356.

Berman, H. M., Westbrook, J., Feng, Z., Gilliland, G., Bhat, T.N., Weissig, H., Shindyalov, I.N., Bourne, P.E. (2000). "The Protein Data Bank." Nucleic Acids Research **28**: 235-242.

Blow, D. (2002). Outline of crystallography for biologists New York, Oxford University Press.

Bodurka, D. C., Levenback, C., Wolf, J.K, Gano, J., Wharton, J.T., Kavanagh, J.J., Gershenson, D.M. (2003). "Phase II trial of irinotecan in patients with metastatic epithelial ovarian cancer or peritoneal cancer." J. Clin. Oncol. **21**: 291-297.

Bornemann, S., Cassells, J. M., Dordick, J. S., Hacking, A. J. (1992). "The use of enzymes to regioselectively deacylate sucrose esters." Biocatalysis **7**: 1-12.

Bornscheuer, U. T. (2002). "Methods to increase enantioselectivity of lipases and esterases." Curr. Opin. Biotechnol. **13**: 543-547.

Bornscheuer, U. T. (2002). "Microbial carboxyl esterase: classification, properties and application in biocatalysis." FEMS Microbiol. Rev. **26**: 73-81.

Botstein, D., Shortle, D. (1985). "Strategies and applications of in vitro mutagenesis." Science. **229**: 1193-1201.

Bradford, M. M. (1976). "A rapid and sensitive method for the quantitation of microgram quantities of protein utilizing the principle of protein-dye binding." Anal Biochem. **7**: 248-254.

Brenner, S. (1988). "The Molecular evolution of genes and proteins: a tale of two serines." Nature(London) **334**: 528-530.

Brunger, A. T., Adams, P. D., Clore, G. M., DeLano,W. L., Gros, P., Grosse-Kunstleve, R. W., Jiang, J. S., Kuszewski, J., Nilges, M., Pannu, N. S., Read, R. J., Rice, L. M., Simonson, T., Warren, G. L. (1998). "Crystallography & NMR system: a new

software suite for macromolecular structure determination." Acta Crystallogr. D **54**: 905-921.

Brzezinski, M. R., Abraham, T.L., Stone, C.L., Dean, R.A., Bosron, W.F. (1994). "Purification and characterization of a human liver cocaine carboxylesterase that catalyzes the production of benzoylecgonine and the formation of cocaethylene from alcohol and cocaine." Biochem. Pharmacol. **48**: 1747-1755.

Brzezinski, M. R., Spink, B. J. Dean, R. A., Berkman, C. E., Cashman, J. R., Borson, W. F. (1997). "Human liver carboxylesterase hCE-1: binding specificity for cocaine, heroin, and their metabolites and analogs." Drug Metab. Dispos. **25**: 1089-1096.

Canet-Aviles, R. M., Wilson, M.A., Miller, D.W., Ahmad, R., McLendon, C., Bandyopadhyay, S., Baptista, M.J., Ringe, D., Petsko, G.A., Cookson, M.R. (2004). "The Parkinson's disease protein DJ-1 is neuroprotective due to cysteine-sulfinic acid-driven mitochondrial localization." Proc Natl Acad Sci U S A. **101**: 9103-9108.

Chitapanarux, I., Tonusin, A., Sukthomya, V., Charuchinda, C., Pukanhapan, N., Lorvidhaya, V. (2003). "Phase II clinical study of irinotecan and cisplatin as first-line chemotherapy in metastatic or recurrent cervical cancer." Gynecol. Oncol. **89**: 402-407.

Christians, F. C., Scapozza, L., Crameri, A., Folkers, G., Stemmer, W.P. (1999). "Directed evolution of thymidine kinase for AZT phosphorylation using DNA family shuffling." Nat Biotechnol. **3**: 259-264.

Coco, W. M., Levinson, W.E., Crist, M.J., Hektor, H.J., Darzins, A., Pienkos, P.T., Squires, C.H., Monticello, D.J. (2001). "DNA shuffling method for generating highly recombined genes and evolved enzymes." Nat Biotechnol. **19**: 354-359.

Cohen, G. E. (1997). "ALIGN: a program to superimpose protein coordinate, accounting for insertions and deletions." J. Appl. Crystallog. **30**: 1160-1161.

Comella, P., Casaretti, R., De, Rosa.V., Avallone, A., Izzo, F., Fiore, F., Lapenta, L., Comella, G. (2002). "Oxaliplatin plus irinotecan and leucovorin-modulated 5-fluorouracil triplet regimen every other week: a dose-finding study in patients with advanced gastrointestinal malignancies. ." Ann. Oncol. **13**: 1874-1881.

Cowie, D. B., Cohen, G.N. (1957). "Biosynthesis by *Escherichia coli* of active altered proteins containing selenium instead of sulfur." Biochim. Biophys. Acta **26**: 252-261.

Crameri, A., Raillard, S.A., Bermudez, E., Stemmer, W.P. (1998). "DNA shuffling of a family of genes from diverse species accelerates directed evolution." Nature **391**: 288-291.

Cuff, M. E., Zhou, M., Collart, F., Joachimiak, A. "Structure of a carboxylesterase from *Bacillus stearothermophilus*. ." to be published.

Dale, S. H., Elsegood, M.R., Holmes, K.E., Kelly, P.F. (2005). "The effect of hydrogen-bonding anions on the structure of metal-sulfimide complexes." Acta Crystallogr. C **61**: m34-m39.

Danks, M. K., Morton, C.L., Krull, E.J., Cheshire, P.J., Richmond, L.B., Naeve, C.W., Pawlik, C.A., Houghton, P.J., Potter, P.M. (1999). "Comparison of activation of CPT-11 by rabbit and human carboxylesterases for use in enzyme/prodrug therapy." Clin Cancer Res. **5**(4): 917-924.

Danks, M. K., Morton, C.L., Pawlik, C.A., Potter, P.M. (1998). "Overexpression of a rabbit liver carboxylesterase sensitizes human tumor cells to CPT-11." **58**: 20-22.

Danks, M. K., Potter, P.M. (2004). "Enzyme-prodrug systems: carboxylesterase/CPT-11." Methods Mol. Med. **90**: 247-262.

De Simone, G., Galdiero, S., Gluseppe, M., Lang, D., Rossl, M., Pedone, C. (2000). "A snapshot of a transition state analogue of a novel thermophilic esterase belonging to the subfamily of mammalian hormone-sensitive lipase." J. Mol. Biol. **10**: 761-771.

De Simone, G., Menchise, V., Manco, G., Mandrich, L., Sorrentino, N., Lang, D., Rossi, M., Pedone, C. (2001). "The crystal structure of a hyper-thermophilic carboxylesterase from the *Archaeon Archaeoglobus Fulgidus*." J. Mol. Biol. **314**: 507-518.

Dean, R. A., Zhang, J., Brzezinski, M.R., Bosron, W.F. (1995). "Tissue distribution of cocaine methyl esterase and ethyl transferase activities: correlation with carboxylesterase protein." J. Pharmacol. Exp. Ther. **275**: 965-971.

DelaFlor-Weiss, E., Richardson, C., Ward, M., Himelstein, A., Smith, L., Podda, S., Gottesman, M., Pastan, I., Bank, A. (1992). "Transfer and expression of the human multidrug resistance gene in mouse erythroleukemia cells." Blood **80**: 106-111.

Dueker, S. R., Lame, M. W., Morin, D., Wilson, D.W., Segall, H. J. (1992). "Guinea pig and rat hepatic microsomal metabolism of monocrotaline." Drug Metab. Dispos. **20**: 275-280.

Dueker, S. R., Lame, M. W., Segall, H. J. (1992). "Hydrolysis of pyrrolizidine alkaloid by guinea pig hepatic carboxylesterase." Toxicol. Appl. Pharmacol. **117**: 116-121.

Dueker, S. R., Lame, M. W., Segall, H. J. (1995). "Hydrolysis rates of pyrrolizidine alkaloids derived from *Senecio jacobaea*." Arch. Toxicol. **69**: 725-728.

Esnouf, R. M. (1999). "Further additions to MolScript version 1.4, including reading and contouring of electron-density maps." Acta Crystllogr D **55**: 938-940.

Ewis, H. E., Abdelal, A. T., Lu, C. D. (2004). "Molecular cloning and characterization of two thermostable carboxylesterases from *Geobacillus stearothermophilus*." Gene **329**: 187–195.

Falconnier, B., Lapierre, C., Lesage-Meessen, G., Yonnet, G., Brunerie, P., Colonna-Ceccald, B., Corrieu, G., Asther, M (1994). "Vanillin as a product of ferulic acid biotransformation by the white-rot fungus *Pycnoporus cinnabarinus* I-937: identification of metabolic pathways." J. Biotechnol. **37**: 123-132.

Farinas, E. T., Bulter, T., Arnold, F.H. (2001). "Directed enzyme evolution." Curr Opin Biotechnol. **6**: 545-551.

Ferro, D. R., Hermans, J. (1977). "A different best rigid-body molecular fit routine." Acta Crystallogr. A **33**: 345-347.

Foa, R., Guarini, A., Gansbacher, B. (1992). "IL2 treatment for cancer: from biology to gene therapy." Br J Cancer. **6**: 992-998.

Frey, P. A., Whitt, S.A., Tobin, J.B. (1994). "A low-barrier hydrogen bond in the catalytic triad of serine proteases." Science. **264**: 1927-1930.

Friedman, H. S., Keir, S.T., Houghton, P.J. (2003). "The emerging role of irinotecan (CPT-11) in the treatment of malignant glioma in brain tumors. ." Cancer **97**: 2359-2362.

Gasson, M. J. (1998). "Metabolism of ferulic acid to vanillin." J. Biol. Chem. **273**: 4163-4170.

Gibbs, M. D., Nevalainen, K.M., Bergquist, P.L. (2001). "Degenerate oligonucleotide gene shuffling (DOGS): a method for enhancing the frequency of recombination with family shuffling." Gene **271**: 13-20.

Greener, A., Callahan, M., Jerpseth, B. (1997). "An efficient random mutagenesis technique using an E. coli mutator strain." Mol. Biotechnol. **2**: 189-195.

Guichard, S. M., Morton, C.L., Krull, E.J., Stewart, C.F., Danks, M.K., Potter, P.M. (1998). "Conversion of the CPT-11 metabolite APC to SN-38 by rabbit liver carboxylesterase." Clin Cancer Res. **4**(12): 3089-3094.

Gupta, E., Mick, R., Ramirez, J., Wang, X., Lestingi, T.M., Vokes, E.E., Ratain, M.J. (1997). "Pharmacokinetic and pharmacodynamic evaluation of the topoisomerase inhibitor irinotecan in cancer patients." J Clin Oncol. **15**(4): 1502-1510.

Habib, N. A. (2001). Cancer gene therapy past achievements and future challenges. New York, Kluwer Academic/Plenum Publishers.

Hakulinen, N., Tenkanen, M., Rouvinen, J. (2000). "Three-dimensional structure of the catalytic core of acetylxylan esterase from *trichoderma reesei*: insights into the deacetylation mechanism." J. Struc. Biol. **132**: 180-190.

Hamstra, D. A., Rice, D.J., Fahmy, S., Ross, B.D., Rehemtulla, A. (1999). " Enzyme/prodrug therapy for head and neck cancer using a catalytically superior cytosine deaminase." Hum Gene Ther. **10**: 1993-2003.

Heikinheimo, P., Goldman, A., Jeffries, C., Ollis, D. L. (1999). "Of barn owls and bankers: a lush variety of alpha/beta hydrolases." Struct. Fold. Des. **7**: 141-146.

Hendrickson, W. A., Pahler, A., Smith, J.L., Satow, Y., Merritt, E.A. and Phizackerley, R.P. (1989). "Crystal structure of core streptavidin determined from multiwavelenght anomalous diffraction of synchrotron radiation." Proc. Natl. Acad. Sci. USA **86**: 2190-2194.

Hosokawa, M., Endo, Y., Fujisawa, M., Hara, S., Iwata, N., Sato, Y. Satoh, T. (1995). "Interindividual variation in carboxylesterase levels in human liver microsomes." Drug Metab. Dispos. **23**: 1022-1027.

Hosokawa, M., Maki, T., Satoh, T. (1987). "Multiplicity and regulation of hepatic microsomal carboxylesterases in rats." Mol. Pharmacol. **31**: 579-584.

Hosokawa, M., Maki, T., Satoh, T. (1990). "Characterization of molecular species of liver microsomal carboxylesterases of several animal species and humans." Arch. Biochem. Biophys. **277**: 219-227.

Hosokawa, M., Suzuki, K., Takahashi, D., Mori, M., Satoh, T., Chiba, K. (2001). "Purification, molecular cloning, and functional expression of dog liver microsomal acyl-CoA hydrolase: a member of the carboxylesterase multigene family." Arch. Biochem. Biophys. **389**: 245-253.

Howard B, B. M., McCallister T, Chong K, Gangavalli R, Severinsson L, Jolly DJ, Darrow T, Vervaert C, Abdel-Wahab Z, et al.(1994) (1994). "Retrovirus-mediated

gene transfer of the human gamma-IFN gene: a therapy for cancer. ." Ann N Y Acad Sci. **716**: 167-187.

Humerickhouse, R., Lohrbach, K., Li, L., Bosron, W.F., Dolan, M.E. (2000). "Characterization of CPT-11 hydrolysis by human liver carboxylesterase isoforms hCE-1 and hCE-2." Cancer Res. **60**(6): 1189-1192.

Ichiki, M., Rikimaru, T., Gohara, R., Koga, T., Kawayama, T., Matunami, M., Oshita, Y., Kamimura, T., Aizawa, H. (2003). "Phase II study of irinotecan and isophosphamide in patients with advanced non-small cell lung cancer. ." Oncology(64): 306-311.

Ivanova, N., Sorokin, A., Anderson, I., Galleron, N., Candelon, B., Kapatral, V., Bhattacharyya, A., Reznik, G., Mikhailova, N., Lapidus, A., Chu, L., Mazur, M., Goltsman, E., Larsen, N., D'Souza, M., Walunas, T., Grechkin, Y., Pusch, G., Haselkorn, R., Fonstein, M., Ehrlich, S.D., Overbeek, R., Kyrpides, N. (2003). "Genome sequence of Bacillus cereus and comparative analysis with *Bacillus anthracis*." Nature. **423**: 87-91.

Joly, J. M., Brown, T. M. (1986). "Metabolism of aspirin and procaine in mice pretreated with O-4-nitrophenyl methyl(phenyl)phosphinate or O-4-nitrophenyl diphenylphosphinate." Toxicol Appl Pharmacol. **84**: 523-532.

Jones, A. T., Zou, J. Y., Cowan, S.W., Kjeldgaard (1991). "Improved methods for building protein models in electron density maps and the location of errors in these models." Acta Crystallogr. A **47**: 110-119.

Jones, R. M., Collier, L.S., Neidle, E. L., Williams, P. A. (1999). "arcABC genes determine the catabolism of aryl esters in *Acinetobacter sp.* strain ADP1." J. Bacteriol. **181**: 4568-4575.

Kamendulis, L. M., Brzezinski, M.R., Pindel, E.V., Bosron, W.F., Dean, R.A. (1996). "Metabolism of cocaine and heroin is catalyzed by the same human liver carboxylesterases." J Pharmacol Exp Ther. **279**: 713-717.

Khanna, R., Morton, C.L., Danks, M.K., Potter, P.M. (2000). "Proficient metabolism of irinotecan by a human intestinal carboxylesterase." Cancer Res. **60**(17): 4725-4728.

Kim, K. K., Song, H. K., Shin, D. H., Hwang, K. Y., Choe, S., Yoo, O. J., Suh, S. W. (1997). "Crystal structure of carboxylesterase from *Pseudomonas fluorcens*, an a/ß hydrolase with broad substrate specificity." Structure **15**: 1571-1584.

Kim, R. H., Smith, P.D., Aleyasin, H., Hayley, S., Mount, M.P., Pownall, S., Wakeham, A., You-Ten, A.J., Kalia, S.K., Horne, P., Westaway, D., Lozano, A.M., Anisman, H., Park, D.S., Mak, T.W. (2005). "Hypersensitivity of DJ-1-deficient mice to 1-methyl-4-phenyl-1,2,3,6-tetrahydropyrindine (MPTP) and oxidative stress." Proc Natl Acad Sci U S A. **102**: 5215-5220. .

Kim, Y. H., Yoon, D. C. (1988). "Efficient oxidation of sulfides to the sulfoxides using a new sulfinylperoxy intermediate generated from 2-nitrobenzenesulfinyl chloride and superoxide." Tetrahedron Lett **29**: 6453-6456.

Kojima, A., Hackett, N.R., Crystal, R.G. (1998). "Reversal of CPT-11 resistance of lung cancer cells by adenovirus-mediated gene transfer of the human carboxylesterase cDNA." Cancer Res. **58**: 4368-4374.

Kojima, A., Hackett, N.R., Ohwada, A., Crystal, R.G. (1998). "*In vivo* human carboxylesterase cDNA gene transfer to activate the prodrug CPT-11 for local treatment of solid tumors." J Clin Invest **101**(8): 1789-1796.

Kolkman, J. A., Stemmer, W.P. (2001). "Directed evolution of proteins by exon shuffling." Nat Biotechnol. **5**: 423-428.

Koukourakis, M. I., Bizakis, J.G., Skoulakis, C.E., Kyrmizakis, D., Giatromanolaki, A., Papadakis, C.E., Prokopakis, E., Amanakis, Z., Hellidonis, E.S. (1999). "Combined irinotecan, docetaxel and conventionally fractionated radiotherapy in locally advanced head and neck cancer. A phase I dose escalation study." Anticancer Res. **19**: 2305-2309.

Kraulis, P. J. (1991). "MOLSCRIPT: a program to produce both detailed and schematic plots of protein structures." J. Appl. Cryst. **24**: 946-950.

Krish, K. (1971). Carboxylic ester hydrolysis. New York, Academic Press.

Kunimoto, T., Nitta, K., Tanaka, T., Uehara, N., Baba, H., Takeuchi, M., Yokokura, T., Sawada, S., Miyasaka, T., Mutai, M. (1987). "Antitumor activity of 7-ethyl-10-[4-(1-piperidino)-1-piperidino]carbonyloxy-camptothec in, a novel water-soluble derivative of camptothecin, against murine tumors." Cancer Res. **47**: 5944-5947.

Kunst, F., Ogasawara, N., Moszer, I., Albertini, A. M., Alloni, G., Azevedo, V., Bertero, M.G., Bessieres, P., Bolotin, A., Borchert, S., Borriss, R., Boursier, L., Brans, A., Braun, M., Brignell, S.C., Bron, S., Brouillet, S., Bruschi, C.V., Caldwell, B., Capuano, V., Carter, N. M., Choi, S. K., Codani, J. J., Connerton, I. F., Danchin, A., et al (1997). "The complete genome sequence of the gram-positive bacterium *Bacillus subtilis*." Nature. **390**: 249-256.

Lamzin, V. S., Wilson, K. S. (1993). "Automated refinement of protein models." Acta Crystallogr. D **49**: 129-149.

Laskowski, R. A., MacArthur, M. W., Moss, D. S., Thornton, J. M. (1993). "PROCHECK - a program to check the stereochemical quality of protein structures." J. Appl. Crystallog. **26**: 283-291.

Lehmann, M. (2004). Concepts for protein engineering. New York, Marcel Dekker.

Lesage-Meessen, G., Delattre, M., Haon, M., Thibault, J.-F., Colonna-Ceccaldi, B., Brunerie, P., Asther, M. (1996). "A two-step conversion process for vanillin production from ferulic acid combining *Aspergillus niger* and *Pycnoporus cinnabarinus*." J. Biotechnol. **50**: 107-113.

Leung, D. W., Chen, E., Goeddel, D.V. (1989). "A method for random mutagenesis of a defined DNA segment using a modified polymerase chain reaction." Technique **1**: 11-15.

Liu, P., Wang, Y. F., Ewis, H. E., Abdelal, A., Lu, C. D., Weber, I. T. (2003). "Crystallization and preliminary X-ray diffraction data for the carboxylesterase Est30 from *Bacillus stearothermophilus*." Acta Crystallogr. D **59**: 1472-1473.

Liu, P., Wang, Y.F., Ewis, H.E., Abdelal, A.T., Lu, C.D., Harrison, R.W., Weber, I.T. (2004). "Covalent reaction intermediate revealed in crystal structure of the *Geobacillus stearothermophilus* carboxylesterase Est30." J Mol Biol. **342**: 551-561.

Lodge, J. A., Maier, T., Liebl, W., Hoffmann, V., Strater, N. (2003). "Crystal structure of Thermotoga maritima alpha-glucosidase AglA defines a new clan of NAD+-dependent glycosidases." J Biol Chem. **278**: 19151-19158.

Lotti, M., Ketterman, A., Waskell, L., Talcott, R.E. (1983). "Meperidine carboxylesterase in mouse and human livers." Biochem Pharmacol. **32**: 3735-3738.

Lund-Pero, M., Jeppson, B., Arneklo-Nobin, B., Sjogren, H.O., Holmgren, K., Pero, R.W. (1994). "Non-specific steroidal esterase activity and distribution in human and other mammalian tissues." Clin. Chim. Acta **224**: 9-20.

Mande, S. S., Parsonage, D., Claiborne, A., Hol, W.G. (1995). "Crystallographic analyses of NADH peroxidase Cys42Ala and Cys42Ser mutants: active site structures,

mechanistic implications, and an unusual environment of Arg 303." Biochemistry. **34**: 6985-6992.

Margolin, A. L. (1993). "Enzymes in the synthesis of chiral drugs." Enzyme Microb. Technol. **15**(262-280).

Matsuzaki, T., Yokokura, T., Mutai, M., Tsuruo, T. (1998). "Inhibition of spontaneous and experimental metastasis by a new derivative of camptothecin, CPT-11, in mice." Cancer Chemother. Pharmacol. **21**: 308-312.

Matthews, B. W. (1968). "Solvent content of protein crystals." J. Mol. Biol. **33**: 491-497.

McCracken, N. W., Blain, P. G., Williams, F.M. (1993). "Nature and role of xenobiotic metabolizing esterases in rat liver, lung, skin and blood." Biochem. Pharmacol. **45**: 31-36.

Merritt, E. A., Bacon, D. J. (1997). "Raster3D photorealistic Molecular Graphics." Methods Enzymol. **277**: 505-524.

Mizohata, E., Sakai, H., Fusatomi, E., Terada, T., Murayama, K., Shirouzu, M., Yokoyama, S. (2005). "Crystal structure of an archaeal peroxiredoxin from the aerobic hyperthermophilic crenarchaeon Aeropyrum pernix K1. ." J Mol Biol. **354**: 317-329.

Mnisi, S. M., Louw, M.E., Theron, J. (2005). "Cloning and characterization of a carboxylesterase from *Bacillus coagulans* 81-11." Curr Microbiol. **50**: 196-201.

Moher, P., Rosslein, L., Tamm, C. (1989). "Kinetic resolution of racemic β -γ epoxy esters with pig esterse." Tetrahedron Lett(30): 2513-2516.

Moore, D. J., Zhang, L., Troncoso, J., Lee, M.K., Hattori, N., Mizuno, Y., Dawson, T.M., Dawson, V.L. (2005). "Association of DJ-1 and parkin mediated by pathogenic DJ-1 mutations and oxidative stress." Hum Mol Genet. **14**: 71-84.

Moore, J. C., Arnold , F. H. (1996). "Directed evolution of a para-nitrobenzyl esterase from aqueous-organic solvents." Nat. Biotechnol. **14**: 458-467.

Morana, A., Di Prizito, N., Aurilia, V., Rossi, M., Cannio, R. (2002). "A carboxylesterase from the hyperthermophilic archaeon Sulfolobus solfataricus: cloning of the gene, characterization of the protein." Gene **283**: 107-115.

Mori, M., Hosokawa, M., Ogasawara, Y., Tsukada, E., Chiba, K. (1999). "cDNA cloning, characterization and stable expression of novel human brain carboxylesterase. ." FEBS Lett. **458**: 17-22.

Myers, R. M., Lerman, L.S., Maniatis, T. (1985). "A general method for saturation mutagenesis of cloned DNA fragments." Science. **229**: 242-247.

Nakamura, M., Shirasawa, E., Hikida, M. (1992). "Characterization of esterases involved in the hydrolysis of dipivefrin hydrochloride." Ophthalmic. Res. **25**: 46-51.

Nambu, K., Miyazaki, H., Nakanishi, Y., Oh-e, Y., Matsunaga, Y., Hashimoto, M. (1987). "Enzymatic hydrolysis of haloperidol decanoate and its inhibition by proteins." Biochem. Pharmacol. **36**: 1715-1722.

Nardini, M., Dijkstra, B. W. (1999). "a/ß hydrolase fold enzymes: the family keeps growing." Curr. Opin. Struct. Biol. **9**: 732-737.

Navaza, J. (1994). "AMoRe: an automated package for molecular replacement." Acta Crystallogr. A **50**: 157-163.

Nicholas, K. B., Nicholas H. B. Jr., Deerfield, D.W. II. (1997). "1997 GeneDoc: Analysis and Visualization of Genetic Variation,." EMBNEW.NEWS **4**(14).

Nishizawa, M., Shimizu, M., Ohkawa, H., Kanaoka, M. (1995). "Stereoselective production of (+)-trans-chrysanthemic acid by a microbial esterase: cloning, nucleotide sequence, and overexpression of the esterase gene of Arthrobacter globiformis in *Escherichia coli*." Appl Environ Microbiol. **61**: 3208-3215.

Ollis, D. L., Cheah, E., Cygler, M., Dijkstra, B., Frolow, F., Franken, S.M., Harel, M., Remington, S.J., Silman, I., Schrag, J., Sussman, J.L. (1992). "The alpha/beta hydrolase fold." Protein Eng. **5**: 197-211.

Oosterhoff, D., Overmeer, R.M., de Graaf, M., van der Meulen, I.H., Giaccone, G., van Beusechem,V.W., Haisma, H.J., Pinedo, H.M., Gerritsen, W.R. (2005). "Adenoviral vector-mediated expression of a gene encoding secreted, EpCAM-

targeted carboxylesterase-2 sensitises colon cancer spheroids to CPT-11." Br J Cancer. **92**: 882-887.

Oosterhoff, D., Witlox, M.A., van Beusechem, V.W., Haisma, H.J., Schaap, G.R., Bras, J., Kruyt, F.A., Molenaar, B., Boven, E., Wuisman, P.I., Pinedo, H.M., Gerritsen, W.R. (2003). "Gene-directed enzyme prodrug therapy for osteosarcoma: sensitization to CPT-11 in vitro and in vivo by adenoviral delivery of a gene encoding secreted carboxylesterase-2." Mol Cancer Ther. **8**: 765-771.

Otwinowski, Z., Minor, W. (1997). "Processing of the X-ray diffraction data collected in oscillation mode." Methods Enzymol. **276**: 307-326.

Park, Y. H., Less, S.S. (1994). "Identification and characterization of capsaicin-hydrolyzing enzymes purified from rat liver microsomes. ." Biochem. Mol. Biol. Int. **34**: 351-360.

Pindel, E. V., Kedishvili, N.Y., Abraham, T.L., Brzezinski, M.R., Zhang, J., Dean, R.A., Bosron, W.F. (1997). "Purification and cloning of a broad substrate specificity human liver carboxylesterase that catalyzes the hydrolysis of cocaine and heroin." J. Biol. Chem. **272**: 14769-14775.

Pohlenz, H. D., Boidol, W., Schuttke, I., Streber, W.R. (1992). "Purification and properties of an *Arthrobacter oxydans* P52 carbamate hydrolase specific for the herbicide phenmedipham and nucleotide sequence of the corresponding gene." J Bacteriol. **174**: 6600-6607.

Potter, P. M., Pawlik, C.A., Morton, C.L., Naeve, C.W., Danks, M.K. (1998). "Isolation and partial characterization of a cDNA encoding a rabbit liver carboxylesterase that activates the prodrug irinotecan (CPT-11)." Cancer Res. **58**(12): 2646-2651.

Potterton, E., Briggs, P., Turkenburg, M., Dodson, E. (2003). "A graphical user interface to the CCP4 program suite." Acta Crystallogr D Biol Crystallogr. **59**: 1131-1137.

Quax, W. J., Broekhuizen, C.P. (1994). "Development of a new Bacillus carboxyl esterase for use in the resolution of chiral drugs." Appl. Microbiol. Biotechnol. **41**: 425-431.

Read, T. D., Salzberg, S. L., Pop, M., Shumway, M., Umayam, L., Jiang, L., Holtzapple, E., Busch, J. D., Smith, K. L., Schupp, J. M., Solomon, D., Keim, P., Fraser, C. M. (2002). "Comparative genome sequencing for discovery of novel polymorphisms in *Bacillus anthracis*." Science. **296**: 2028-2033.

Redinbo, M. R., Potter, P.M. (2005). "Mammalian carboxylesterases: from drug targets to protein therapeutics." Drug Discov. Today. **10**: 313-325.

Rhodes, G. (2000). Crystallography made crystal clear : a guide for users of macromolecular models San Diego, Calif. : Academic, c2000.

Rice, G. C., Goeddel, D.V., Cachianes, G., Woronicz, J., Chen, E.Y., Williams, S.R., Leung, D.W. (1992). "Random PCR mutagenesis screening of secreted proteins by direct expression in mammalian cells." Proc Natl Acad Sci U S A. **89**: 5467-5471.

Rivory, L. P., Haaz, M.C., Canal, P., Lokiec, F., Armand, J.P., Robert, J. (1997). "Pharmacokinetic interrelationships of irinotecan (CPT-11) and its three major plasma metabolites in patients enrolled in phase I/II trials." Clin Cancer Res. **3**(8): 1261-1266.

Roth, J. A., Swisher, S.G., Meyn, R.E. (1999). "p53 tumor suppressor gene therapy for cancer." Oncology (Williston Park). **10 Suppl 5**: 148-154.

Rothenberg, M. L., Oza, A. M, Bigelow, R.H., Berlin, J. D., Marshall, J.L., Ramanathan, R.K., Hart, L. L., Gupta, S., Garay, C.A., Burger, B.G., Le, Bail N, Haller, D.G. (2003). "Superiority of oxaliplatin and fluorouracil-leucovorin compared with either therapy alone in patients with progressive colorectal cancer after irinotecan and fluorouracil-leucovorin: interim results of a phase III trial. ." J. Clin. Oncol. **21**: 2059-2069.

Satoh, T., Hosokawa, M. (1998). "The mammalian carboxylesterases: from molecules to functions." Annu. Rev. Pharmacol.Toxicol. **38**: 257-288.

Satoh, T., Hosokawa, M., Atsumi, R., Suzuki, W., Hakusui, H., Nagai, E. (1994). "Metabolic activation of CPT-11, 7-ethyl-10-[4-(1-piperidino)-1-piperidino]carbonyloxycamptothecin, a novel antitumor agent, by carboxylesterase." Biol. Pharm. Bull. **5**: 662-664.

Senter, P. D., Marquardt, H., Thomas, B.A., Hammock, B.D., Frank, I.S., Svensson, H.P. (1996). "The role of rat serum carboxylesterase in the activation of paclitaxel and camptothecin prodrugs." Cancer Res.. **56**: 1471-1474.

Senter, P. D., Springer, C.J. (2001). "Selective activation of anticancer prodrugs by monoclonal antibody-enzyme conjugates." Adv Drug Deliv Rev. **53**: 247-264.

Sevilla, M. D., Becker, D., Yan, M. (1990). "The formation and structure of the sulfoxyl radicals RSO-, RSOO-, RSO_2-, and RSO_2OO- from the reaction of cysteine, glutathione and penicillaminethiyl radicals with molecular oxygen." Int. J. Raciat. Biol. **57**: 65-81.

Sheldrick, G. M. (1997). SHELX97. Program for Crystal Structure Analysis, University of Gottingen, Germany.

Sheldrick, G. M., Sheldrick, W. S. (1970). "Crystal structure of trimethylammonium iodine; refinement of absorption for a laminar crystal." Acta Crystallogr. B **26**: 1334-1338.

Sieber, V., Martinez, C.A., Arnold, F.H. (2001). "Libraries of hybrid proteins from distantly related sequences." Nat Biotechnol. **5**: 456-460.

Spiller, B., Gershenson, A., Arnold, F.H., Stevens, R.C. (1999). "A structural view of evolutionary divergence." Proc Natl Acad Sci U S A. **96**(22): 12305-12310.

Stehle, T., Claiborne, A., Schulz, G.E. (1993). "NADH binding site and catalysis of NADH peroxidase." Eur. J. Biochem. **211**: 221-226.

Svendsen, A. (2004). Enzyme functionality : design, engineering,and screening New York Marcel Dekker.

Taguchi, T., Wakui, A., Hasegawa, K., Niitani, H., Furue, H., Ohta, K., Hattori, T. (1990). "Phase I clinical study of CPT-11. Research group of CPT-11." Gan To Kagaku Ryoho **17**(1): 115-120.

Takayama, H., Watanabe, A., Hosokawa, M., Chiba, K., Satoh, T., Aimi, N. (1998). "Synthesis of a new class of camptothecin derivatives, the long-chain fatty acid esters of 10-hydroxycamptothecin, as a potent prodrug candidate, and their *in vitro* metabolic conversion by carboxylesterases." Bioorg Med Chem Lett. **8**: 415-418.

Tang, B. K., Kalow, W (1995). "Variable activation of lovastatin by hydrolytic enzymes in human plasma and liver." Eur. J. Clin. Pharmacol.(47): 449-451.

Taylor, P., Radic, Z (1994). "The cholinesterases: from gene to proteins." Annu. Rev. Pharmacol.Toxicol. **34**: 281-320.

Terwilliger, T. C. (2001). "Maximum-likehood density modification with pattern recognition of structural motifs." Acta Crystallogr. D **57**: 1755-1762.

Terwilliger, T. C., Berendzen, J. (1997). "Bayesian MAD phasing." Acta Crystllogr. D **53**: 571-579.

Thompson, J. D., Gibson, T. J., Plewniak, F., Jeanmougin, F., Higgins, D. G. (1997). "The ClustalX windows interface: flexible strategies for multiple sequence alignment aided by quality analysis tools." Nucleic Acids Res. **24**: 4876-4882.

Tsuji, T., Kaneda, N., Kado, K., Yokokura, T., Yoshimoto, T., Tsuru, D. (1991). "CPT-11 converting enzyme from rat serum: purification and some properties." J Pharmacobiodyn. **14**: 341-349.

Vagin, A., Teplyakov, A. (1997). "MOLREP: an automated program for molecular replacement." J. Appl. Cryst. **30**: 1022-1025.

Walker, C. H., Mackness, M. I. (1983). "Esterases: Problems of identification and classification." Biochem. Pharmacol. **32**: 3265-3269.

Watanabe, Y. (1992). "Transfection of interferon-gamma gene in animal tumors--a model for local cytokine production and tumor immunity." Semin Cancer Biol. **1**: 43-46.

White, K. N., Vale, V.L., Hope, D.B. (1994). "Identification of common from salicylates esterases in guinea-pig tissues similar to the microsomal aspirinase of liver." Biochem. Soc. Trans. **22**: 220S.

Wierdl, M., Morton, C.L., Nguyen, N.K., Redinbo, M.R., Potter, P.M. (2004). "Molecular Modeling of CPT-11 Metabolism by Carboxylesterases (CEs): Use of Pnb CE as a Model." Biochemistry **43**: 1874-2882.

Wierdl, M., Morton, C.L., Weeks, J.K., Danks, M.K., Harris, L.C., Potter, P.M. (2002). "Sensitization of human tumor cells to CPT-11 via adenoviral-mediated delivery of a rabbit liver carboxylesterase." Cancer Res. **61**: 5078-5082.

Wilson, M. A., Ringe, D., Petsko, G.A. (2005). "The atomic resolution crystal structure of the YajL (ThiJ) protein from Escherichia coli: a close prokaryotic homologue of the Parkinsonism-associated protein DJ-1." J Mol Biol. **353**: 678-691.

Xu, G., McLeod, H.L. (2001). "Strategies for enzyme/prodrug cancer therapy." Clin Cancer Res. **7**: 3314-3324.

Yamada, T., Hosokawa, M., Satoh, T., Moroo, I., Takahashi, M., Akatsu, H. Yamamoto, T. (1994). "Immunohistochemistry with an antibody to human liver carboxylesterase in human brain tissues. ." Brain Res. **658**: 163-167.

Yamada, Y., Otsuka, M., Takaiti, O. (1992). "Metabolic fate of the new angiotensin-converting enzyme inhibitor imidapril in animals. 7th communization: in vitro metabolism. ." Arzneimittel Forsch **42**: 507-512.

Yang, W., Hendrickson, W.A., Crouch, R.J. and Satow, Y. (1990). "Structure of ribonuclease H phased at 2 Å resolution by MAD analysis of the selenomethionyl protein." Science. **272**: 1606-1614.

Zhao, H., Giver, L., Shao, Z., Affholter, J.A., Arnold, F.H. (1998). "Molecular evolution by staggered extension process (StEP) *in vitro* recombination." Nat. Biotechnol. **16**: 258-261.

Zhao, H. M., Zha, W.J. (2004). Evolutionary methods for protein engineering. New York, Marcel Dekker.

Zock, J., Cantwell, C., Swartling, J., Hodges, R., Pohl, T., Sutton, K., Rosteck, P. Jr, McGilvray, D., Queener, S. (1994). "The *Bacillus subtilis* pnbA gene encoding p-nitrobenzyl esterase: cloning, sequence and high-level expression in *Escherichia coli*." Gene **151**: 37-43.